AN ANALYSIS OF THE INCOMPRESSIBLE TWO-DIMENSIONAL JET EJECTOR

Thesis by

James R. Rose

In Partial Fulfillment of the Requirements

For the Degree of

Doctor of Philosophy

California Institute of Technology

Pasadena, California

1969

(Submitted March 10, 1969)

ACKNOWLEDGEMENTS

The author would like to express his appreciation to Dr. Peter B. S. Lissaman for his essential guidance in the analysis of this problem, to Dr. Gordon Harris for his many valuable suggestions, and to Mrs. E. Fox for her assistance in the preparation of this dissertation. To all the above, and most especially to his wife, for their unfailing encouragement the author is deeply indebted.

The financial support of the National Research Council of Canada, and the Ford Foundation, during the course of this study, is gratefully acknowledged.

ABSTRACT

A general method for calculating the performance of two-dimensional jet ejector systems is presented, with special emphasis on those qualities desired in thrust augmenter devices. The nature of the viscous-inviscid interaction problem is examined and a "frictionless" model is defined. The equations are solved for the particular parametric problem of a single jet in a finite length shroud of uniform height. The flow in the "recovery" or confined-mixing region is discussed for this model and techniques are developed which may be applied to devices with diffusing systems.

The solutions presented for the free-mixing or interaction region are shown to agree with the simple channel flow studied analytically and experimentally by Curtet.

TABLE OF CONTENTS

TABLE OF CONTENTS (Continued)

TABLE OF CONTENTS (Continued)

LIST OF SYMBOLS

a	primary nozzle half-height
A	velocity profile parameter $= \int_0^1 f d\eta$
B	velocity profile parameter $= \int_0^1 f^2 d\eta$
c_t	turbulent coefficient
C_i i=0, N	coefficients in potential solutions
C_f	skin friction coefficient
f	velocity profile function
$\tilde{f}(z)$	complex transformation function
$F(z)$	complex velocity potential
g	turbulent shear stress function
$\tilde{g}(z)$	complex transformation function
h	shroud half height
$I(\xi')$	function in potential solution
J_i i=0, N	function in potential solution
k_i	coefficients in expansion near X = 0
K_i i=0, N	function in potential solution
L	shroud length
L_1	nozzle position relative to shroud lip
M	momentum flux/unit depth
M_T	total momentum flux/unit depth
N	number of match points in the potential solution
p	static pressure
p_∞	free stream static pressure (ambient)

LIST OF SYMBOLS (Continued)

P_0	static pressure at jet edge
Q	volume flux/unit depth-half plane model
Q_T	total volume flux/unit depth-full model
u	velocity in X-direction (axial)
$\tilde{u}$	supervelocity in jet
U	velocity at edge of mixing region
u_j	primary jet velocity
v	velocity in Y-direction (transverse)
w	complex velocity = u-iv
x	axial coordinate referred to shroud lip (nondimensional)
x_i	potential flow stations in approximated solution
X	axial coordinate referred to nozzle position
X_{m_i}	match points in approximated solution
X_f	axial distance from nozzle to shroud trailing edge
y	transverse coordinate (nondimensional)
Y	transverse coordinate
α	momentum coefficient
γ	velocity profile parameter = B/A
δ	turbulent jet boundary
ϵ	parameter of complex transformation
ζ	complex transformation of z into half-plane
η	imaginary component of ζ
κ_t	turbulent coefficient
λ	velocity profile factor

LIST OF SYMBOLS (Continued)

Λ	nondimensional shroud length = L/h
Λ_1	nondimensional nozzle position = L_1/h
Λ_2	nondimensional nozzle height = a/h
Λ_M	nondimensional length of mixing = $\Lambda + \Lambda_1$
ξ	real component of ζ
ξ_i	mapping points of x_i
ρ	fluid density
φ_T	thrust augmentation = M_T/M_j
φ_{T_∞}	limiting value of φ_T for infinite shroud
ψ	incompressible stream function
Ψ	stream function evaluated on boundary

Subscripts (except where noted above)

1	-	value at the shroud nozzle plane
2	-	value at the shroud exit plane
e	-	value at the end of free-mixing region
δ	-	complex quantity evaluated on jet boundary
j	-	primary jet value
t	-	turbulent parameter

Superscripts

*	-	normalized value
-	-	time averaged value
'	-	fluctuating component
^	-	normalized value (edge position δ)

I. PRINCIPLES OF JET EJECTORS

I. 1 Introduction

The turbulent mixing processes associated with a high energy jet exhausting into a free ambient medium have been of interest to many investigators in the past half-century. This flow affords a comparatively simple experimental medium for the measurement of turbulence phenomena, and a good verification of the similarity arguments used in shear flow models.

The fundamental effect of putting a body in the vicinity of a high energy jet is to distort and direct the flow which is induced by the entraining action of the jet. A free jet normally spreads into the secondary medium by the diffusion of momentum, but the total momentum flux in the jet direction at any station downstream remains constant. When a body is placed in the induced flow, however, it is acted upon by pressure and viscous forces due to the induced flow, and in general these forces have a component in the direction of the primary jet flow. The reaction forces of the body on the fluid then produce a change in the jet streamwise momentum flux, which represents a change in the thrust of the system. For thrust augmentors, this change is an increase in thrust, and the design criterion is the maximization of this momentum exchange between the forces on the body and the jet momentum flux. We will concentrate in this study on the mechanism of momentum exchange applied to two-dimensional jets with a symmetric external geometry (shroud), as illustrated in figure 1.

Designing the outer geometry in order to utilize this influence, several practical devices have been produced. Jet pumps are designed to maximize the induced/primary mass flow rates, and to deliver this flow into regions of higher pressure. In thrust augmentors, the desired characteristic is the maximum total/primary momentum flux ratio, in order to produce large increases in thrust.

In principle the ejector phenomenon could be used to improve the performance of primary thrust systems and such auxiliary devices as jet flap aerofoils and boundary-layer-control blowing systems. The effective design of such systems requires fundamental knowledge of the characteristics of shrouded or confined jets, which is as yet not available.

With the use of the momentum theorem T. von Kármán[1] investigated the possibilities of obtaining thrust augmentation in a uniform shroud system as a function of the assumed inlet and exhaust velocity profiles. His results (discussed in Section I. 4) indicated the possibilities of large increases in thrust but could not close the problem by relating the thrust augmentation to the geometry and primary thrust of a particular configuration. In this study we will present a method for relating the mixing processes to a generalized ejector configuration, and use the method to define the limits of operation for a simple class of two-dimensional ejectors.

To this end we define a "frictionless" model as one in which friction effects (boundary layers on the shroud surfaces) are neglected. This model represents the limiting case for the real system, whose performance characteristics will in general be degraded

by friction. Even though for some configurations this model will be somewhat imprecise, it has been found by various authors (Curtet[2], Hill[3]) that the frictionless model is quite good in the specific geometries investigated. In any case, the effect of friction will best be estimated as a "correction" to the ideal model.

I. 2 The Frictionless Model

The basic fluid-mechanical problem in a shrouded jet system is the evaluation of the mixing effectiveness in the region of entrainment. The nature of this process enables us to conveniently divide the flow into two fundamentally distinct regions, with an unsteady interface (figure 2). This same division occurs in the classic free jet spreading into an ambient medium. A look at this associated problem will illustrate the characteristics of the two regions. In the mixing region, viscous effects predominate, and for most practical cases the flow is rotational and turbulent. The assumption that the flow in this region can be adequately described by the boundary-layer equations was shown to be valid by many investigators (Goldstein[4]). They have also shown that a wide variety of phenomenological laws describing the behavior of the turbulence terms allow excellent predictions of the mean velocity profile of the jet, the growth of the jet thickness, and the rate of increase of mass flux (the entrainment).

G. I. Taylor[5], referring to some earlier work in the calculation of the external streamlines, showed that the smoke pictures of Lippisch[6] could be reproduced by an assumed sink distribution along the jet axis in potential flow. He generated the first-order

solution to the flow in the outer region by matching the sink distribution to the entrainment rate of a turbulent jet. The outer flow is thus essentially inviscid and irrotational, and may be handled by the classical method of potentials.

These results suggest singular perturbation methods should be used for the jet mixing, in which the simple free jet and Taylor's potential flow represent the first-order inner and outer solutions respectively. In these flows, the inner or free-mixing solution is the dominating solution, and is not changed to first order by the external geometry, as demonstrated by the fact that Taylor's solutions for the infinite region and the semi-infinite region (the jet issuing normal to an infinite wall) can use the same sink distribution on the jet boundary to generate the induced flow.

Another class of turbulent jet mixing is represented by the mixing of jets in constant area ducts, where the flow external to the mixing region can be assumed to be uniform and in the direction of the primary jet, as in the analyses of Curtet for the two-dimensional problem, and Hill for the round jet in a coaxial duct. In this type of flow, the external flow has a fundamental effect on the development of the mixing region through the first-order effects of the pressure gradient and entrainment as represented by the non-zero edge velocity. This strong interaction is solved by simultaneously calculating the mixing and entrained flow problems, which must be matched at some boundary.

The problem of a body in the neighborhood of a high energy jet issuing into an ambient medium contains the two simple flows

mentioned above as limiting cases. To clarify this point we can divide the problem into two classes, remembering that we are discussing only those flows with symmetry about the axis of the primary jet.

Type I flows (figure 2) include those in which the bodies are totally enclosed by entrained or external flow, and hence do not influence the mixing by direct contact with the mixing region, but by modifying and directing the external entrained flow. These flows have the free jet as the limit when the body is far removed from the mixing region.

Type II flows (figure 3) include those where some part of the body is in direct contact with, and hence modulating the mixing process, as well as influencing the external flow. Thus the limit as the body becomes a very long duct in which the mixing process is confined, is represented by the second simple case discussed above.

The problems in the type I category could clearly be calculated by the same perturbation technique as the free jet problem, since the body is totally immersed in irrotational flow and potential solutions can be found. For the case where the body is far from the mixing region, the solution to the first-order potential problem, which would have the boundary conditions imposed by the free jet entrainment rate, would give a good approximation of the forces exerted on the body. As the body is moved closer to the primary jet, second-order terms would become important, but the perturbation scheme would still be straightforward. In this type of problem, the boundary conditions to the outer flow problem would be imposed

on the axis of symmetry, but the potential flow region must exclude that part of the region occupied by the turbulent mixing.

The use of this method is not so straightforward in the type II problems, where a portion of the body is submerged in the mixing region. Applying the boundary conditions to the outer flow on the axis of symmetry would imply that the entire body was in the entrained flow region. In particular the application of a Kutta condition on a sharp trailing edge would then appear as an artificial condition if that part of the body was in the mixing flow. It seems practical for this type of problem to find a solution of the inner and outer flows simultaneously and to choose a matching boundary which would realistically represent the confining effect of the body on the turbulent mixing, and the blocking effect of the turbulent mixing on the potential flow solution.

The problem which we will solve here is of the second type, since it seems that the strong interaction of the viscous and inviscid regions, and the increase in mixing efficiency due to the confining effect of the body are necessary to produce large changes in the jet momentum flux, and hence large forces on the body. In addition, we will assume that the symmetric pair of external bodies, (the shroud), is long enough to prevent the viscous-inviscid mixing of the flow downstream of the shroud from affecting the flow at the shroud entrance. Thus the entraining efficiency of the jet is determined by the jet mixing in that region upstream of the jet impingement on the shroud.

I. 3 Geometrical Parameters

The complete ejector configuration can be described by the

shroud geometry and the position and distribution of the primary nozzle system. A complete study of any practical device would necessitate the definition of parameters to represent each geometric detail (for example the shroud shape, lip shape, number of jets). In this study we confine ourselves to the uniform shroud with a zero thickness lip and a single center-line primary nozzle (figure 4).

The parameters to be studied now are reduced to

$\Lambda = L/h$ the nondimensional shroud length

$\Lambda_1 = L_1/h$ the nondimensional position of the primary nozzle relative to the lip of the shroud

An additional parameter, the relative nozzle height $\Lambda_2 = a/h$ is considered here to be much smaller than 1. The nozzle can now be represented as a point momentum source, a model which gives good agreement with experiments for free jets at distances downstream of the nozzle greater than a few nozzle heights.

The symmetry of the model allows us to represent the ejector by a half-plane model with boundary conditions

$$v = 0$$

$$\frac{\partial u}{\partial Y} = 0$$

on $Y = 0$

I. 4 Conservation Laws

Since we are neglecting friction on the shroud, we can generate a "law" for this system corresponding to the conservation of momentum for the free jet. In figure 4, we designate a velocity u(Y) with an associated static pressure p(Y) at a general station X downstream of the jet nozzle. The corresponding quantities at the nozzle

station and exit plane are designated with subscripts 1 and 2 respectively.

The equations of conservation of mass and momentum lead to the following "laws"

$$\int_{-h}^{h} u dY = \int_{-h}^{h} u_2 dY = Q_T \tag{1.1}$$

$$\int_{-h}^{h} (p + \rho u^2) dY = \int_{-h}^{h} (p_\infty + \rho u_2^2)\, dY = M_T \tag{1.2}$$

where p_∞ is the ambient pressure of the outer flow, and M_T is the total momentum flux. If M_j is the primary jet momentum flux, we can define the Thrust Augmentation, φ_T, as

$$\varphi_T = M_T/M_j \tag{1.3}$$

and this parameter, which is dependent upon the configuration of the ejector, describes the efficiency of the thrust augmentor since it is a ratio of the thrust of the system to the thrust of the primary (or the jet thrust in the absence of the shroud).

Assuming a uniform velocity, uniform pressure primary jet, M_j is given by

$$M_j = 2a(p_j + \rho\, u_j^2) \tag{1.4}$$

The induced flow at, and upstream of, station 1 is inviscid and irrotational, and hence the pressure is determined from Bernoulli's theorem.

I. 5 Fundamental Ejector Behavior

We can obtain an idea of the performance of uniform shroud

ejectors by considering the asymptotic behavior of the frictionless model in a uniform external flow U_∞ when the shroud is long enough to allow the induced flow upstream of the primary and the mixed flow downstream of the primary to become uniform with velocity U (figure 5). For the ideal momentum source primary, the finite momentum flux $M_j \left\{ \lim_{a \to 0} 2\rho a u_j^2 = M_j \right\}$ makes the mass flux $\left\{ \lim_{a \to 0} 2a\rho u_j \right\}$ of the primary negligible. All of the flow in the shroud is then entrained flow. The external streamlines contract as the flow which is entrained into the shroud is given an increase in velocity $(U-U_\infty)$, and hence near the lip of the shroud on the outside, there is a stagnation point. The mass flux in the shroud is given by

$$Q_T = 2\rho h U \tag{1.5}$$

and the thrust of the system is given by the increase in momentum flux of the entrained flow

$$M_T = 2hU\,\rho\,(U-U_\infty) \tag{1.6}$$

The flow inside the shroud may be calculated by considering the conservation of momentum in the control volume shown in figure 5, where the pressure in the uniform entrained flow is given by

$$p = p_\infty + \frac{\rho}{2}\,(U_\infty^2 - U^2) \tag{1.7}$$

We find then that

$$M_j = \rho h (U^2 - U_\infty^2) \tag{1.8}$$

and hence from 1. 3, the thrust augmentation is given by

$$\varphi_T = 2/(1 + \frac{U_\infty}{U}) \tag{1.9}$$

When the ejector is stationary, the asymptotic value is obtained

$$\varphi_{T_\infty} = 2 \tag{1.10}$$

This remarkable number is a convenient standard with which to compare the performance of finite ejectors, and deserves some comment. It is independent of ejector geometry near the entrance as long as the region in which the control volume is considered is of uniform height. Thus in this limit the lip shape plays no role, and the pressure forces generated there are similar to those generated at the leading edge of an aerofoil. In particular, the zero thickness lip generates the same thrust as the finite lip, due to the negative infinite pressures developed. This is exactly analogous to the flat plate aerofoil nose suction.

For finite U_∞ the thrust augmentation is a function of the conventional jet momentum coefficient

$$C_j = \frac{M_j}{2h(\frac{\rho}{2} U_\infty^2)} \tag{1.11}$$

since the velocity ratio $\frac{U}{U_\infty}$ can be obtained from the momentum balance, equation 1. 8. Hence φ_T can be written as

$$\varphi_T = 2\left(1 - \frac{1}{1+\sqrt{1+C_j}}\right) \tag{1.12}$$

Thus for a given primary, the augmentation is degraded by forward speed, and the analysis presented here for zero forward speed must be modified if the device is to operate at flight speeds where $C_j \sim O(1)$. For the limiting case where $C_j \to 0$, or $U \to U_\infty$, the shroud produces no augmentation in thrust since then the stagnation point moves up to the lip and the infinite negative pressure there disappears.

To introduce the analysis for finite ejectors in an ambient medium, it is useful to look at the results obtained by the method used by von Kármán, which was referred to earlier. If we assume that nonuniform velocity profiles occur in ejectors of moderate length, we can assign a parametric description of the nonuniformity by defining

$$\lambda = \frac{\frac{1}{h}\int_0^h u^2 \, dY}{\left(\frac{1}{h}\int_0^h u \, dY\right)^2}$$

where then $\lambda > 1$ for nonuniform profiles. We use Bernoulli's equation to relate the pressure to the velocity in the entrained flow and then make the critical assumption that the entrained flow is unidirectional ($v \equiv 0$). Referring again to figure 4 we can evaluate the two conservation laws, equations 1.1 and 1.2 at station 1, and thus calculate the thrust augmentation as a function of the dimensionless primary nozzle height Λ_2 and the velocity parameters λ_1 and λ_2 evaluated at sections 1 and 2 respectively. The results are shown in figure 6.

It is apparent that highly nonuniform entrance profiles and profiles approaching uniformity at the exit produce the highest thrust augmentations. The apparently unbounded values of φ_T possible stem from the assumption that highly nonuniform inlet velocity profiles may be attained in the induced flow, with no accompanying transverse velocity components. We will make the more realistic assumption of potential entrained flow to show that the thrust augmentation is constrained to a much narrower range, and reaches the asymptotic value

$$\varphi_{T_\infty} = 2$$

for the "frictionless" model of infinite length.

II. THE FLOW FIELD (TYPE II)

II. 1 The Nature of the Flow

In addition to the distinction made in the previous section between the mixing region and the outer region, it is convenient to divide the turbulent flow field into two parts, the free-mixing region, where the turbulent processes are controlled by the free boundary, and the confined-mixing region which is enclosed by solid surfaces (figure 7).

This difference is expressed in the behavior of the pressure term in the confined-mixing region. Because there is no longer any boundary condition linking the pressure to the velocity field, it must be treated as a separate variable, with values prescribed at the point of impingement of the jet and at the exit, where it must equal p_∞.

The exit plane is assumed to be downstream far enough that the outer entrained flow is not affected by the discharging flow, and hence the flow downstream of the exit plane may be neglected.

II. 2 The Interaction Problem

As has already been discussed, this type of interaction problem is most conveniently solved as a strong interaction, in which both the inviscid region and the viscous region must be solved simultaneously. Moreover, the boundary conditions must be so specified that the entraining effect of the mixing is limited to that part of the jet which is bounded by fluid, and hence the matching conditions will be specified off the axis of symmetry. We choose to match both the pressure and mass flux at the edge of the jet, which then will be

considered to be the boundary of the potential flow region. This seems to be the most obvious matching point from a physical point of view, but no mathematical justification exists for choosing it over other positions, for example the half-velocity point.

We must now formulate the equations of motion in each region, and apply the conditions at the boundary that mass flux and pressure, or edge velocity, be the same for the inner and outer regions. We will then calculate the flow in the confined mixing region, and determine the length of shroud necessary for the pressure to return to ambient pressure.

II. 3 The Free-Mixing Region

We will define two axial scales for the inner and outer flow for convenience. In the inner flow, the distance from the nozzle will be denoted by X, while in the outer flow, x will be measured from the shroud lip, and is made dimensionless by the shroud height.

(a) The Mixing Layer Equations

We represent the velocities and pressure in the two-dimensional Navier-Stokes equations by

$$u = \overline{u} + v'$$

$$v = \overline{v} + v'$$

$$p = \overline{p} + p'$$

where barred quantities are time averaged and primed quantities are fluctuations with zero mean. The equations can be written as

$$\frac{\partial \overline{u}}{\partial X} + \frac{\partial \overline{v}}{\partial Y} = 0 \qquad (2.1)$$

$$\frac{\partial \overline{u}^2}{\partial X} + \frac{\partial \overline{u}\,\overline{v}}{\partial Y} = -\frac{1}{\rho}\frac{\partial \overline{p}}{\partial X} - \frac{\partial \overline{u'^2}}{\partial X} - \frac{\partial \overline{u'v'}}{\partial Y} \qquad (2.2)$$

$$\frac{\partial \overline{u}\,\overline{v}}{\partial X} + \frac{\partial \overline{v}^2}{\partial Y} = -\frac{1}{\rho}\frac{\partial \overline{p}}{\partial Y} - \frac{\partial \overline{u'v'}}{\partial X} - \frac{\partial \overline{v'^2}}{\partial Y} \qquad (2.3)$$

In addition to the transverse scale $\delta \sim O(h)$ previously mentioned, we note that L represents an axial length scale which is large compared with h. That is $\Lambda = L/h >> 1$.

Thus if $\frac{\partial}{\partial X} \sim \frac{1}{L}$ and $\frac{\partial}{\partial Y} \sim \frac{1}{h}$, from 2.1 we get

$$\frac{\overline{v}}{\overline{u}} = O\left(\frac{1}{\Lambda}\right)$$

In addition, we assume that the mean products of the turbulent quantities are of the same order, that is $O(\overline{u'^2}) = O(\overline{v'^2}) = O(\overline{u'v'})$.

Examining the roles of the inertia and pressure terms in 2.2 and 2.3 we see that if they are of the same order in 2.2, the inertia terms must be of order $(1/\Lambda)^2$ compared with the pressure term in 3.3. Thus

$$\frac{\overline{p}}{\rho} = \frac{P_0(X)}{\rho} - \overline{v'^2}$$

where P_0 is the pressure evaluated at the jet boundary. This implies that

$$P_0 = O(\Lambda^2)\,\overline{v}^2\Big|_{Y=\delta}$$

and hence that Bernoulli's equation reduces to

$$P_0 = p_\infty - \frac{\rho}{2} U^2(X)$$

where U(x) is the edge velocity. The model equations are reduced to

$$\frac{\partial \overline{u}^2}{\partial X} + \frac{\partial \overline{u}\,\overline{v}}{\partial Y} = -\frac{1}{\rho}\frac{dP_0}{dX} - \frac{\partial}{\partial Y}\overline{u'v'} + \frac{\partial}{\partial X}(\overline{u'^2} - \overline{v'^2}) \qquad (2.4)$$

$$\frac{\partial \overline{u}}{\partial X} + \frac{\partial \overline{v}}{\partial Y} = 0 \qquad (2.5)$$

The assumption on the turbulence terms leads us to exclude the last term of 2.4 as $O(\frac{1}{\Lambda})$ compared with the others. We use 2.5 to eliminate $\overline{v}$ and obtain the basic equation

$$\frac{\partial \overline{u}^2}{\partial X} - \frac{\partial}{\partial Y}\left(\overline{u}\int_0^Y \frac{\partial \overline{u}}{\partial X}\,dY\right) = -\frac{1}{\rho}\frac{dP_0}{dX} - \frac{\partial \overline{u'v'}}{\partial Y} \qquad (2.6)$$

(b) Similarity Solutions

In order to make some progress in solving 2.6, a relationship connecting the turbulent shear stress to the mean flow must be found. One procedure is to postulate a "law" through some simple argument such as the mixing length. For shear flows of this type investigators (see Schlichting [7]) have formed several such laws which seem to have virtually the same validity in predicting development of mean flow quantities.

In addition the mean velocity profiles in the region downstream of the jet potential core can be reasonably well correlated onto a single universal curve, as has been demonstrated for cases of free jet spreading (Reichardt [8]), jets in co-flowing constant velocity streams (Weinstein [9]) and self-similar jet spreading (Harris [10]). For this reason we will represent u(X, Y) by a universal function

$$\overline{u}(X, Y) = U(X) + \tilde{u}(X)\, f(\frac{Y}{\delta(X)}) \qquad (2.7)$$

where $\delta(X)$ is the edge of the jet, $U(X)$ the axial velocity measured there, and the supervelocity $\tilde{u}(X)$ is the difference between the jet maximum velocity and the edge velocity. The edge will be defined in the next section as the line at which the inner and outer flows are to be matched, and we then avoid the conventional difficulties in locating the point where the physics of the flow changes.

We choose to represent the universal velocity profile with the function

$$f = \tfrac{1}{2}(1 + \cos(\pi \frac{Y}{\delta})) \qquad (2.8)$$

since this represents the experimental curve in the inner region as well as any other, and has a finite radius of curvature at $Y = 0$.

Before discussing the representation of the turbulent shear stress, we note that truly self-preserving flow can only satisfy 2.6 for certain relationships between U, $\tilde{u}$ and δ. The integral form of the equation, however, with the assumed velocity profile, together with enough auxiliary equations to solve the problem, predicts well the required functions when they are mutually independent. Integrating 2.6 across the shear layer, we obtain the basic integral equation

$$\frac{dU}{dX}(2\delta\tilde{u}) + \frac{d\tilde{u}}{dX}(\delta(U + 2\gamma\tilde{u})) + \frac{d\delta}{dX}(\tilde{u}(U + \gamma\tilde{u})) = 0 \qquad (2.9)$$

where γ, B and A are constants defined as

$$A = \int_0^1 f \, d(\frac{Y}{\delta}) = \frac{1}{2}$$

$$B = \int_0^1 f^2 \, d(\frac{Y}{\delta}) = \frac{3}{8}$$

and

$$\gamma = \frac{B}{A} = \frac{3}{4}$$

For this two-parameter model of the free-mixing region we need two additional relationships. One will bring in the forcing term through the shear stress term, and the other will be supplied by the matching at the boundary.

(c) The Auxiliary Equation

Forms of the auxiliary equation commonly used are the integral mechanical energy equation for the mean flow, and the moment of momentum equation, both derived by integrating the product of equation 2.6 and the appropriate weighting function. For this study we choose as our auxiliary equation the momentum equation evaluated on the axis of symmetry. While it is recognized that the physical applicability is perhaps not as direct, in that it emphasizes the mechanics of the flow at one particular transverse position as opposed to the averaging effect of the other equations, it has the advantage of being in the simplest form, and more important, it gives the same general results as the other forms.

In terms of our assumed velocity profile, it has the form

$$\frac{dU}{dX}(\delta\tilde{u}) + \frac{d\tilde{u}}{dX}(\delta(U + \tilde{u})) = -\frac{1}{\rho}\frac{\partial}{\partial Y}(\overline{u'v'})\Big|_{Y=0} \qquad (2.10)$$

(d) The Turbulent Shear Stress

We need not specify at this time which representation of the Reynolds stress term we will use, but only its form at Y = 0. We

denote $-\overline{u'v'} = \frac{\tau}{\rho}$ by the general form

$$\frac{\tau}{\rho} = \kappa_t u^2(X)\, g\left(\frac{Y}{\delta(X)}\right) \tag{2.11}$$

since experiments in a wide range of jet expansion flows justify the assumption that the shear stress is in local equilibrium with the mean flow parameters as scaling factors. We thus seek to extend this assumption to our problem with the condition that those regions where large X-gradients occur must be held suspect. Since no data are presently available on the behavior of jets departing from or relaxing to equilibrium, any correction is not justified in this model.

For the auxiliary equation used here, the forcing term is of the form

$$\left.\frac{\partial \overline{u'v'}}{\partial Y}\right|_{Y=0} = c_t \frac{\tilde{u}^2}{\delta} \tag{2.12}$$

where $c_t = \kappa_t g'(0)$ is an empirical constant which must be obtained from the limiting cases of the flow.

(e) Matching Conditions

The quantities to be matched in this problem are those most naturally associated with the mixing process, the pressure and the entrainment. In our model, these are represented by U(X) and Q(X) where

$$Q = \int_0^\delta \bar{u}\, dY = \delta(U + A\tilde{u}) \tag{2.13}$$

We therefore replace $\tilde{u}$ by Q and rearrange equations 2.9 and 2.10, using 2.12 to evaluate the forcing term. The set of equations to be solved is then

$$F_1 \frac{dQ}{dX} + F_2 \frac{d\delta}{dX} + F_3 \frac{dU}{dX} = 0 \qquad (2.14)$$

$$G_1 \frac{dQ}{dX} + G_2 \frac{d\delta}{dX} + G_3 \frac{dU}{dX} = - c_t (Q - U\delta)^2 \qquad (2.15)$$

where F_i and G_i are functions of Q, U, δ and are listed in Appendix I. Each coefficient is homogeneous in Q and Uδ.

II. 4 The Inviscid Region

The inviscid region is shown in figure 8 as that area bounded by the upper shroud surface, GF, the lower shroud surface, FE, the free boundary $y = \frac{\delta(X)}{h} = \hat{\delta}$ (EB), and the y = 0 axis from the free boundary to $x \to -\infty$, BA. Since the induced flow is assumed irrotational we may use potential flow theory to solve for $\psi(x, y)$, the incompressible streamfunction defined by

$$u = \frac{\partial \psi}{\partial y}$$

$$v = - \frac{\partial \psi}{\partial x}$$

where

$$\nabla^2 \psi = 0 .$$

For this two-dimensional problem we will use complex variable methods to solve for the complex potential

$$F = \varphi(x, y) + i\, \psi(x, y)$$

where $z = x + iy$

and $F = F(z)$.

We use the outer axial coordinate x which is related to the

inner coordinate X by

$$x = \frac{X}{h} - \Lambda_1 \qquad (2.16)$$

where Λ_1 is the normalized axial separation of the primary nozzle and the shroud leading edge, and hence in the z-plane the shroud is defined by

$$x \geq 0, \quad y = 1 .$$

The solution to the problem is determined by mapping the z-plane into the upper half-plane ζ (figure 9) where $\zeta = \xi + i\eta$ is defined by the mapping functions developed in Appendix III.

At the boundary $y = \hat{\delta}$, the flow is regular and hence the inviscid region may be analytically continued across the free boundary. We choose then to consider the flow as being generated by an artificial distribution of sinks on the line BC, and thus must solve a Dirichlet problem (figure 10) with the boundary conditions

$$\psi = 0 \quad \text{on} \quad AB$$

$$\psi = \Psi(x) \text{ on } BC$$

$$\psi = Q_T/2 \text{ on DFG}$$

and a sink-like behavior at $y \to \infty$

$$\psi \sim \frac{Q_T}{2} \left(1 - \frac{1}{\pi} \tan^{-1}\left(\frac{y}{x}\right)\right)$$

Mapping the function F directly over into ζ, we form the corresponding boundary-value problem on the half-plane (figure 10) with the solution

$$F(\zeta) = -\frac{1}{\pi}\int_{-\epsilon}^{0} I(\xi')\log(\xi'-\zeta)d\xi' \tag{2.17}$$

where

$$I(\xi') = \frac{d\Psi}{d\xi'} = \frac{d\Psi}{dx'}\frac{dx'}{d\xi'} \tag{2.18}$$

and $-\epsilon$ is the mapped nozzle position.

In the physical plane, the complex velocity $w(z) = u-iv$ is calculated from the complex potential as

$$w(z) = \frac{dF}{d\zeta} \Big/ \frac{dz}{d\zeta} \ . \tag{2.19}$$

Defining z_δ, ζ_δ to be the real and transform points which lie on the free boundary $y = \hat{\delta}(x)$, we can calculate from 2.17 and 2.19 the streamfunction and x-velocity at z_δ and equate them to the values $Q(X)$ and $U(X)$ in the inner flow.

The required relationship for Q, U, and $\hat{\delta}$ is then obtained by solving two integral equations

$$Q(X) = \mathcal{I}m\left\{-\frac{1}{\pi}\int_{-\epsilon}^{0} I(\xi')\log(\xi'-\zeta_\delta)d\xi'\right\} \tag{2.20}$$

$$U(X) = Re\left\{\frac{1}{\pi}\frac{d\zeta}{dz}\Big|_{z=z_\delta}\int_{-\epsilon}^{0}\frac{I(\xi')}{\xi'-\zeta_\delta}\,d\xi'\right\} \tag{2.21}$$

simultaneously to eliminate $I(\xi')$.

The interaction problem is now formulated. At this point the problem could be generalized to consider other shroud shapes with their corresponding mappings to the half-plane. Regardless of the shape of the shroud, the transformation must reduce to the scaling

transformation

$$z \alpha \zeta$$

for large ζ.

Using this we can show that 2.17 satisfies boundary conditions

(a) For $\mathrm{Re}\{\zeta\} < -\epsilon$, $\mathcal{I}\mathrm{m}\{\zeta\} = 0$

$$\psi = \mathcal{I}\mathrm{m}\{F(\zeta)\} = 0.$$

(b) For $\mathrm{Re}\{\zeta\} > 0$, $\mathcal{I}\mathrm{m}\{\zeta\} = 0$

$$\log(\xi' - \zeta) = -i\pi + \log(\zeta - \xi')$$

and therefore

$$\psi = \int_{-\epsilon}^{0} I(\xi')d\xi' = \frac{Q_T}{2} .$$

(c) If we consider the limit $|\zeta| \to \infty$

$$\log(\xi' - \zeta) \sim -i(\pi - \arg(\zeta))$$

so that

$$\psi \sim \frac{Q_T}{2}\left(1 - \frac{1}{\pi}\arg(\zeta)\right)$$

$$= \frac{Q_T}{2}\left(1 - \frac{1}{\pi}\tan^{-1}\left(\frac{y}{x}\right)\right) .$$

III. THE INTERACTION PROBLEM

III. 1 The Equations

Quasi-linear differential equations of the type 2. 14 and 2. 15 would ordinarily be handled as an initial value problem and forward-integrated. The elliptic nature of the outer flow, however, makes the coefficients of the equation dependent on the values of the parameters along the entire boundary, and necessitates a more elaborate numerical scheme. Accordingly we will introduce a numerical method which starts by integrating the inner equations using some assumed relationship in place of the equations 2. 20 and 2. 21. With the solution so calculated we will solve one of 2. 20 or 2. 21 for the kernel $I(\xi')$. Rearranging the inner equations so that the remaining equations, 2. 20 or 2. 21, can be considered a forcing function, with a known kernel, we can obtain a second approximation to the inner solution. We must then provide a suitable scheme such that successive iterations will converge to a stable solution in a reasonable manner.

It is important that we establish the correct initial conditions for the inner integration. As was suggested in Section I. 2, we will use the momentum point source model for the primary to avoid the complications of the initial "primary core" region of mixing. We then must look at the behavior of the equations close to the source.

III. 2 Initial Conditions

Assuming that the leading terms of the expansions of the parameters U, Q and δ for small X are of the form

$$Q \simeq Q_0 X^{a_1}$$
$$\delta \simeq \delta_0 X^{a_2} \qquad (3.1)$$
$$U \simeq U_0 X^{a_3}$$

where a_1, a_2 are both greater than zero, with the restrictions

$$Q = \delta(U + A\tilde{u}) \geq 0$$

and $\delta\tilde{u} \geq 0$, we find that

$$\lim_{X \to 0} \quad 0 \leq \frac{\delta_0 U_0}{Q_0} X^{a_2+a_3-a_1} \leq 1$$

and hence $a_4 = a_2 + a_3 - a_1 \geq 0$.

Keeping the lowest-order terms in 2.14 and 2.15 we have

$$k_1 + k_2 X^{a_4} + k_3 X^{2a_4} = 0 \qquad (3.2)$$

and
$$X^{a_2-1}(k_4 + k_5 X^{a_4} + k_6 X^{2a_4}) = -c_t Q_0^2 \left(1 - X^{a_4} \frac{\delta_0 U_0}{Q_0}\right)^2 \qquad (3.3)$$

where

$$k_1 = (2a_1 - a_2)\frac{\gamma}{A}\,\delta_0 Q_0^2$$

$$k_2 = -\left(\left(2\frac{\gamma}{A} - 1\right)a_1 + 2\left(\frac{\gamma}{A} - 1\right)a_3\right)\delta_0^2 U_0 Q_0$$

$$k_3 = \left(\left(2\frac{\gamma}{A} - 3\right)a_3 + \left(\frac{\gamma}{A} - 1\right)a_2\right)\delta_0^2 U_0^2$$

$$k_4 = (a_1 - a_2)\delta_0 Q_0^2$$

$$k_5 = -(1 - A)(a_1 + a_2 - a_3)\,\delta_0^2 U_0 Q_0$$

$$k_6 = (1 - 2A)a_3 \delta_0^3 U_0^2$$

First consider $a_4 > 0$. From 3.2 and 3.3, keeping only the lowest order terms,

$$(2a_1 - a_2)\frac{\gamma}{A}\delta_0 Q_0^2 = 0$$

$$X^{a_2-1}\delta_0(a_1 - a_2) = -c_t$$

with the resulting conditions

$$a_1 = \frac{1}{2}$$

$$a_2 = 1 \qquad (3.4)$$

$$\delta_0 = 2c_t$$

Now consider $a_4 = 0$. 3.2 and 3.3 become

$$k_1 + k_2 + k_3 = 0$$

$$X^{a_2-1}(k_4 + k_5 + k_6) = -c_t Q_0^2\left(1 - \frac{U_0\delta_0}{Q_0}\right)^2$$

Again $a_2 = 1$, and a_1, a_3 and δ_0 are found to be functions of $\frac{\delta_0 U_0}{Q_0}$, such that

$$2a_1 - 1 > 0$$

(This is shown in Appendix II.)

Examining the jet momentum flux

$$M(X) = 2\rho\int_0^{\delta}(U + \tilde{u}f)^2\,dY$$

and using 2.13 to remove $\tilde{u}$, we have

$$\frac{M(X)}{2\rho} = U^2\delta + 2U(Q-\delta U) + \frac{\gamma}{A}\,\frac{(Q-\delta U)^2}{\delta} \qquad (3.5)$$

For $a_4 > 0$, we note that as $X \to 0$

$$\lim_{X\to 0}\ \frac{M(X)}{2\rho} = \frac{\gamma}{A}\,\frac{Q_0^2}{\delta_0}\,X^{2a_1-a_2}\,(1 + O(X^{a_4}))$$

$$\simeq \frac{\gamma}{A}\,\frac{Q_0^2}{2c_t}\ .$$

Setting this limit equal to $M_j/2\rho$, we solve for Q_0 to obtain

$$Q_0 = \left(\frac{2c_t A}{\rho\gamma}\,\frac{M_j}{2}\right)^{\frac{1}{2}}\ . \qquad (3.6)$$

This case corresponds to momentum source flow.

In the case $a_4 = 0$, equation 3.5 becomes

$$\lim_{X\to 0}\ \frac{M(X)}{2\rho} \simeq \frac{\gamma}{A}\,\frac{Q_0^2}{\delta_0}\,X^{2a_1-1}\,f_n\left(\frac{\delta_0 U_0}{Q_0}\right)$$

$$\simeq 0 \quad \text{for } 0 < \frac{\delta_0 U_0}{Q_0} < 1$$

since $2a_1 - 1 > 0$.

This flow is the self-similar flow studied by Harris and does not correspond to momentum source flow.

The behavior of the flow in our problem can be characterized by equations 3.1 within a certain finite radius of convergence for a given accuracy. The magnitude of this radius is determined numerically as described in Appendix VI. Adding further terms to the expansion requires the knowledge of the behavior of U near X = 0, which is initially unaccounted for. We choose X_0 the starting point

within this radius so that the initial conditions become

$$\left.\begin{aligned} Q(X_0) &= \left(\frac{2\,c_t A}{\rho\gamma}\,\frac{M_j}{2}\,X_0\right)^{\frac{1}{2}} \\ \delta(X_0) &= 2\,c_t X_0 \end{aligned}\right\} \qquad (3.7)$$

It is of interest to note for further reference that this one-term expansion is an exact solution for the case $U \equiv 0$, that is, the free jet case. Hence the constant c_t may be simply related to the free jet growth rate $\frac{d\delta}{dx}$. (Appendix V.)

III. 3 Physical Parameters

The homogeneity of the coefficients and forcing terms in equations 2.14, 2.15, 2.20, and 2.21 allows us to express the velocities and lengths in terms of non-dimensional quantities and the global parameters Q_T and h. Then we define

$$Q^* = \frac{2Q}{Q_T}$$

$$X^* = \frac{X}{h}$$

$$U^* = \frac{2h\,U}{Q_T}$$

$$\hat{\delta} = \frac{\delta}{h}$$

(The symbol ˆ is used to avoid confusing the dimensionless edge position with the commonly used displacement thickness δ^*). From 2.14 and 2.15, corresponding coefficients F_i^* and G_i^*, are derived in Appendix I. The full problem can now be stated as

$$F_1^* \frac{dQ^*}{dX^*} + F_2^* \frac{d\hat{\delta}}{dX^*} + F_3^* \frac{dU^*}{dX^*} = 0 \qquad (3.8)$$

$$G_1^* \frac{dQ^*}{dX^*} + G_2^* \frac{d\hat{\delta}}{dX^*} + G_3^* \frac{dU^*}{dX^*} = -c_t(Q^* - \hat{\delta} U^*)^2 \tag{3.9}$$

$$Q^*(X^*) = \mathcal{I}m \left\{ -\frac{1}{\pi} \int_{-\epsilon}^{0} I^*(\xi') \log(\xi' - \zeta_\delta) d\xi' \right\} \tag{3.10}$$

$$U^*(X^*) = Re \left\{ \frac{1}{\pi} \frac{d\zeta}{dz}\Big|_{z=z_\delta} \int_{-\epsilon}^{0} \frac{I^*(\xi')d\xi'}{\xi' - \zeta_\delta} \right\} \tag{3.11}$$

We also define the parameter

$$a = \frac{M_j}{\rho} \frac{2h}{Q_T^2} \tag{3.12}$$

The initial conditions then become

$$\left.\begin{aligned} Q^*(X_0^*) &= \left(\frac{2c_t A}{\gamma} a X_0^*\right)^{\frac{1}{2}} \\ \hat{\delta}(X_0^*) &= 2 c_t X_0^* \end{aligned}\right\} \tag{3.13}$$

and end conditions are, at $X^* = X_e^*$

$$\hat{\delta}\ (X_e^*) = 1$$

$$Q^*(X_e^*) = 1$$

The parameter a is strictly speaking a momentum coefficient, but in a more general sense is the characteristic parameter for jets in uniform channels, as it is exactly analogous to the parameters discussed by Curtet and Hill. As the problem is now stated there are two independent parameters, a and the primary nozzle parameter Λ_1. The conditions at X_e^* fix both X_e^* and U_e^*, the value of the edge velocity at the end of the free-mixing zone. However, the parameter Λ will then fix the length of the confined mixing region and hence

govern the pressure recovery. Thus for this analysis α is determined by the value of Λ for a given Λ_1, and provides the condition which closes the problem.

We can now solve the interaction problem as a parametric problem involving α and Λ_1. The only requirement is that Λ be large enough so that the shroud extends past the end of the free-mixing zone.

III. 4 Method of Solution

(a) Approximation of the Integral Equations

To make the problem tractable, we replace the integral equation with a series of known functions multiplied by unknown constant coefficients. We must now satisfy the equations 3.10 and 3.11 at only a finite number of points along the matching boundary.

The kernel $I(\xi')$ is approximated by a series of the type

$$I(\xi') = C_0 \mathcal{J}_0(\xi') + \sum_{i=1}^{N} C_i \mathcal{J}_i(\xi')$$

Then equations 3.10 and 3.11 can be replaced by

$$Q^*(X^*) = C_0 K_0(\zeta_\delta) + \sum_{i=1}^{N} C_i K_i(\zeta_\delta) \qquad (3.14)$$

$$U^*(X^*) = C_0 J_0(\zeta_\delta) + \sum_{i=1}^{N} C_i J_i(\zeta_\delta) \qquad (3.15)$$

where the functions K_i, J_i are known functions of $(x, \hat{\delta})$. For this analysis we base these functions on an assumed piece-wise linear distribution of $\Psi^*(x')$ of the form (see figure 11)

$$\Psi^*(x') = C_1 \left(\frac{x'+\Lambda_1}{x_1+\Lambda_1}\right) \text{ for } -\Lambda_1 \leq x' \leq x_1 \qquad (3.16)$$

and

$$\Psi^*(x') = C_{i-1} + \left(\frac{x'-x_{i-1}}{x_i-x_{i-1}}\right)(C_i-C_{i-1}) \tag{3.17}$$

for $x_{i-1} \leq x' \leq x_i$ and $i \geq 2$

where $x_i (i = 1, N)$ are the endpoints of the intervals. It was also found to be convenient to add a sink at the downstream infinity of the channel, and this is represented by the zeroth terms in 3.14 and 3.15.

We integrate equations 3.8 and 3.9 in the form

$$\frac{dQ^*}{dX^*} = \frac{NUM1(Q^*, \hat{\delta}, U^*, \frac{dU^*}{dX^*})}{DEN(Q^*, \hat{\delta}, U^*)} \tag{3.18}$$

$$\frac{d\hat{\delta}}{dX^*} = \frac{NUM2(Q^*, \hat{\delta}, U^*, \frac{dU^*}{dX^*})}{DEN(Q^*, \hat{\delta}, U^*)} \tag{3.19}$$

where the right-hand sides of these equations are evaluated in Appendix I. The functions U^* and dU^*/dX^* are known functions of X^* and $\hat{\delta}$ in the integration. A standard Runge-Kutta technique is used since the right-hand sides are regular in the range of integration. The difficulties arising at the initial point are discussed in Appendix VI.

(b) Iteration Procedure

The iteration procedure is carried out for fixed Λ_1 and α. Because of the fixed end conditions which the solutions must reach, it is possible to obtain a stable solution which does not satisfy the end conditions, if all C_i's are allowed to vary. The procedure fixes C_0 therefore and finds a stable solution for the N remaining C_i's. The end condition is checked and if the value of $Q^*(X_e^*) \neq 1$, a new

value of C_0 is chosen and the procedure is repeated. The initial C_i's are chosen to satisfy equation 3.14 at $\hat{\delta} = 1$,

$$C_0 + \sum_{i=1}^{N} C_i = 1 \tag{3.20}$$

since the functions K_i have the value 1 at this point (see Appendix IV).

Equation 3.15 is used to evaluate U* and dU*/dX*, and the inner equations are integrated to give Q* and $\hat{\delta}$. Their values at the N match points X_{m_i} are inserted in 3.14 to generate a set of N linear algebraic equations in C_i (i = 1, N). The solution to this set of equations is used to generate a new set of coefficients, and the inner equations are again integrated using 3.15 with the new C_i's. A stable condition is reached when successive iterations produce the same set of coefficients. A more detailed discussion of the method and the nature of the convergence can be found in Appendix VI.

IV. SOLUTIONS IN THE FREE-MIXING REGION

The numerical solutions for $\hat{\delta}$, Q* and U* were carried out as described for values of the momentum coefficient α ranging from 0.3 to 1.0, and nozzle positions Λ_1 from -2.0 (downstream of the lip) to 5.0 (upstream of the lip). The results for $\alpha = 0.5$ and $\alpha = 1.0$ are representative of these solutions and are shown in figures 12 to 17.

The mean boundary position $\hat{\delta}$ is plotted in figure 12 against a turbulent axial coordinate defined by

$$\overline{X} = \frac{9}{2}\frac{A}{\gamma} c_t x^*$$

with Λ_1 as a parameter. The corresponding values of Q* are shown in figure 13 and the plots of U*, generated by the potential solution, are shown in figure 14. We note in figure 14 that the edge velocity curves are somewhat irregular, reflecting the fact that the solutions are "matched" at only a finite number of points (5 in this study, for all cases). Various values of N, the number of matching points, were tried, and checked against the limiting analytic solution obtained from the simple theory (which is discussed in Section IV. 2), for the case when the nozzle is downstream of the region of influence of the shroud lip. This simple solution is shown in the figures to illustrate the agreement obtained for N = 5.

In figure 15, the boundary position $\hat{\delta}$ is plotted for $\alpha = 1.0$. The same qualitative behavior is observed as for $\alpha = 0.5$, with the mixing distance X* considerably reduced. The volume flux Q* is shown in figure 16 for $\alpha = 1.0$, and the edge velocity U* is plotted in figure 17 against $\overline{X}$. Again excellent agreement is obtained with

the simple solution for $\Lambda_1 = -2$, $N = 5$. The nature of the solution will be discussed in Section IV. 3.

IV. 1 Limiting Cases

The lip parameter Λ_1 has an upstream limit imposed by the expansion rate of the free jet. For $\Lambda_1 = \Lambda_{1_{max}}$, the free jet expanding from the nozzle would just meet the lip of the nozzle at $\hat{\delta} = 1$. This can be physically visualized by considering the "starting" problem of the jet. For $\Lambda_1 < \Lambda_{1_{max}}$, the free jet would spread to the shroud and be "trapped" by the pressure gradient induced by the lip, to be swept downstream to its stable position. For $\Lambda_1 > \Lambda_{1_{max}}$, the jet would not "see" the shroud and spread outside the lip. This phenomenon was indicated by the numerical procedure which became unstable in this regime. The value of $\Lambda_{1_{max}}$ is found from the free jet solution

$$\hat{\delta} = 2\, c_t\, X^*$$

where $X^* = \Lambda_{1_{max}}$ at $\hat{\delta} = 1$.

Thus

$$\Lambda_{1_{max}} = \frac{1}{2c_t} \tag{4.1}$$

The downstream limit is defined as the value of Λ_1 when the lip position ceases to have an effect on the jet spreading, and can be considered removed to upstream infinity. The analysis for this "channel flow" was done by Curtet using a much simpler potential flow model which reflects the localizing behavior of flows in channels.

This limit was found to occur within one or two channel heights from the lip, and will be defined for all values of α as

$$\Lambda_{1_{min}} = -2 \tag{4.2}$$

IV. 2 Simple Channel Solution

Following Curtet's method, the potential flow in the channel is assumed to be uniform, and this allows us to replace equations 3.14 and 3.15 by the much simpler continuity equation

$$Q^* + (1 - \hat{\delta})\, U^* = 1 \tag{4.3}$$

The solution to equations 3.8, 3.9 and 4.3 can be found in closed form and is presented in Appendix VII. The comparison with Curtet's results can be seen in figures 18 and 19. That this should be a good approximation for the potential flow is not surprising since classical solutions for potential flows in channels indicate that the actual distribution of singularities at any x-station has an effect on the flow only in the neighborhood of 1/2 channel heights upstream and downstream. The flow is "localized" in the sense that derivatives of $\hat{\delta}$, Q^* and U^* at any x-station are dependent only on their values at that station. Near the lip, this localization breaks down and the elliptic nature of the potential flow becomes important.

IV. 3 Discussion of Free-Mixing Solutions

The solutions presented in figures 12 to 17 were obtained by a five-point match (N = 5) in the numerical iteration process. The momentum coefficient values $\alpha = 0.5$ and $\alpha = 1.0$ were chosen as

representative of the range of α possible for a non-diffused pressure recovery. For values of $\alpha > 1$, the edge velocity becomes negative at the end of the free-mixing region and the applicability of potential flow for these regions of reverse flow is uncertain. Since this is an unfavorable condition for thrust augmentation in any case, as we will see in Section VI, we have considered $\alpha = 1$ to be the upper limit of interest. Values of $\alpha < 0.5$ were investigated numerically but not included in these results, and $\alpha = 0.5$ will be shown to be the maximum achievable with a uniform shroud.

The simple channel solutions are shown in comparison with the numerical results for the mixing boundary $\hat{\delta}$, the volume flux Q^* and the edge velocity U^*. It is noted that the numerical solutions $\hat{\delta}$ and Q^* for the channel flow are virtually indistinguishable from the simple theory, while the U^* curves (figures 14 and 17) reflect the matching process in that they are linear combinations of the assumed potential functions. Nevertheless their agreement with the channel solutions is good except near the point source, where they exhibit a singular behavior characteristic of the potential model used. The agreement of the numerical solutions supports our assumption that the mixing in this initial region has a weak dependence on the outer flow.

The presence of the singularity in the potential solution at the shroud lip becomes important for nozzle positions Λ_1 near $\Lambda_{1_{max}}$. The jet spreading (figures 12 and 15) is seen to be depressed by the favorable pressure gradient ahead of the lip, and swept into the shroud. At the same time, the volume flux (figures 13 and 16)

increases more rapidly than in the channel flow case, which suggests that the role of the transverse velocity at the jet boundary in the potential flow is significant. The increasing X-derivatives of the flow quantities for Λ_1 near $\Lambda_{1_{max}}$ also indicate that the assumptions for the formation of the boundary-layer equations are poor. Again however we will see that these values of Λ_1 produce poor thrust augmentations, and need not be emphasized.

V. THE CONFINED-MIXING REGION

V. 1 Introduction

In order to determine the thrust augmentation of the complete system, we must determine the manner in which the pressure in the confined flow rises to ambient pressure at the shroud exit plane. Some assumptions about the turbulent mixing are necessary to replace our lack of knowledge of the detailed behavior of the Reynolds stress terms in the equation of motion. In Hill's analysis for a co-axial geometry, the integral methods which we employed in the free-mixing region predicted quite well the pressure rise in the confined mixing, except in the immediate transition from free mixing. For his analysis an eddy viscosity model represents the effect of the turbulent mixing, and can be extended to this study.

The basis for the applicability of the integral methods is the assumption that we can approximate the y-dependence of the pressure term in 5. 1 through some experimental evidence or physical argument. Hill assumes that the pressure is constant across the channel for the axisymmetric case, and Ferguson[11] does the same in a much cruder analysis of the two-dimensional ejector. The success of the calculation in matching the experimental data, with the exception of the transition region which is of the order of one channel height in length, supports the extension of our methods into the confined-mixing region.

The nature of the turbulent flow in this region is expressed by the integrated momentum equation

$$\frac{d}{dX}\int_0^h (\bar{p} + \rho\bar{u}^2)dY = -C_f \frac{\rho U^2 h}{2} \qquad (5.1)$$

where the retarding effect of the viscous layers adjacent to the shroud is represented by the friction coefficient C_f. The experiments of Hill and Ferguson indicate that pressure and momentum flux terms are more significant than the friction term and hence that the loss in momentum flux due to mixing is almost entirely recovered by the pressure term in channels of moderate length. For this reason and in accord with our "frictionless" model, we will make the assumption that the right-hand side of 5.1 is zero.

V.2 Integral Equations

The pressure recovery in the confined-mixing region depends through 5.1 on the manner in which the momentum flux integral decays toward the uniform state. The possibility of a filling-out of the velocity profile due to the redistribution of momentum across the channel must be allowed. To this end Hill suggests a velocity profile of the form

$$\bar{u}(X, Y) = U(X) + \tilde{u}(X)\,(f(y) + \Xi(X)\, f_1(y)) \qquad (5.2)$$

where $y = Y/h$.

Here the addition to the old profile 2.7 takes the form of some suitable function $f_1(y)$ which has the value

$$f_1 = 0 \quad \text{at} \quad y = 0, 1$$

and $\Xi(X)$, which represents the magnitude of the distortion from the free jet profile.

The unknown functions to be determined are the pressure $\bar{p}$, the edge velocity U, the supervelocity $\tilde{u}$, and the form parameter Ξ. To calculate these Hill uses the integral continuity equation and three successive integral moments of the momentum equation. His results indicate that the choice of $f_1(y)$ is not a sensitive factor in the calculations since the changes in the velocity profiles for moderate length shrouds are not great. This result is substantiated by taking a closer look at the momentum equation.

V. 3 Similarity Solution

Making the same assumptions as in the free-mixing region about the relative importance of the terms in the momentum equation, we may write from the boundary-layer equation 2. 6

$$\bar{u}\frac{\partial\bar{u}}{\partial X} - \frac{\partial\bar{u}}{\partial Y}\int_0^Y \frac{\partial\bar{u}}{\partial X}\,dY = -\frac{1}{\rho}\frac{d\bar{p}}{dX} - \frac{\partial\overline{u'v'}}{\partial Y} \tag{5.3}$$

and from 2. 11 for the turbulent shearstress

$$\frac{\tau}{\rho} = -\overline{u'v'} = \kappa_t \tilde{u}^2(X)g(y) \tag{5.4}$$

It can be easily shown (Appendix VIII) that substituting the free-jet velocity profile in 5. 3 gives an equation of the form

$$\frac{d\tilde{u}^*}{dX^*}\left(\frac{\cos\pi y}{2}\right) + \frac{d}{dX^*}\left(p^* + \frac{\tilde{u}^{*2}}{8}\right) = \kappa_t \tilde{u}^{*2} g'(y) \tag{5.5}$$

where

$$p^* = \frac{(\bar{p} - p_\infty)}{\rho(Q_T/2h)^2}$$

and the other starred quantities have been defined in Section III. 3.

If the eddy viscosity is assumed constant across the channel,

then g(y) is related to f(y) by

$$g = \frac{df}{dy}$$

and 5. 5 can be rearranged as

$$\cos\pi y \left(\tfrac{1}{2} \frac{d\tilde{u}^*}{dX^*} + \kappa_t \frac{\pi^2}{2} \tilde{u}^{*2} \right) + \frac{d}{dX^*} \left(p^* + \frac{\tilde{u}^{*2}}{8} \right) = 0 \qquad (5.6)$$

Thus the momentum equation is exactly satisfied if

$$\frac{d}{dX^*} \left(p^* + \frac{\tilde{u}^{*2}}{8} \right) = 0 \qquad (5.7)$$

and

$$\frac{d\tilde{u}^*}{dX^*} + \kappa_t \pi^2 \tilde{u}^{*2} = 0 \qquad (5.8)$$

Since the conditions at the start of the confined-mixing region must be matched to the values at the end of the free-mixing region where the velocity profile is represented by the cosine distribution, the initial value of $\Xi(X)$ is zero. Thus the momentum equation 5. 3 evaluated at the station $X^* = X^*_e$ and using the velocity profile 5. 2 would have the terms in equation 5. 6 plus the derivative of the second parameter $\Xi(X)$ in the form

$$\cos\pi y \left(\tfrac{1}{2} \frac{d\tilde{u}^*}{dX^*} + \kappa_t \frac{\pi^2}{2} \tilde{u}^{*2} \right) + \frac{d}{dX^*} \left(p^* + \frac{\tilde{u}^{*2}}{8} \right)$$

$$+ \frac{d}{dX^*} (\tilde{u}^* \Xi) \mathcal{J}_n (X^*_e, y) = 0 \qquad (5.9)$$

Applying the arguments used above, the first two terms result in equations 5. 7 and 5. 8, and either the coefficient $\mathcal{J}_n$ or $\frac{d}{dX^*} (\tilde{u}^* \Xi)$ must be zero to satisfy the equation exactly. Since $\mathcal{J}_n$ includes the

initial conditions and the function $f_1(y)$, it will not be zero in general and hence $\frac{d}{dX^*}(\tilde{u}^* \Xi) = 0$.

In other words Ξ and $\frac{d\Xi}{dX^*}$ are zero at $X^* = X_e^*$ and in a numerical integration Ξ will then be zero at the next step in the integration. Equation 5. 9 then holds throughout the confined mixing region and Ξ is identically zero. This result supports Hill's assertion that the additional parameter is a correction to the first order solution.

Other phenomenological laws may represent the turbulent shear stress as well as the eddy viscosity model, in which case non-zero values of $\Xi(X)$ would be generated. They must however have a small effect on the profile for these conditions where friction is neglected, and hence the simple solution represented by 5. 7 and 5. 8 can be significantly improved only by a more detailed model of the turbulent mixing. We will use this solution to obtain the parametrical dependence of the momentum coefficient α, and the thrust augmentation φ_T, on Λ and Λ_1.

V. 4 Pressure Recovery

The initial conditions for the first order equations 5. 7 and 5. 8 are found from the solution in the free-mixing region evaluated at $X^* = X_e^*$. That is

$$U^* = U_e^*$$

and from the integrated continuity equation

$$Q_e^* = U_e^* + A\tilde{u}_e^* = 1 \tag{5.10}$$

Also the pressure is given by

$$p_e^* = -\frac{U_e^{*2}}{2} \tag{5.11}$$

Integrating 5.7 and 5.8 and applying 5.10 and 5.11 the solutions have the form

$$\tilde{u}^* = 2(1-U_e^*)/(1+2\pi^2\kappa_t(1-U_e^*)(X^*-X_e^*)) \tag{5.12}$$

$$p^* = \tfrac{1}{2}-U_e^* - \tfrac{1}{2}((1-U_e^*)/(1+2\pi^2\kappa_t(1-U_e^*)(X^*-X_e^*)))^2 \tag{5.13}$$

$$U^* = U_e^*+2\pi^2\kappa_t(1-U_e^*)^2(X-X_e^*)/(1+2\pi^2\kappa_t(1-U_e^*)(X-X_e^*)) \tag{5.14}$$

Equations 5.13 and 5.14 are shown in figures 20 and 21 respectively.

VI. EVALUATION OF THRUST AUGMENTATION

VI. 1 Length of the Confined Mixing Region

We will now formulate the parametric representation of the ejector characteristics. The analysis of the free-mixing region provided the quantities X_e^* and U_e^*, the length of the free-mixing region and the edge velocity at the end of the free-mixing region as functions of Λ_1 and the momentum coefficient α. These are shown in figures 22 to 25. In order to relate these quantities to the shroud length, Λ, we must calculate the length of the confined-mixing region, $X_f - X_e$ (figure 7).

Since the pressure must reach ambient at the end of the shroud, and the flow as modelled by equations 5. 12 to 5. 14 is a purely local flow, exhibiting no downstream dependence, we can estimate the length of the confined region by setting

$$p^* \Big|_{X^*=X_f^*} = 0 \tag{6.1}$$

From 5. 13 then

$$X_f^* - X_e^* = \frac{1}{2\pi^2 \kappa_t} \left(\frac{1}{\sqrt{1-2U_e^*}} - \frac{1}{1-U_e^*} \right) \tag{6.2}$$

which is shown in figure 26 for $\kappa_t = .021$ (κ_t is assumed to be derivable from free-jet data--see Appendix V).

The total shroud length Λ can now be calculated as

$$\Lambda = (X_e^* - \Lambda_1) + (X_f^* - X_e^*) \tag{6.3}$$

VI. 2 Thrust Augmentation

For our frictionless model, we may evaluate the integral momentum equation 1. 2 at any axial position providing the pressure term is accounted for. At the free-confined-mixing boundary, $X^* = X_e^*$, this relationship is given by 5. 11. The velocity profile is the free jet profile 2. 7 and the supervelocity $\tilde{u}_e^*$ is related to U_e^* by 5.10. The total momentum flux is then given by

$$M_T = 2\rho h\left(\frac{Q_T}{2h}\right)^2 \left(2U_e^* - \frac{3}{2} U_e^{*2} + \frac{\gamma}{A} (1-U_e^*)^2\right) \qquad (6.4)$$

Using the definition of the momentum coefficient α (3. 12) and the thrust augmentation φ_T (1. 3), we may express φ_T as

$$\varphi_T = \frac{1}{\alpha}\left(\frac{\gamma}{A} + 2(1-\frac{\gamma}{A})U_e^* - (\frac{\gamma}{A} - \frac{3}{2}) U_e^{*2}\right) \qquad (6.5)$$

which for the cosine profile reduces to

$$\varphi_T = \frac{1}{\alpha} (1.5 - U_e^*) \qquad (6.6)$$

VI. 3 Parametric Analysis

We now have enough information to derive the thrust augmentation. We will consider the implicit functional relationships established and invert in terms of the independent parameters Λ and Λ_1.

From equation 6. 2 and the parametric solution for $X_e^* - \Lambda_1$, we can write equation 6. 3 in functional form as

$$\Lambda = \Lambda(\Lambda_1, \alpha, U_e^*) \qquad (6.7)$$

From figure 18 we write

$$U_e^* = U_e^*(\Lambda_1, \alpha) \qquad (6.8)$$

Using 6. 8 in 6. 7 and solving the functional relationship for α, we obtain

$$\alpha = \alpha(\Lambda, \Lambda_1) \tag{6.9}$$

Substituting back in 6. 8 we have

$$U_e^* = U_e^*(\Lambda, \Lambda_1) \tag{6.10}$$

Now we can use equation 6. 6 to write the thrust augmentation as

$$\varphi_T = \varphi_T(\Lambda, \Lambda_1) \tag{6.11}$$

The parametric dependence represented by equation 6. 11 is displayed in figures 27 and 28. It is evident that there is an optimum thrust coefficient for each value of the shroud length Λ. This optimum and the corresponding nozzle position Λ_1 which produces it are plotted in figures 29 and 30 respectively.

For $\Lambda_1 < -2$, the functional dependence on Λ_1 expressed in equation 6. 8 disappears. Equation 6. 3 can be rewritten as

$$\Lambda_M = \Lambda + \Lambda_1 = X_e^* + (X_f^* - X_e^*) \tag{6.12}$$

which can be inverted to give

$$\alpha = \alpha(\Lambda_M) \tag{6.13}$$

Since U_e^* is now only a function of α, we can write in this limiting case, from 6. 11

$$\varphi_T = \varphi_T(\Lambda_M) \tag{6.14}$$

This curve is plotted in figure 31. For the limit of very long mixing chamber lengths, the edge velocity at transition, U_e^*, approaches the limit $U_e^* = 0.5$. From the channel solution of the free-mixing region, a is related to U_e^* by

$$a = 1 - U_e^* \tag{6.15}$$

and hence approaches $a = 0.5$.

The limiting value of X_e^* is obtained from the simple channel solution as $X_e^* = 8.14$.

From equation 6.2, as $X_f^* - X_e^*$ becomes large, the limiting behavior of U_e^* is obtained and with equation 6.15 inserted into the thrust augmentation equation, 6.6, we get the asymptotic dependence of φ_T as

$$\varphi_T = 1 + \frac{1}{1 + \frac{6.25}{(\Lambda_M - 3.1)^2}} \tag{6.16}$$

as $\Lambda_M >> 1$.

We note that as $\Lambda_M \to \infty$, the thrust coefficient for this channel flow condition approaches the value $\varphi_{T_\infty} = 2$. Since the lip is now effectively at upstream infinity, it has no effect on the flow. In addition, the number and transverse positions of the primary jets have no effect on the asymptotic value, so long as they can be considered as point momentum sources. We will discuss the significance of φ_{T_∞} in the next section and correlate the von Kármán results with those presented here.

VII. GENERAL DISCUSSION

VII.1 Frictionless Model Characteristics

The idealized model as constituted in this study has a number of important properties. The presence of an optimum primary nozzle position emphasizes the interaction of the free-mixing process and the confined-mixing process in a shroud of given length. The asymptotic performance of the frictionless model gives rise to a characteristic number, $\varphi_{T_\infty} = 2$, which has been previously recognized as an ejector "magic number," but has not been fully understood as to its significance.

The existence of an optimum nozzle position indicates the tradeoff in the lengths of the free-mixing and confined-mixing regions. The length of the free-mixing region is relatively insensitive to nozzle position, although the edge velocity at the free-confined boundary, U_e^*, rises as the nozzle is moved forward. The length of the confined-mixing region however has a strong sensitivity to U_e^* for high U_e^*, and is insensitive at low U_e^* (figure 26). The mixing in this region is an increasing function of the length of the region, while the free-mixing becomes less effective as the lip is moved forward. These two processes produce a total mixing which has an optimum at some particular nozzle position.

For larger Λ, the optimum nozzle position moves downstream out of the region of influence of the lip. That is, the confined-mixing process determines the characteristics of the system. In particular the limiting value φ_{T_∞} is the thrust augmentation of a shroud which effectively extends upstream and downstream to infinity. This allows

complete mixing to occur, in that the exit velocity profile is uniform, and in addition the flow at the lip is that due to a sink at downstream infinity. Thus the thrust produced by the pressure on the lip is independent of the shape of the lip, and, for the zero thickness lip, is analogous to the lip thrust of a flat plate aerofoil. An "infinite" shroud in principle doubles the thrust of a primary system of any configuration provided that the primary cross-section is small compared to the shroud cross-section.

VII. 2 Effects of Wall Friction

The performance of the real ejector simulated by our frictionless model will of course be reduced by the drag of the wall viscous shear stress. This friction effect manifests itself in the wall boundary layers which extend from the lip through the free and confined-mixing regions, and through this mechanism the system size and velocity magnitudes directly influence performance. A Reynolds number thus becomes an additional independent variable in the problem. In addition, the high pressure gradients around the lip make the lip design an important factor, in maintaining an attached flow and depressing the initial boundary-layer growth. For certain ranges of the parameter, α, where the edge velocity U(X) becomes small in the free-mixing region, the boundary layer can grow rapidly and produce regions of non-potential flow outside the turbulent mixing. Curtet found that increases in α for his experimental geometry eventually produce regions of reverse flow leading to dynamic instabilities where the jet oscillates between the channel walls. These values of α are higher than the region of interest in this analysis, but would be

important for ejectors with non-constant height mixing regions. No attempt has been made in this study to assess the reductions in performance due to these effects.

In the confined-mixing region, friction has two important effects. First, it produces the possibility of a pressure maximum occurring in the shroud axial direction, and effectively reduces the optimum length of the shroud from infinity to some finite value. Again this is a Reynolds number effect which for reasonable initial skin friction coefficients seems to be small. Hill and Ferguson both show experimental results which differ little from the frictionless solution for lengths on the order of 20-30 shroud heights, where the pressure maxima occur. For lengths beyond these maxima the flow becomes primarily pipe flow, with the internal mixing effect reducing in importance. Hence our study is not extended beyond moderate shroud lengths. Even then, the numerical estimate of confined-mixing region lengths is extremely sensitive to even small friction effects, while the attainable thrust augmentations are less sensitive. The curves produced in this study must in this light be considered as illuminating the principles involved and the qualitative dependence of the physical quantities on geometry rather than as pure engineering data. For any given diffusion system (pressure recovery) a much more detailed analysis is required.

VII. 3 The Real Ejector

Many of the simplifying assumptions made in this study were necessary because the real fluid mechanics cannot be modeled in more accurate ways. The model for the effects of velocity

fluctuations is one such case. Two basic simplifications were introduced here which are certainly not universally accurate, and probably are misleading in certain areas. Nevertheless, without a much more detailed and comprehensive experimental investigation than has yet been attempted, they are the best models that can reasonably be used.

The modeling of the transverse behavior of the $\overline{u'v'}$ Reynolds term by a universal function of the transverse position in the shear layer has been questioned in shear flows where a pressure gradient exists in the flow direction. Most extensive work has been done in boundary layers, however, and the applicability of boundary-layer techniques is not obvious, since the wall effect on the boundary layer is not present in this case. The extension of this universal function through the free/confined mixing transition and into the pressure recovery region is also a matter which needs much experimental work, and can only be supported at this stage by the results of a few experiments, which have been cited previously.

The proportionality of the turbulent shear term to the super-velocity $\tilde{u}$ and the shear layer width or channel height in the two mixing regions is also inadequately supported by experimental work, especially in the regions of strong pressure gradients. The effect is manifested in the "universality" of the turbulent coefficient c_t, which might be more accurately modeled as a function of X* or a function of the mean flow quantities. Certainly however the agreement within 30% of the c_t derived from Curtet's experiments on shrouded water jets, with that derived from free air jet data suggests that the

non-universality might be quite small.

Other areas where the model is probably over-simplified are the immediate vicinity of the shroud lip, which has been discussed in Section IV. 3, and the transition region between free and confined mixing. The discontinuity in pressure gradient between the two regions as exhibited by this model is smoothed out into an area a few channel heights in length, at the end of which the confined mixing calculations are quite accurate. The correlation of the dynamic quantities seems to be quite good in the experiments cited, so that the error again primarily affects the length estimates of the confined-mixing region. This is not a surprising result as the flow is quite complicated in this region, and is quite sensitive to viscous effects in the boundary layer there. Any improvement in the calculations for transition and confined mixing will necessarily take all these effects into account.

Another complication in most ejector systems is the finite height of the primary nozzle, and the effect of the jet potential core in the mixing analysis. This core region can be analyzed in the same manner as the self-similar region, with good qualitative results as shown by Curtet. His model includes the finite primary height, and in this case the α parameter assumes a slightly different meaning and is more easily related to the primary/secondary mass flux ratio. Since this feature does not include any fundamental differences from, but considerably complicates, our analytical procedure, we have considered it an unessential addition to the problem.

VII. 4 Extensions of the Model

The analysis of the free-mixing region, which was the major problem in this study, has enough flexibility that it can be used to treat a much wider range of jet ejectors. The primary restriction is that of incompressible irrotational outer flow. The case of a compressible or even supersonic primary could in principle be investigated with this analysis if the compressible turbulent mixing could be adequately modeled. The numerical technique would require few changes. On the other hand, the analysis for changes in shroud geometry, lip shape and groups or off-axis positions of primary nozzles needs only minor changes in the equations describing the physics, but probably significant redesign of the potential flow solution in the complex plane. Similarly, analysis of diffusing sections at the end of the shroud requires special treatment of the confined mixing regions but could be handled in the same manner as uniform height shrouds.

The extension of the study to three-dimensional, axisymmetric configurations could conveniently be handled, if a suitable numerical scheme could be devised to solve the potential flow of the entrained fluid. This extension from a practical point of view is essential since the ejector principle is most applicable to co-axial systems.

VII. 5 Conclusions

This study provides a closed solution to the jet ejector problem for a simple model of a jet in a shroud of uniform height and finite length. The thrust augmentations achieved with the axial geometry

of the primary are less than the theoretical limit thrust augmentation φ_{T_∞}, and friction effects further reduce the performance of the shroud. We note that for the frictionless model in all cases the shroud should be as long as possible, but that friction effects will limit this optimum length. For fixed shroud length on the other hand, an optimum primary nozzle position is defined, and for moderate shroud lengths the effect of friction drag is probably small, if the lip is correctly designed to minimize the initial growth of the shear layer.

The ejector analysis presented here represents the maximum performance which could be achieved if all the effects of friction could be overcome. The fact that the asymptotic value of $\varphi_T = 2.0$ is the maximum obtainable suggests that the center-line ejector is best operated with the lip effect removed. However, if the design requirements limit the ejector shroud length, we have shown that an optimum nozzle position exists, and that the lip area of the shroud plays an important role in the mixing process. The analysis of von Kármán has been shown to correctly estimate the effect of non-uniform velocity profiles at the exit of the ejector, but to be misleading in the assumption that highly nonuniform, unidirectional potential flows can be generated at the entrance section.

The addition of diffusers, and changes in shroud geometry and nozzle position are amenable to the techniques developed here and seem attractive, in particular the case for the primary jet on the shroud wall.

In conclusion, this study has put the mechanisms involved into perspective, and provided some important guidelines for the design of straight center-line ejectors, as well as provided the necessary first step in understanding the principles of jet ejectors.

REFERENCES

1. von Kármán, T.: "Theoretical Remarks on Thrust Augmentation," Reissner Anniversary Volume, J. W. Edwards, 1949, pp. 461-468.

2. Curtet, R.: "Sur l'Écoulement d'un Jet Entre Parois," Publications Scientifiques et Techniques de l'Air, 359, March 1960.

3. Hill, P. G.: "Turbulent Jets in Ducted Streams," JFM 22, Part 1, May 1965, pp. 161-186.

4. Goldstein, S.: Modern Developments in Fluid Mechanics, Vol. II, Dover Publications, New York 1965, p. 592.

5. Taylor, G. I.: "Flow Induced by Jets," JAS 25, 1958. pp. 464-465.

6. Lippisch, A. M.: "Flow Visualization," Aero. Eng. Review, February 1958, pp. 28-29.

7. Schlichting, H.: Boundary Layer Theory, 4th Ed., McGraw-Hill, 1960, p. 605.

8. Reichardt, H.: "Laws of Free Turbulence," VDI-Forschungshaft 414, 1942.

9. Weinstein, A. S., Osterle, J. F., Forstall, N.: "Momentum Diffusion from a Slotted Jet into a Moving Secondary," Trans. ASME 23, 1956, pp. 437-443.

10. Lissaman, P. B. S., Harris, G. L.: "The Mechanics of Ejector Thrust Augmentation," GALCIT Ae TR 67-1, May 1967.

11. Ferguson, C. V.: "Mixing of Parallel Flowing Streams in a Pressure Gradient," Proc. Ht. Trans. and Fl. Mech. Inst., May 1949, pp. 77-88.

REFERENCES (Cont'd)

12. Newman, B. G.: "Turbulent Wakes and Jets," Symposium on the Fluid Mechanics of Internal Flows--Warren, Mich., 1965, Elsevier Publishing Co., New York, 1967.

LIST OF APPENDICES

APPENDIX I

COEFFICIENTS OF THE FREE-MIXING TURBULENT EQUATIONS

The coefficients in equations 2.14 and 2.15 are

$$F_1 = \delta\left(2\frac{\gamma}{A}Q - (2\frac{\gamma}{A} - 1)\,\delta U\right)$$

$$F_2 = -\left(\frac{\gamma}{A}Q^2 - (\frac{\gamma}{A} - 1)\,\delta^2 U^2\right)$$

$$F_3 = -\delta^2\left(2(\frac{\gamma}{A} - 1)\,Q - (2\frac{\gamma}{A} - 3)\,\delta U\right)$$

$$G_1 = \delta(Q-(1-A)\delta U)$$

$$G_2 = -Q(Q-(1-A)\delta U)$$

$$G_3 = -\delta^2\left((1-A)Q-(1-2A)\delta U\right)$$

The corresponding coefficients F_i^* and G_i^* in equations 3.8 and 3.9 are defined by

$$F_i^*(Q^*, U^*, \hat{\delta}) = k_{p_i}(Q_T, h)F_i(Q, U, \delta)$$

where the k_{p_i}, the dimensional factors, are

$$k_{p_1} = \frac{2}{Q_T h}$$

$$k_{p_2} = \frac{4}{Q_T^2}$$

$$k_{p_3} = \frac{2}{Q_T h^2}$$

and the G_i^* are similarly given as

$$G_i^*(Q^*, U^*, \hat{\delta}) = k_{p_i}(Q_T, h)G_i(Q, U, \delta)$$

The solution of equations 3.8 and 3.9 with U*, dU*/dx* as forcing functions is found by inverting the matrix equation

$$\begin{bmatrix} F_1^* & F_2^* \\ G_1^* & G_2^* \end{bmatrix} \begin{Bmatrix} \frac{dQ^*}{dX^*} \\ \frac{d\hat{\delta}}{dX^*} \end{Bmatrix} = \begin{Bmatrix} -F_3^* \frac{dU^*}{dX^*} \\ -c_t(Q^* - \hat{\delta} U^*)^2 - G_3^* \frac{dU^*}{dX^*} \end{Bmatrix}$$

Then in 3.18 and 3.19

$$NUM1 = c_t F_2^* (Q^* - \hat{\delta} U^*)^2 + \frac{dU^*}{dX^*} (F_2^* G_3^* - F_3^* G_2^*)$$

$$NUM2 = -c_t F_1^* (Q^* - \hat{\delta} U^*)^2 - \frac{dU^*}{dX^*} (F_1^* G_3^* - F_3^* G_1^*)$$

$$DEN = F_1^* G_2^* - F_2^* G_1^*$$

Examining DEN, we find the roots

$$DEN = -\frac{\gamma}{A} \hat{\delta} Q^{*3} (1 - \frac{\hat{\delta} U^*}{Q^*}) (1 - t_1 \frac{\hat{\delta} U^*}{Q^*}) (1 - t_2 \frac{\hat{\delta} U^*}{Q^*})$$

where

$$t_1 = 1 - \frac{A}{\gamma} < 1$$

$$t_2 = 1 - A < 1$$

The denominator has no zeroes in the range of integration since

$$\frac{\hat{\delta} U^*}{Q^*} = 1 - A \frac{\hat{\delta} \tilde{u}^*}{Q^*} < 1$$

for jet-like flows.

APPENDIX II

BEHAVIOR OF INITIAL CONDITIONS FOR SELF-SIMILAR FLOWS

For the case

$$a_2 + a_3 - a_1 = 0 \tag{A2. 1}$$

equation 3. 2 becomes

$$k_1 + k_2 + k_3 = 0 \tag{A2. 2}$$

where

$$k_1 = (2a_1 - a_2)\,\frac{\gamma}{A}\,\delta_0 Q_0^2$$

$$k_2 = -\left((2\,\frac{\gamma}{A} - 1)a_1 + 2(\frac{\gamma}{A} - 1)a_3\right)\delta_0^2 U_0 Q_0$$

$$k_3 = \left((\frac{2\gamma}{A} - 3)a_3 + (\frac{\gamma}{A} - 1)a_2\right)\delta_0^2 U_0^2$$

With $a_2 = 1$ and $\frac{\delta_0 U_0}{Q_0} = \beta$, using A2. 1 to eliminate a_3, leads to the solution for a_1

$$a_1 = \tfrac{1}{2}(1 + \frac{A}{2\gamma}\,\frac{\beta}{(1 - t_3\beta)}) \tag{A2. 3}$$

when $t_3 = 1 - \frac{3}{2}\,\frac{A}{\gamma} < 1$.

Since $0 < \beta < 1$ from Section III. 2 we can conclude that

$$2a_1 - 1 > 0$$

APPENDIX III

THE COMPLEX TRANSFORMATION

The real and auxiliary planes are shown in figure 9. The conformal transformation which maps

$$z = x + iy \quad \text{into} \quad \zeta = \xi + i\eta$$

is

$$\tilde{g}(\zeta) = \frac{dz}{d\zeta} = \frac{1}{\pi}\left(\frac{\zeta - 1}{\zeta}\right) \tag{A3.1}$$

The mapping points are defined as

$z = i$ $\qquad$ $\zeta = 1$

$y > 1$

$|x| \to \infty$ $\qquad$ $|\zeta| \to \infty$

$y < 1$

$|x| \to \infty$ $\qquad$ $|\zeta| \to 0$

Then

$$\tilde{f}(\zeta) = z = \frac{1}{\pi}(\zeta - \log \zeta) + i - \frac{1}{\pi} \tag{A3.2}$$

The nozzle position $x = -\Lambda_1$ maps into the point

$$\zeta = -\epsilon \qquad (\epsilon > 0)$$

so that

$$\Lambda_1 = \frac{1}{\pi}(\epsilon + \log \epsilon + 1) \tag{A3.3}$$

The inverse transform

$$\zeta = \zeta(z)$$

is accomplished with the use of Newton's Method, when the n^{th} iteration gives

$$\zeta_n = \zeta_{n-1} + \frac{Z-\tilde{f}(\zeta_{n-1})}{\tilde{g}(\zeta_{n-1})}$$

and Z is the point $z = Z$ at which ζ is required.

The number of iterations n is determined by requiring the error

$$\left| \frac{Z - \tilde{f}(\zeta_{n-1})}{\zeta_{n-1}\,\tilde{g}(\zeta_{n-1})} \right| < \Delta$$

for a fixed upper bound Δ.

The method is quite rapid for a reasonable choice of the initial point ζ. (In general $n < 6$ for $\Delta = 10^{-5}$ for any Z in the range of interest.)

A check is provided to keep the value to which the process converges on the correct branch of ζ.

APPENDIX IV

EVALUATION OF THE CHARACTERISTIC FUNCTIONS OF THE POTENTIAL FLOW

The line in the physical plane $-\Lambda_1 < x' < \infty$ is divided into N sections by the N stations

$$-\Lambda_1 < x_1 < \ldots < x_N$$

over which $\Psi(x')$ is approximated by 3.16 and 3.17.

Then

$$I(\xi') = \frac{d\Psi}{dx'} \frac{dx'}{d\xi'}$$

$$= \tilde{g}(\xi') \sum_{i=1}^{N} \left(\frac{H(x'-x_{i-1}) - H(x'-x_i)}{x_i - x_{i-1}} \right) C_i \qquad \text{(A4.1)}$$

where $H(t) = 0$ for $t < 0$

$= 1$ for $t > 0$

and $\tilde{g}(\xi')$ is the transformation function defined by A3.1. The matching points map into the corresponding points

$$-\epsilon < \xi_1 < \ldots < \xi_N < 0 \qquad \text{in the auxiliary plane.}$$

Hence the fundamental solution 2.17 becomes

$$F(\zeta) = C_0 \mathcal{K}_0(\zeta) + \sum_{i=1}^{N} C_i \mathcal{K}_i(\zeta) \qquad \text{(A4.2)}$$

where

$$\mathcal{K}_0(\zeta) = -\frac{1}{\pi} \log(-\zeta)$$

$$1 \leq i \leq N \qquad \mathcal{K}_i(\zeta) = -\frac{1}{\pi(x_i - x_{i-1})} \int_{\xi_{i-1}}^{\xi_1} \log(\xi' - \zeta) \tilde{g}(\xi') d\xi' \qquad \text{(A4.3)}$$

The zeroth term represents the sink at downstream infinity.

The complex velocity is obtained from

$$w(z) = \frac{1}{\tilde{g}(\zeta)} \frac{dF}{d\zeta}$$

or
$$w(z) = C_0 \mathcal{J}_0(\zeta) + \sum_{i=1}^{N} C_i \mathcal{J}_i(\zeta) \qquad \text{(A4. 4)}$$

where

$$\mathcal{J}_0(\zeta) = - \frac{1}{\pi \zeta \tilde{g}(\zeta)}$$

$$1 \leq i \leq N \qquad \mathcal{J}_i(\zeta) = - \frac{1}{\pi(x_i - x_{i-1})\tilde{g}(\zeta)} \int_{\xi_{i-1}}^{\xi_i} \frac{\tilde{g}(\xi')d\xi'}{(\xi' - \zeta)} \qquad \text{(A4. 5)}$$

In A4. 5, the integrals may be evaluated using A3. 1 to give

$$\mathcal{J}_0(\zeta) = - \frac{1}{\zeta - 1}$$

$$\mathcal{J}_i(\zeta) = \frac{1}{\pi(x_i - x_{i-1})} \left(\log\left(\frac{\xi_i - \zeta}{\xi_{i-1} - \zeta}\right) + \frac{1}{\zeta - 1} \log\left(\frac{\xi_i}{\xi_{i-1}}\right) \right) \qquad \text{(A4. 6)}$$

$1 \leq i \leq N$

The integrals in A4. 4 cannot be directly integrated, however, and must be approximated. This is most easily done by considering that

$$\mathcal{K}_i(\zeta) = \int \tilde{g}(\zeta) \mathcal{J}_i(\zeta) d\zeta + C \qquad \text{(A4. 7)}$$

If we look at A4. 7 for the three cases

(a) $|\zeta| > |\xi_{i-1}|$

(b) $|\xi_{i-1}| > |\zeta| > |\xi_i|$

(c) $|\xi_i| > |\zeta|$

and expand in terms of $|\frac{\zeta}{\xi_i}|^{m_1}$, $|\frac{\zeta}{\xi_{i-1}}|^{m_2}$

where m_1 and m_2 are positive or negative integers, we obtain the form

$$\mathcal{K}_i(\zeta) = -\frac{1}{\pi^2(x_i-x_{i-1})}\left(\mathcal{I}_{1i}(\zeta)+\mathcal{I}_{2i}(\zeta)\right) \tag{A4.8}$$

where

$$\mathcal{I}_{1i}(\zeta) = (\xi_i-\zeta)\log(\xi_i-\zeta)-(\xi_{i-1}-\zeta)\log(\xi_{i-1}-\zeta)-\log(\frac{-\xi_i}{-\xi_{i-1}})\log\zeta \tag{A4.9}$$

and

$\mathcal{I}_{2i}(\zeta)$ is expanded for each case.

(a) $$\mathcal{I}_{2i} = -\sum_{n=1}^{\infty}\frac{1}{n^2}\left(1-(\frac{\xi_i}{\xi_{i-1}})^n\right)(\frac{\xi_{i-1}}{\zeta})^n + C \tag{A4.10}$$

(b) $$\mathcal{I}_{2i} = \frac{(\log\zeta)^2}{2} - \log(-\xi_{i-1})\log\zeta + \sum_{n=1}^{\infty}\frac{1}{n^2}\left((\frac{\xi_i}{\zeta})^n+(\frac{\zeta}{\xi_{i-1}})^n\right) \tag{A4.11}$$

(c) $$\mathcal{I}_{2i} = \log(\frac{-\xi_i}{-\xi_{i-1}})\log\zeta - \sum_{n=1}^{\infty}\frac{1}{n^2}\left(1-(\frac{\xi_i}{\xi_{i-1}})^n\right)(\frac{\zeta}{\xi_i})^n + C \tag{A4.12}$$

The constant C is determined by matching the three expansions at their common points, and setting $\mathcal{K}_i(-\epsilon) = 0$.

This gives

$$C = i\pi\log(\frac{-\xi_i}{-\xi_{i-1}}) \tag{A4.13}$$

The functions required in 3.14 and 3.15 are then

$$\left.\begin{aligned} K_i(\zeta_\delta) &= \mathcal{I}m\left\{\mathcal{K}_i(\zeta_\delta)\right\} \\ J_i(\zeta_\delta) &= Re\left\{\mathcal{J}_i(\zeta_\delta)\right\} \end{aligned}\right\} \quad 0 \leq i \leq N \tag{A4.14}$$

As $\hat{\delta} = 1$, from Appendix III we see that ζ is real and positive, $\zeta = \overline{\xi}$. Evaluating A4.8 at $\zeta = \overline{\xi}$ and taking the imaginary part we have

$$K_i(\overline{\xi}) = \frac{1}{\pi(x_i - x_{i-1})}\left(\xi_i - \xi_{i-1} - \log\left(\frac{-\xi_i}{-\xi_{i-1}}\right)\right) \tag{A4.15}$$

but from A3.2, this is

$$K_i(\xi) = \frac{\tilde{f}(\xi_i) - \tilde{f}(\xi_{i-1})}{x_i - x_{i-1}} = 1 \tag{A4.16}$$

Evaluation of dU/dx

The velocity derivative on the free boundary depends upon the local tangent at the boundary $d\delta/dx$. We can express it as

$$\frac{dU}{dX} = Re\left\{\frac{dw}{dz}\frac{dz_\delta}{dX}\right\} \tag{A4.17}$$

The derivative of the complex velocity can be expressed as

$$\frac{dw}{dz} = \frac{1}{\tilde{g}(\zeta)}\left(C_0\mathcal{J}_0'(\xi) + \sum_{i=1}^{N} C_i\mathcal{J}_i'(\xi)\right) \tag{A4.18}$$

and $\frac{dz_\delta}{dX}$ is written as

$$\frac{dz_\delta}{dX} = 1 + i\frac{d\delta}{dX}$$

Equation A4.17 is now composed of two parts

$$\frac{dU}{dX} = \sum_{i=0}^{N} C_i Re\left\{\frac{\mathcal{J}_i'}{\tilde{g}}\right\} - \frac{d\delta}{dX}\sum_{i=0}^{N} C_i\,\mathcal{I}m\left\{\frac{\mathcal{J}_i'}{\tilde{g}}\right\} \tag{A4.19}$$

Since the real and imaginary parts of the complex functions $\frac{\mathcal{J}_i'}{\tilde{g}}$ are of the same order of magnitude throughout the range, and we have assumed $\frac{d\delta}{dx} \ll 1$, in practice and in agreement with our use of the boundary-layer equations, we use only the first term of A4.19 as the forcing term in the differential equations.

APPENDIX V

EVALUATION OF TURBULENT COEFFICIENTS

The coefficient c_t which arises as a physical property of the turbulent mixing must be determined experimentally. Since there is insufficient data available from shrouded turbulent jet measurements, we must use free jet data, assuming that the mixing coefficient is the same for this case.

From Section III, we see that c_t is defined as

$$c_t = \frac{1}{2} \frac{d\delta}{dX} \tag{A5.1}$$

For the cosine velocity distribution

$$\frac{\bar{u}-U}{\tilde{u}} = \frac{1}{2} \left(1 + \cos \left(\frac{\pi Y}{\delta}\right)\right) \tag{A5.2}$$

We note that $Y_{\frac{1}{2}} = \frac{\delta}{2}$ gives the half-velocity point in the profile, and this distance has been well established in the literature. Newman[12] has tabulated these results and has found the average to be

$$\frac{dY_{\frac{1}{2}}}{dX} = 0.104 \tag{A5.3}$$

From A5.1 we see that

$$c_t = 0.104$$

Coefficient of Eddy-Viscosity

In the confined mixing region the turbulent Reynolds stress is modeled as

$$\tau = \rho \kappa_t \tilde{uh} \frac{\partial \tilde{u}}{\partial \tilde{Y}} \tag{A5. 4}$$

where $\kappa_t \tilde{uh}$ has the function of a viscosity coefficient.

Substituting for the velocity the distribution given by A5. 2 where now $\delta = h$, we can form the non-dimensional forcing term in the momentum equation

$$\left(\frac{2h}{Q_T}\right)^2 \frac{1}{\rho} \frac{\partial \tau}{\partial y} = -\kappa_t \frac{\pi^2}{2} \tilde{u}^{*2} \cos \pi y \tag{A5. 5}$$

where $y = \frac{Y}{h}$.

Since the momentum equation is exactly satisfied by the cosine distribution and one-dimensional pressure function, we can equate the forcing term derived in Section II. 3 from equation 2. 10 to the above expression which gives

$$-\kappa_t \frac{\pi^2}{2} \tilde{u}^{*2} \cos \pi y \Big|_{y=0} = -c_t \tilde{u}^{*2} \tag{A5. 6}$$

or

$$\kappa_t = 0.021 \tag{A5. 7}$$

Comparison with Experiments of Curtet

To fit Curtet's results for the channel flow solution, we define a turbulent axial scale

$$\overline{X} = \frac{9}{2} \frac{A c_t}{\gamma} X^* \tag{A5. 8}$$

which for the cosine distribution has a best fit for

$$\frac{9}{2} \frac{A c_t}{\gamma} = 0.26$$

or

$$c_t = 0.087 \qquad \text{(A5. 9)}$$

This value is somewhat lower than that for a free jet, which indicates that the presence of shrouds might inhibit the turbulent jet mixing. However there is still insufficient evidence to substantiate any correction to the free jet value.

APPENDIX VI

NUMERICAL TECHNIQUES

All numerical methods used in the calculations are standard CIT 7090/94 library routines since all equations are well behaved in the region of interest and, with the exception of the initial region, exhibit no significant sensitivity to changes in program parameters.

(A) The Initial Point

Solution curves generated for a given set of initial conditions were quite sensitive to the choice of initial point and initial step size in the numerical integration scheme. To ensure that the correct solution was obtained, it was necessary to vary both the initial point X_0^* and the step size Δ_m until the solution generated showed little sensitivity to the variations. To check the result, the second order initial conditions for the simple channel solution were used with the same initial points. The variation in the final point X_e^* and the volume flux Q_e^* with X_0^* and Δ_m are shown in figure 32. The numerical inaccuracies in the large X_0^* range are due to the error in choosing only a finite number of terms in the expansion around $X^* = 0$ in the initial conditions. The error in the small X_0^* range is due to the inability of the relatively large step size to adequately represent the derivatives. We choose as our operating points the largest X_0^* and Δ_m at which the high X_0^* and low X_0^* errors do not overlap. They are

$$\left.\begin{aligned} X_0^* &= 0.0001 \\ \Delta_m &= 0.001 \end{aligned}\right\} \qquad (A6.1)$$

When the integration has proceeded into higher ranges of X*, the step size is increased to $\Delta_m = 0.1$.

(B) The Iteration Scheme

The numerical program is illustrated in the flow diagram in figure 33. The mechanics of transforming from the physical plane to the ζ-plane, and the calculation of the forcing functions are handled in subprograms, while the step-wise integration is done in the main program. At the end of an iteration, a subprogram is again used to calculate new coefficients in the potential flow solution.

At the end of each integration, arrays are generated consisting of values of Q* and $\hat{\delta}$ evaluated at the chosen match points. The match points are selected during the integration to be near the downstream end of the particular interval, $x_i - x_{i-1}$ (see figure 11), and are labeled $X^*_{m_i}$. The arrays generated, Q^*_i and $\hat{\delta}_i$ are substituted in 3.14 to calculate ζ_δ and hence the potential functions $K_i(\zeta_\delta)$ (Appendix IV). The set of algebraic equations produced with the non-homogeneous terms $\{Q^*_i\}$ are solved for the coefficients C_i.

If these C_i's are now used as the new coefficients in 3.15 for the forcing term U*, the iteration procedure often produces a looping condition whereby a stable solution does not appear. To prevent this, the new coefficients are obtained by an averaging of the old coefficients and those obtained from solving the algebraic equations. This method produces an essentially stable solution for all cases within four iterations.

APPENDIX VII

SIMPLE CHANNEL THEORY

The equations are written in terms of the parameters U^*, $\tilde{u}^*$ and $\hat{\delta}$ as, from 2.9

$$2\hat{\delta}\tilde{u}\frac{dU^*}{dX^*} + \hat{\delta}(U^* + 2\gamma\tilde{u}^*)\frac{d\tilde{u}^*}{dX^*} + \tilde{u}^*(U^* + \gamma\tilde{u}^*)\frac{d\hat{\delta}}{dX^*} = 0 \qquad (A7.1)$$

from 2.10 and 2.12

$$\hat{\delta}\tilde{u}^*\frac{dU^*}{dX^*} + \hat{\delta}(U^* + \tilde{u}^*)\frac{d\tilde{u}^*}{dX^*} = -c_t\frac{\tilde{u}^{*2}}{\hat{\delta}} \qquad (A7.2)$$

and the continuity equation

$$U^* + A\hat{\delta}\tilde{u}^* = 1 \qquad (A7.3)$$

with the definition

$$Q^* = \hat{\delta}(U^* + A\tilde{u}^*)$$

Equation A7.1 can be rewritten in the form

$$\frac{d}{dX^*}(\hat{\delta}\tilde{u}^*U^* + \gamma\hat{\delta}\tilde{u}^{*2}) + \hat{\delta}\tilde{u}^*\frac{dU^*}{dX^*} = 0$$

and substituting for U^* from A7.3, this becomes

$$\hat{\delta}\tilde{u}^*(\gamma\tilde{u}^* - \frac{3}{2}\hat{\delta}\tilde{u}^* + 1) = \frac{a}{A} \qquad (A7.4)$$

where a is the momentum parameter defined by equation 3.12.

This is solved for $\hat{\delta} = \hat{\delta}(\tilde{u}^*)$, and hence

$$U^* = U^*(\tilde{u}^*)$$

These are substituted into A7.2, resulting in an equation of

the form

$$\mathcal{J}(\tilde{u}^*)\frac{d\tilde{u}^*}{dX^*} = -c_t \qquad \text{(A7.5)}$$

which can be integrated to give

$$X^* = X^*(\tilde{u}^*)$$

Rearranging the solutions and expressing them in terms of the argument $\varphi^* = 1-U^*$

$$Q^* = \varphi^* + \frac{2}{3}\frac{\gamma}{A}\frac{\varphi^{*2}(1-\varphi^*)}{S} \qquad \text{(A7.6)}$$

$$\hat{\delta} = \frac{2}{3}\frac{\gamma}{A}\frac{\varphi^{*2}}{S} \qquad \text{(A7.7)}$$

$$X^* = \frac{2}{9}\frac{\gamma}{Ac_t}\left(\frac{d_1\varphi^*+d_2}{S^2} + \frac{d_3\varphi^*+d_4}{S} + d_5\log(S)+T\right) \qquad \text{(A7.8)}$$

where

$$S(\varphi^*, a) = \varphi^{*2} - \frac{2}{3}\varphi^* + \frac{2}{3}a$$

$$T(\varphi^*, a) = \begin{cases} d_6\tan^{-1}\left(\dfrac{3\varphi^*-1}{\sqrt{6a-1}}\right) + d_7 & a > \frac{1}{6} \\ d_6\log\left(\dfrac{1+\sqrt{1-6a}-3\varphi^*}{1-\sqrt{1-6a}-3\varphi^*}\right) + d_7 & a < \frac{1}{6} \end{cases}$$

The coefficients $d_1 \ldots d_8$ are listed in table I and the form parameters γ, A are defined in Section II. 3(b).

We find the values at $X^* = X^*_e$ by setting $\hat{\delta} = 1$ in A7. 7. Then

$$\varphi^{*2}_e - \frac{2}{3}\varphi^*_e + \frac{2}{3}a = \frac{2}{3}\frac{\gamma}{A}\varphi^{*2}_e \qquad \text{(A7.9)}$$

which must be solved for φ^*_e. We must pick that root of A7. 9 which

gives a minimum X_e^*, if two real roots exist. We can see that the profile parameter $\frac{2}{3}\frac{\gamma}{A}$ is important in that values less than 1 produce the possibility of no real solutions for a above a critical value. Physically in these cases the boundary turns back upstream. To avoid this apparent anomaly we require $\frac{2}{3}\frac{\gamma}{A} \geq 1$ from our profile. For the cosine profile the limiting value is reached since $(\frac{\gamma}{A})_{cosine}=\frac{3}{2}$. In this case A7. 9 has the simple solution

$$\varphi_e^* = a \tag{A7. 10}$$

Then

$$U_e^* = 1-a \tag{A7. 11}$$

$$\tilde{u}_e^* = 2a \tag{A7. 12}$$

and $$X_e^* = \frac{1}{c_t}\left(\frac{12a^2 + 9a - 2}{8a(6a-1)} + \frac{3a}{4}\, d_8\right) \tag{A7. 13}$$

APPENDIX VIII

SIMILARITY SOLUTION IN CONFINED MIXING

Integrating the assumed velocity profile

$$\overline{u} = U(X) + \tilde{u}(X)f(y) \qquad \text{(A8. 1)}$$

across the channel, the integral continuity equation expressed in non-dimensional variables, can be written as

$$U^*(X^*) + A\tilde{u}^*(X^*) = 1 \qquad \text{(A8. 2)}$$

Substituting A8. 1 into the momentum equation 5. 3 and using A8. 2 to remove U*, we have

$$\frac{d\tilde{u}^*}{dX^*}\left((f-A)+\tilde{u}^*((f-A)^2+f'(Ay-\int_0^y f dy))\right) + \frac{1}{\rho}\frac{dp^*}{dX^*} = \kappa_t \tilde{u}^{*2} g' \qquad \text{(A8. 3)}$$

The right-hand side is the derivative of the turbulent Reynolds term as given in equation 5. 4.

If we represent the profile shape function by the cosine formula,

$$f = \tfrac{1}{2}(1 + \cos\pi y) \qquad \text{(A8. 3)}$$

then A = 1/2 and the coefficient of $d\tilde{u}^*/dx^*$ becomes $(\frac{\cos\pi y}{2} + \frac{\tilde{u}^*}{4})$.

The momentum equation reduces to equation 5. 5. Now if g(y) = df/dy as proposed in Section V. 3, the forcing function can be written as

$$\kappa_t \tilde{u}^{*2}\, g'(y) = -\kappa_t \frac{\pi^2}{2} \tilde{u}^{*2} \cos\pi y \qquad \text{(A8. 4)}$$

TABLE I

CHANNEL FLOW COEFFICIENTS

d_1		$\frac{2\gamma}{27}(3\alpha+2)$
d_2		$-\frac{4\alpha\gamma}{27}(3\alpha+1)$
d_3		$2-\gamma\left(\frac{11\alpha-2}{6\alpha-1}\right)$
d_4		$-2\alpha+\frac{\gamma}{9}\left(\frac{144\alpha^2-15\alpha-2}{6\alpha-1}\right)$
d_5		$\frac{4\gamma-3}{2}$
d_6	$\alpha>\frac{1}{6}$	$\frac{-3}{\sqrt{6\alpha-1}}\left(1-\frac{\gamma}{3}\left(\frac{27\alpha-4}{6\alpha-1}\right)\right)$
	$\alpha<\frac{1}{6}$	$-\frac{3}{2\sqrt{1-6\alpha}}\left(1-\frac{\gamma}{3}\left(\frac{27\alpha-4}{6\alpha-1}\right)\right)$
d_7	$\alpha>\frac{1}{6}$	$3-\frac{\gamma}{2}\left(\frac{36\alpha-7}{6\alpha-1}\right)-d_5\log\left(\frac{2\alpha}{3}\right)+d_6\tan^{-1}\left(\frac{1}{\sqrt{6\alpha-1}}\right)$
	$\alpha<\frac{1}{6}$	$3-\frac{\gamma}{2}\left(\frac{36\alpha-7}{6\alpha-1}\right)-d_5\log\left(\frac{2\alpha}{3}\right)+d_6\log\left(\frac{1-\sqrt{1-6\alpha}}{1+\sqrt{1-6\alpha}}\right)$
d_8	$\alpha>\frac{1}{6}$	$\tan^{-1}\left(\sqrt{6\alpha-1}\right)/(6\alpha-1)^{3/2}$
	$\alpha<\frac{1}{6}$	$\log\left(\frac{1-\sqrt{1-6\alpha}}{1+\sqrt{1-6\alpha}}\right)/2(1-6\alpha)^{3/2}$

LIST OF FIGURES

LIST OF FIGURES (Cont'd)

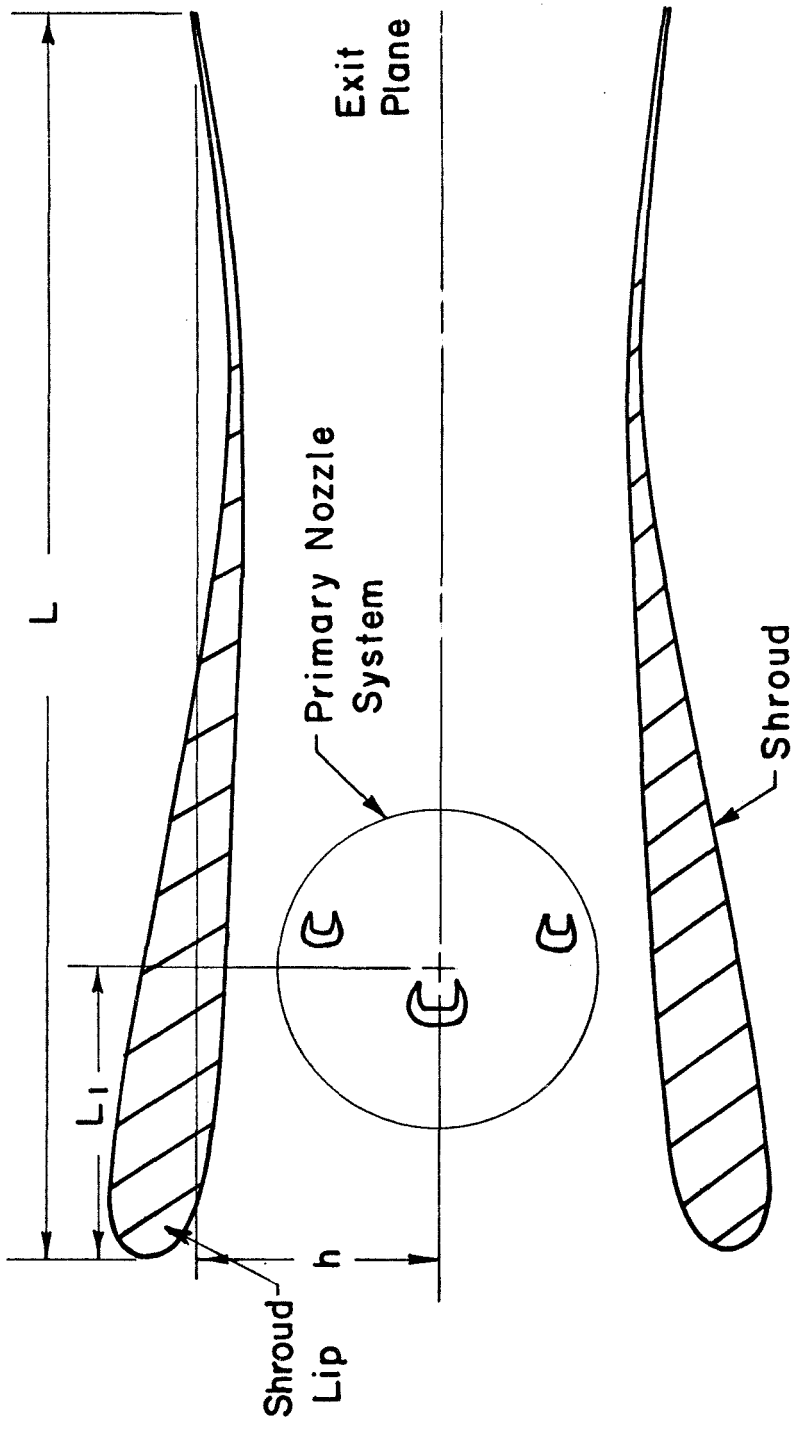

FIG. 1 GENERALIZED TWO-DIMENSIONAL AXIAL JET EJECTOR

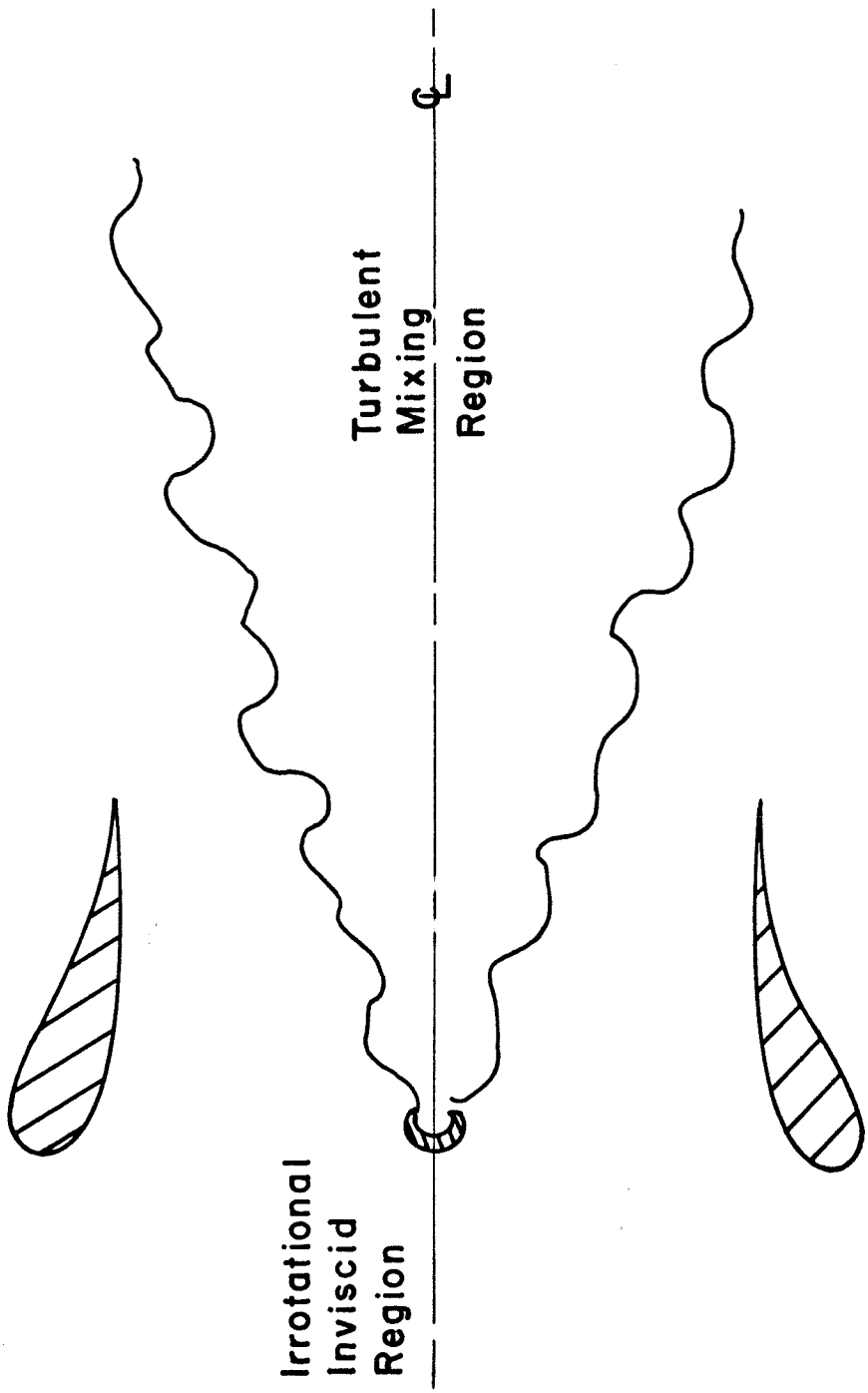

FIG. 2 FLOW REGIONS (TYPE I FLOWS)

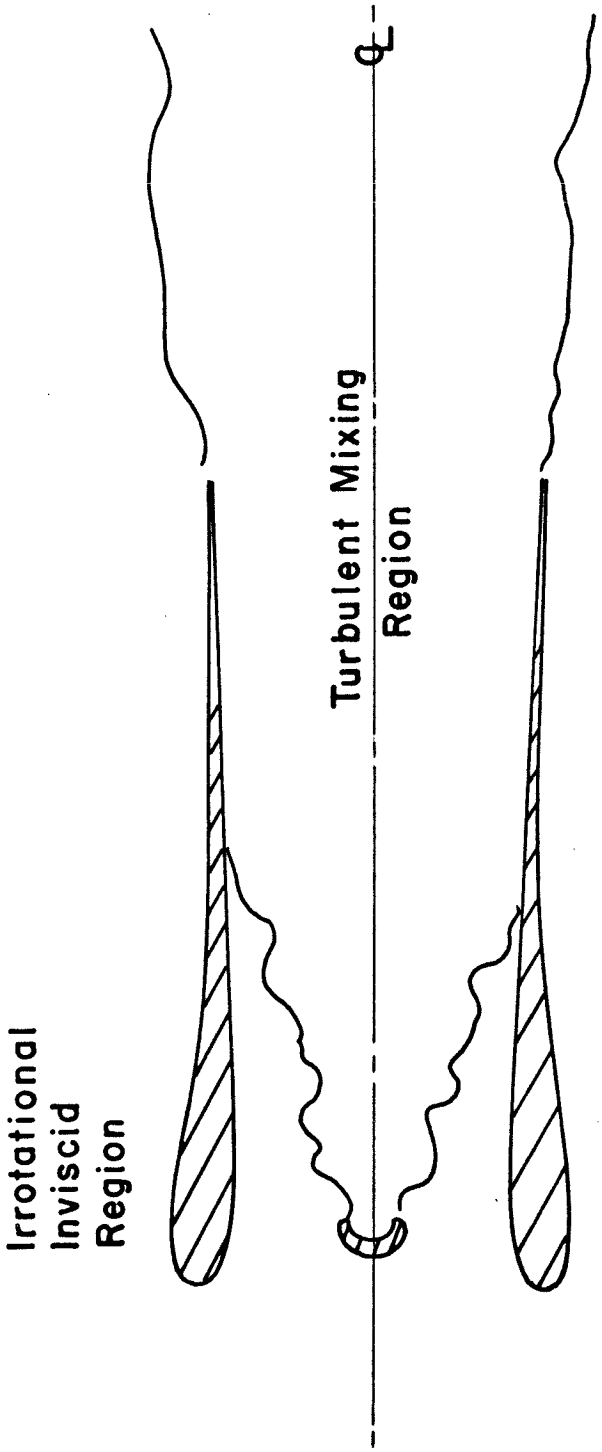

FIG.3 FLOW REGIONS (TYPE II FLOWS)

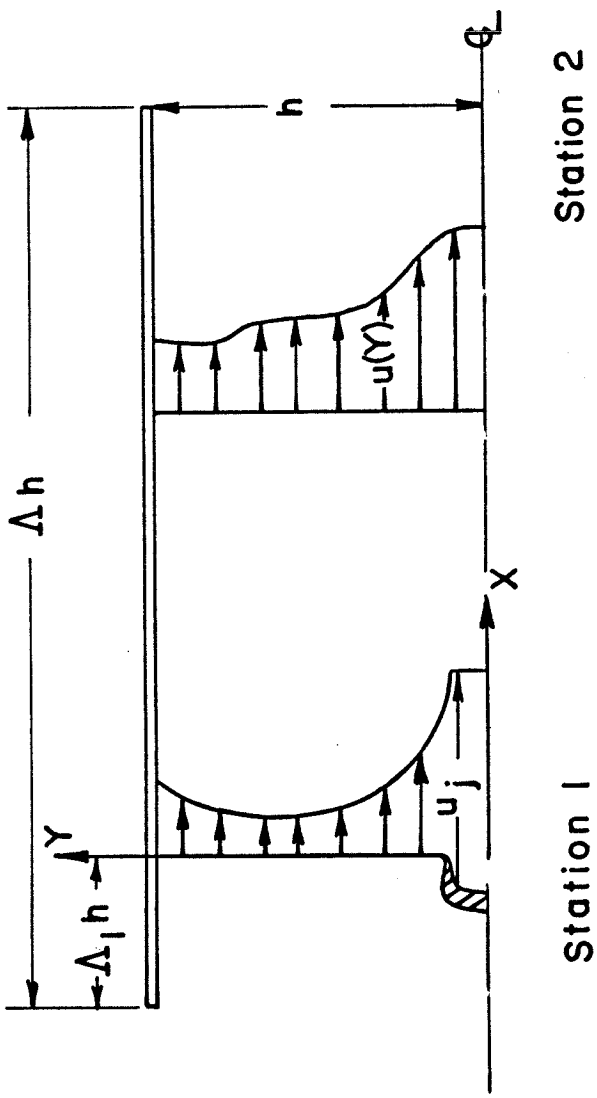

FIG. 4 TWO-PARAMETER MODEL

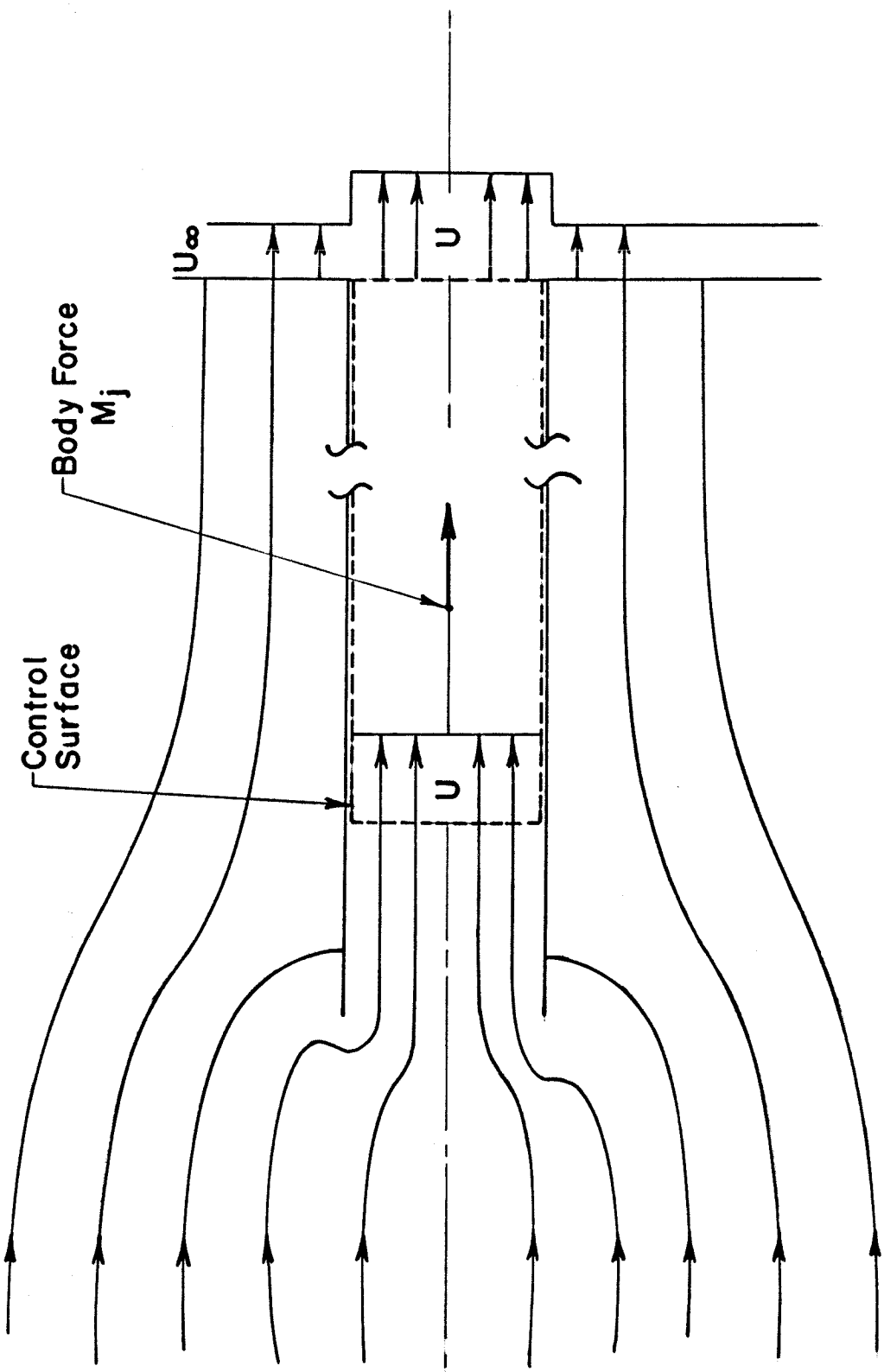

FIG. 5 LONG SHROUD LIMIT

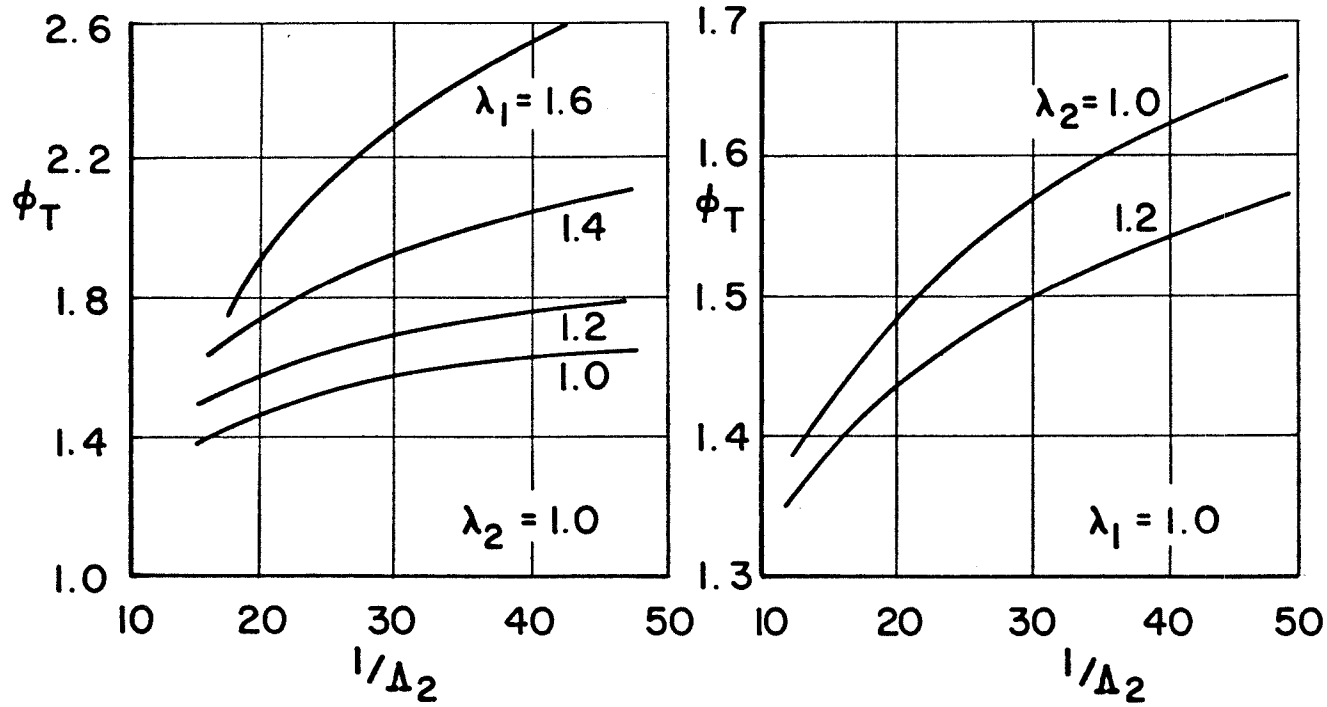

Von Kármán Model

$$\lambda = \frac{\frac{1}{h}\int_0^h u^2 dy}{\left(\frac{1}{h}\int_0^h u dy\right)^2}$$

Taken From Ref. 10

FIG. 6 INFLUENCE OF VELOCITY PROFILES ON THRUST COEFFICIENT

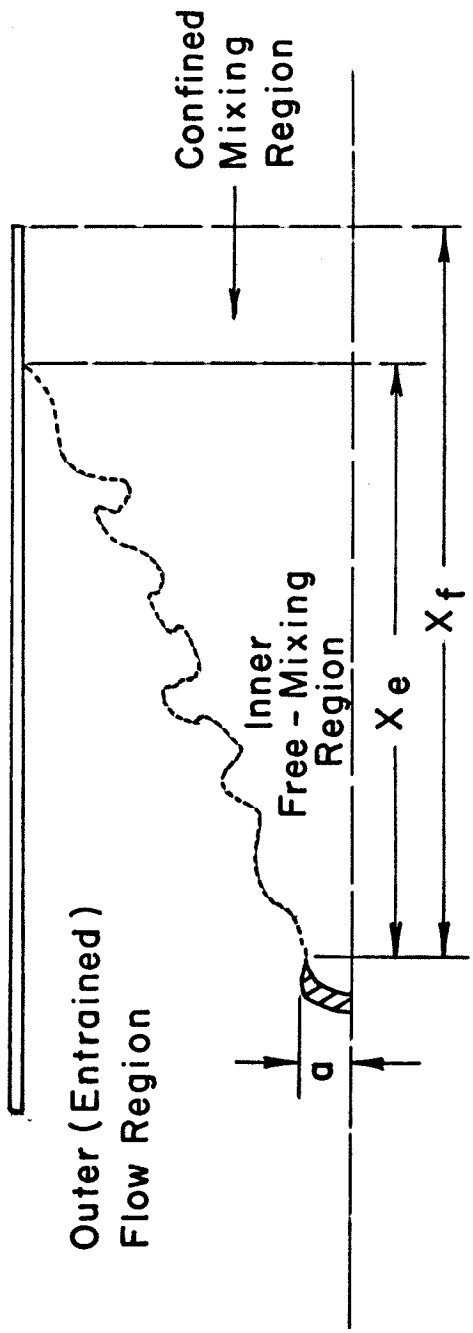

FIG. 7 TWO-PARAMETER MODEL

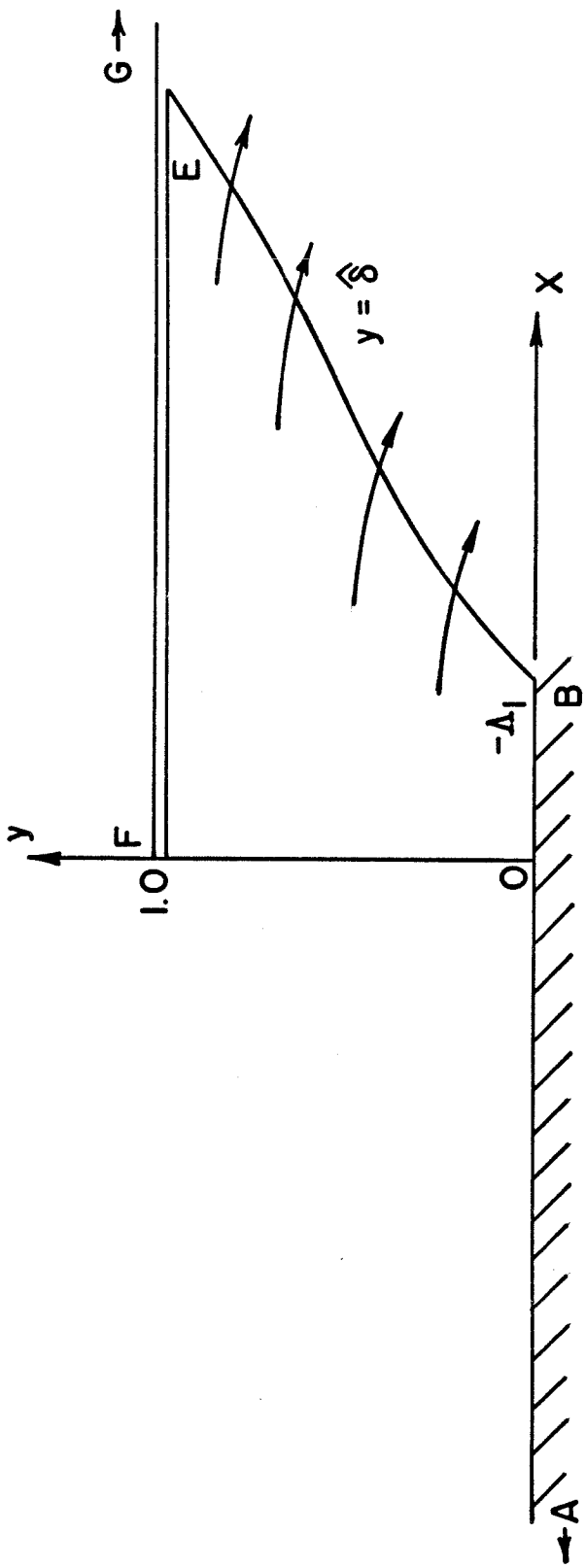

FIG. 8 THE INVISCID REGION

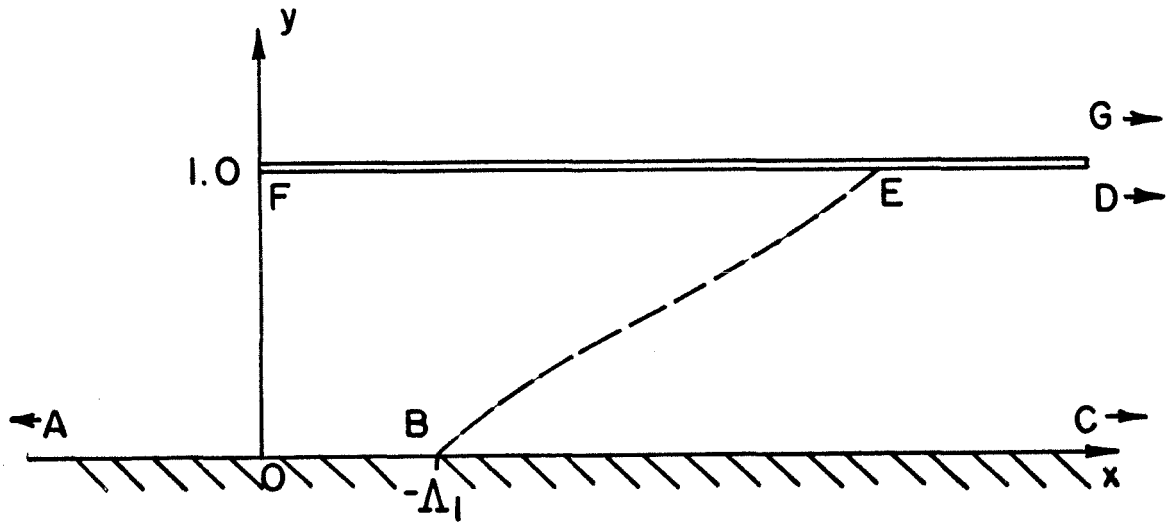

Physical (Z) Plane

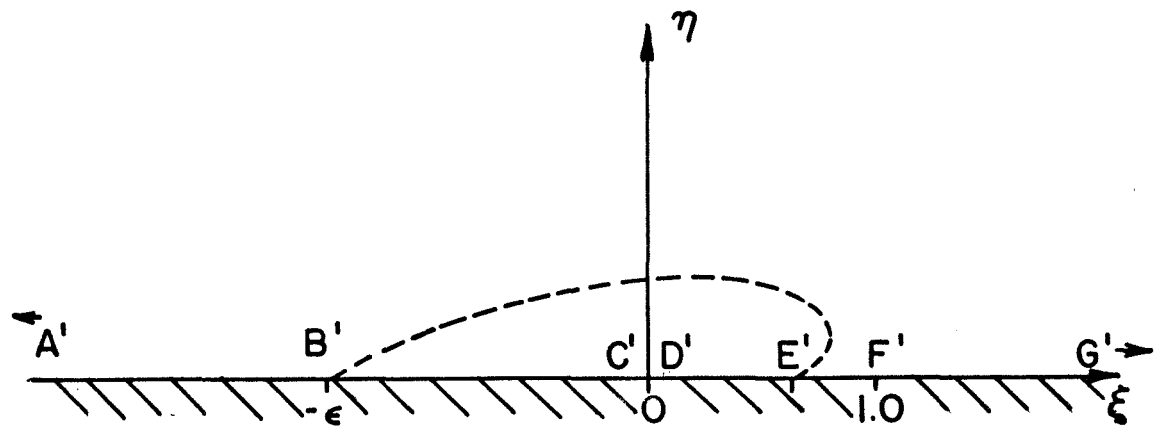

Transform (ζ) Plane

FIG. 9 COMPLEX MAPPING

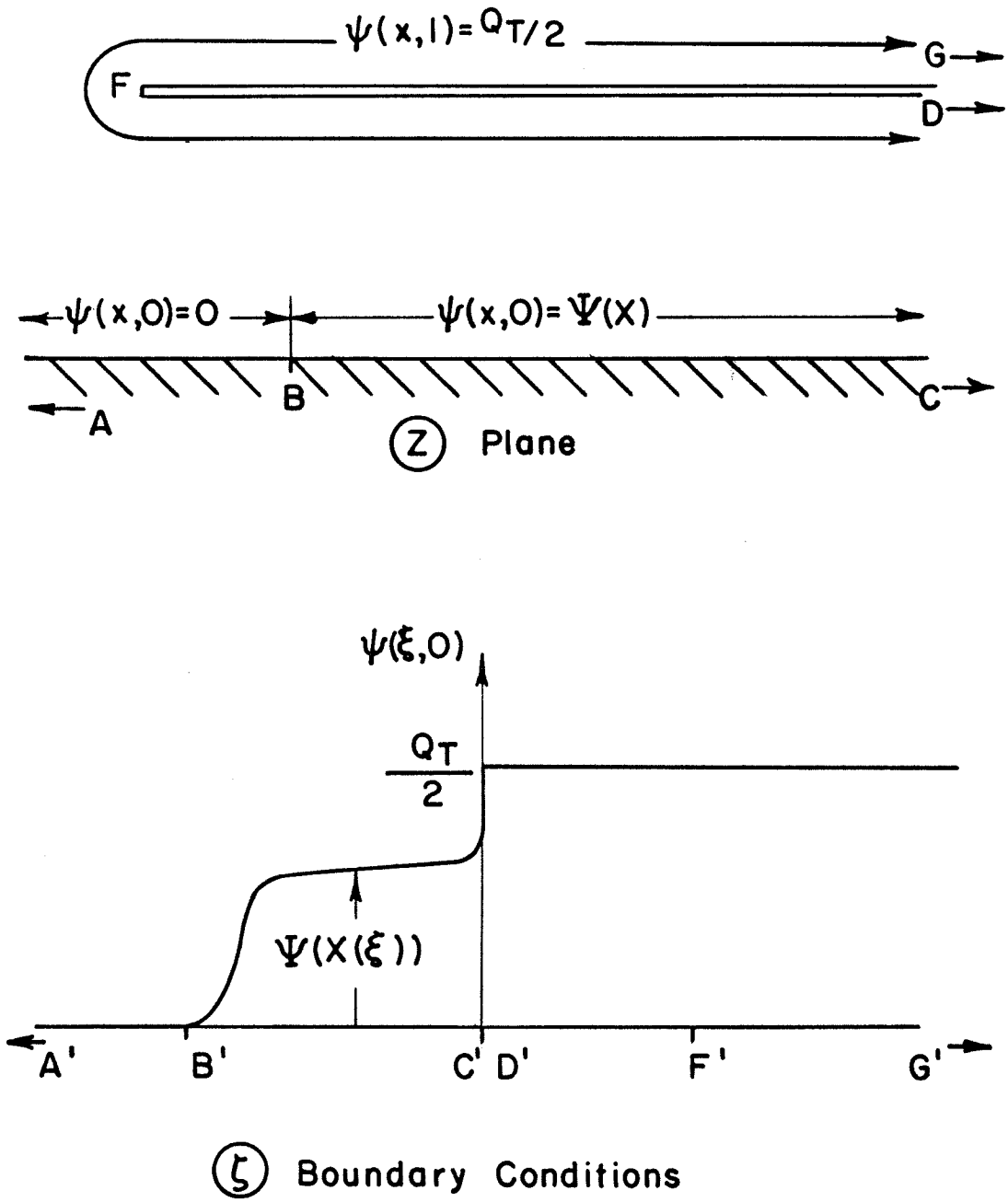

FIG. 10 BOUNDARY VALUE PROBLEM

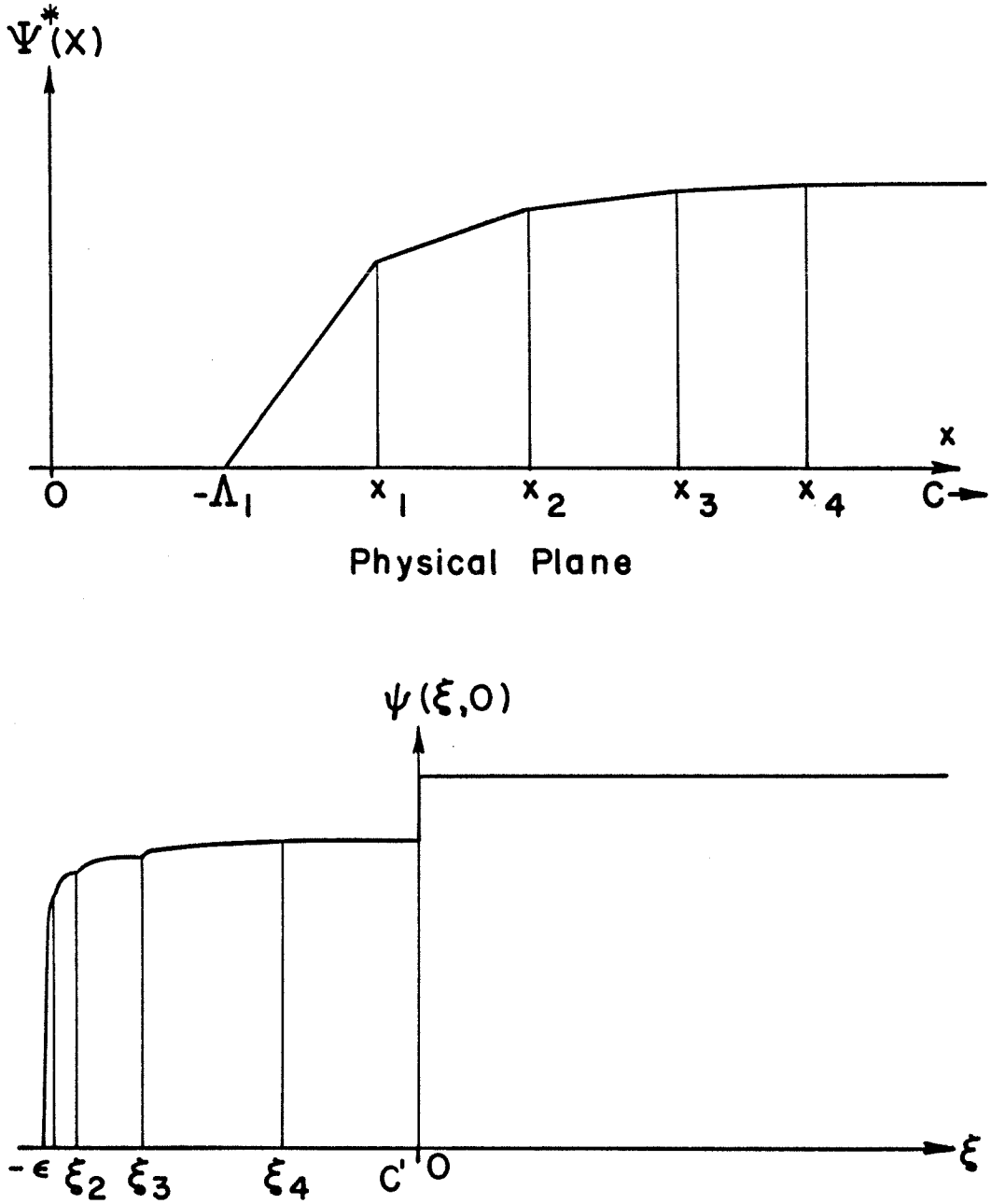

FIG. 11 APPROXIMATE BOUNDARY CONDITIONS

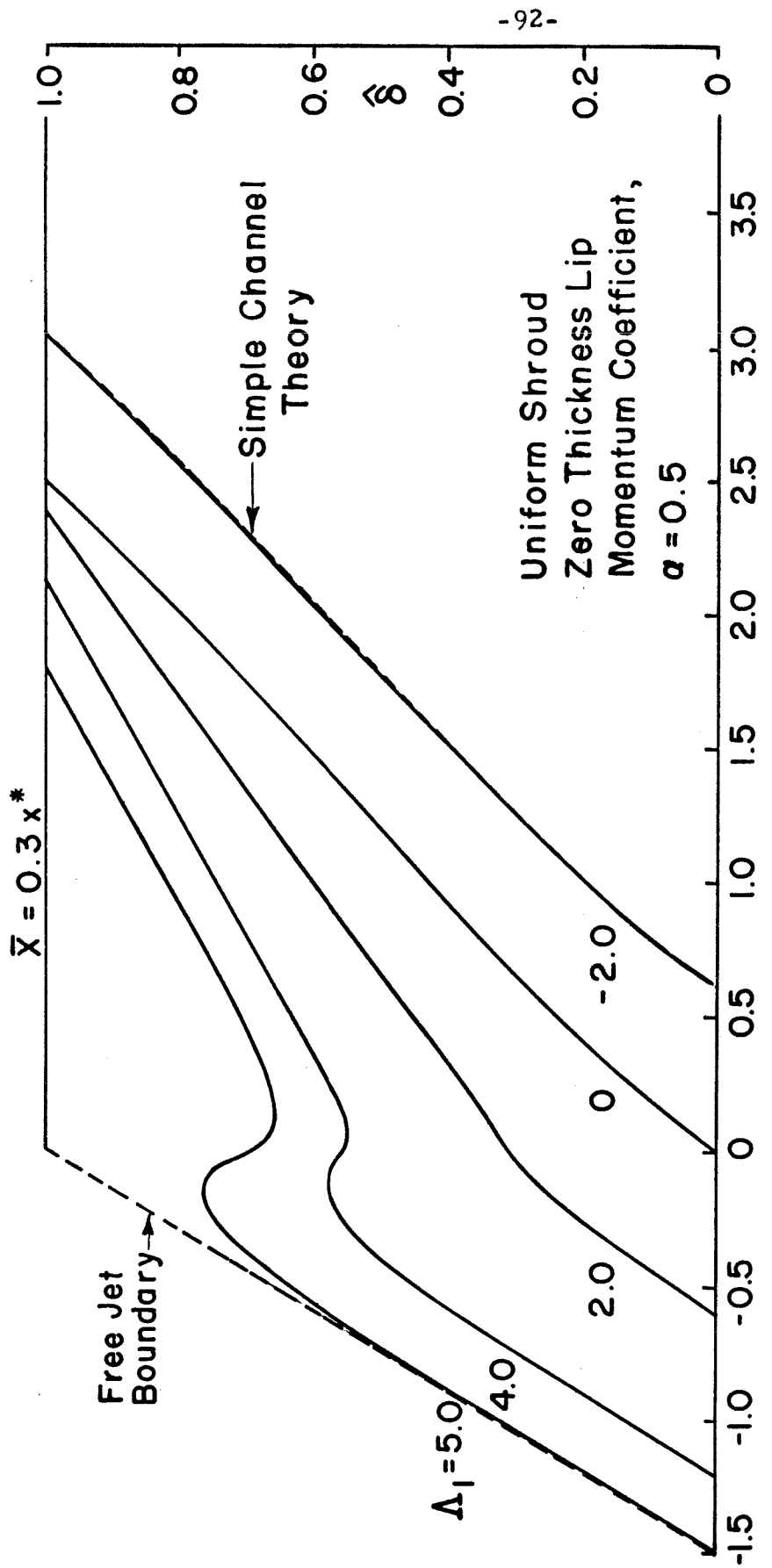

FIG. 12 EFFECT OF Λ_1 ON BOUNDARY POSITION $\bar{\delta}$

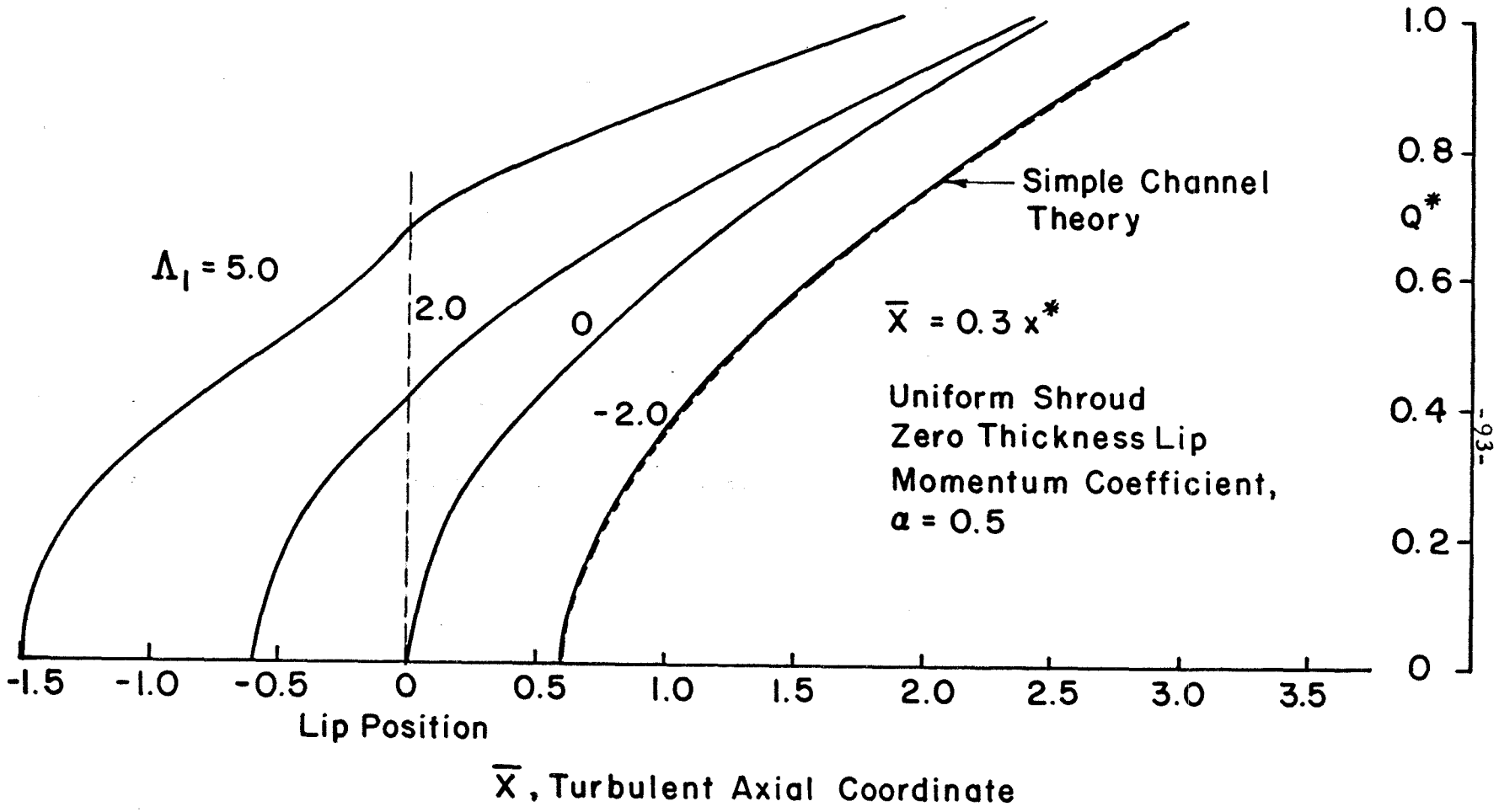

FIG. 13 EFFECT OF Λ_1 ON JET ENTRAINMENT Q^*

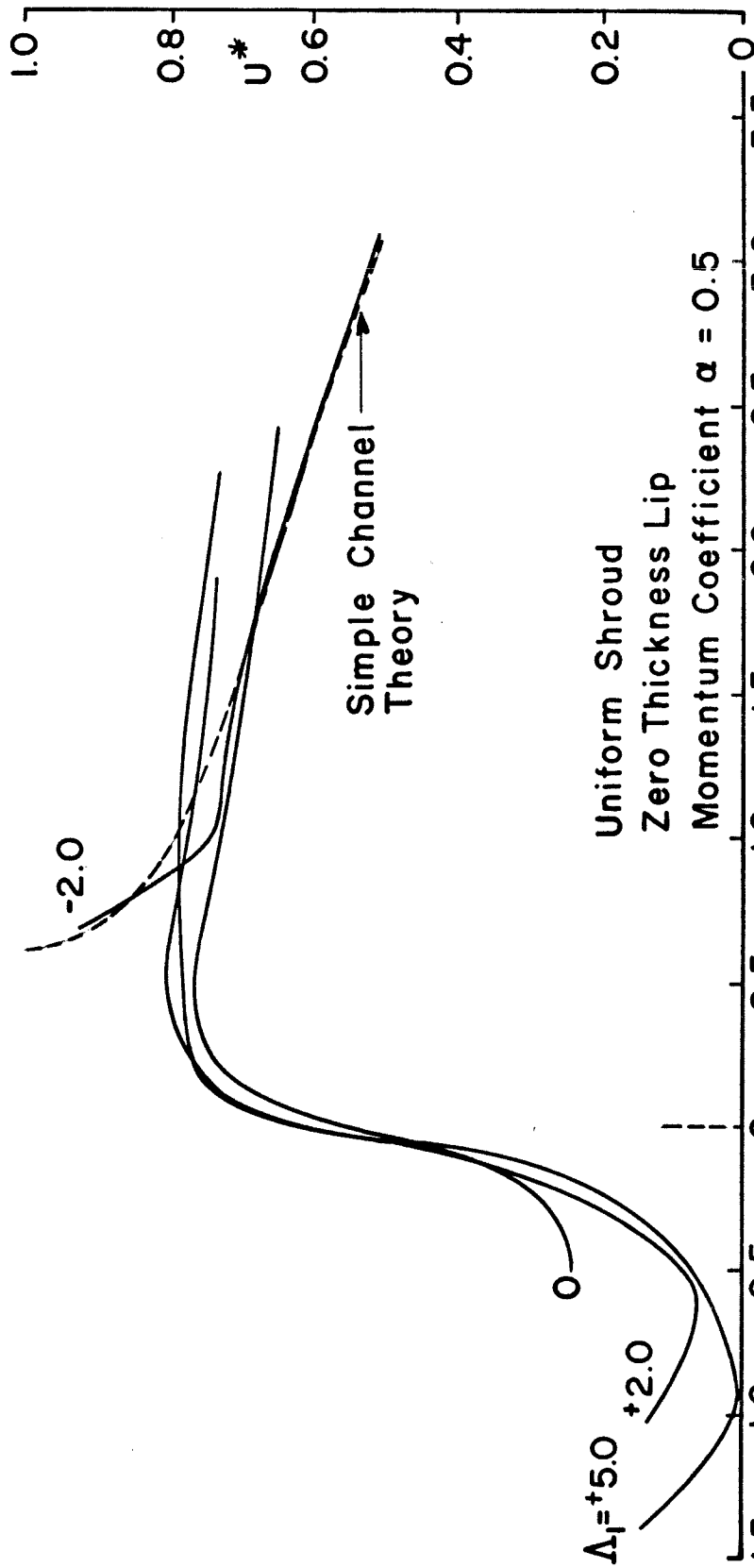

FIG. 14 EFFECT OF Λ_1 ON EDGE VELOCITY U^*

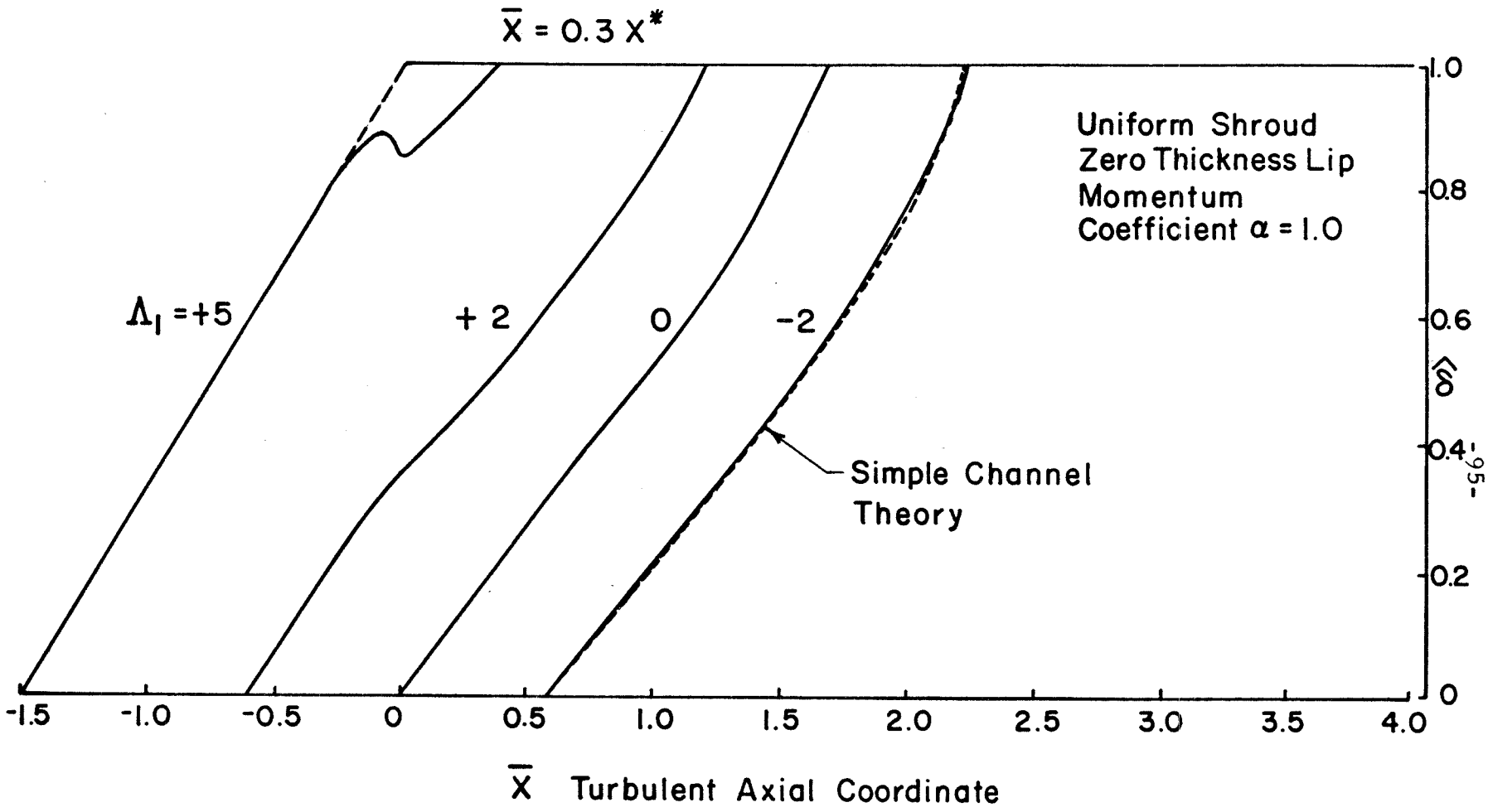

FIG. 15 EFFECT OF Λ_1 ON BOUNDARY POSITION $\hat{\delta}$

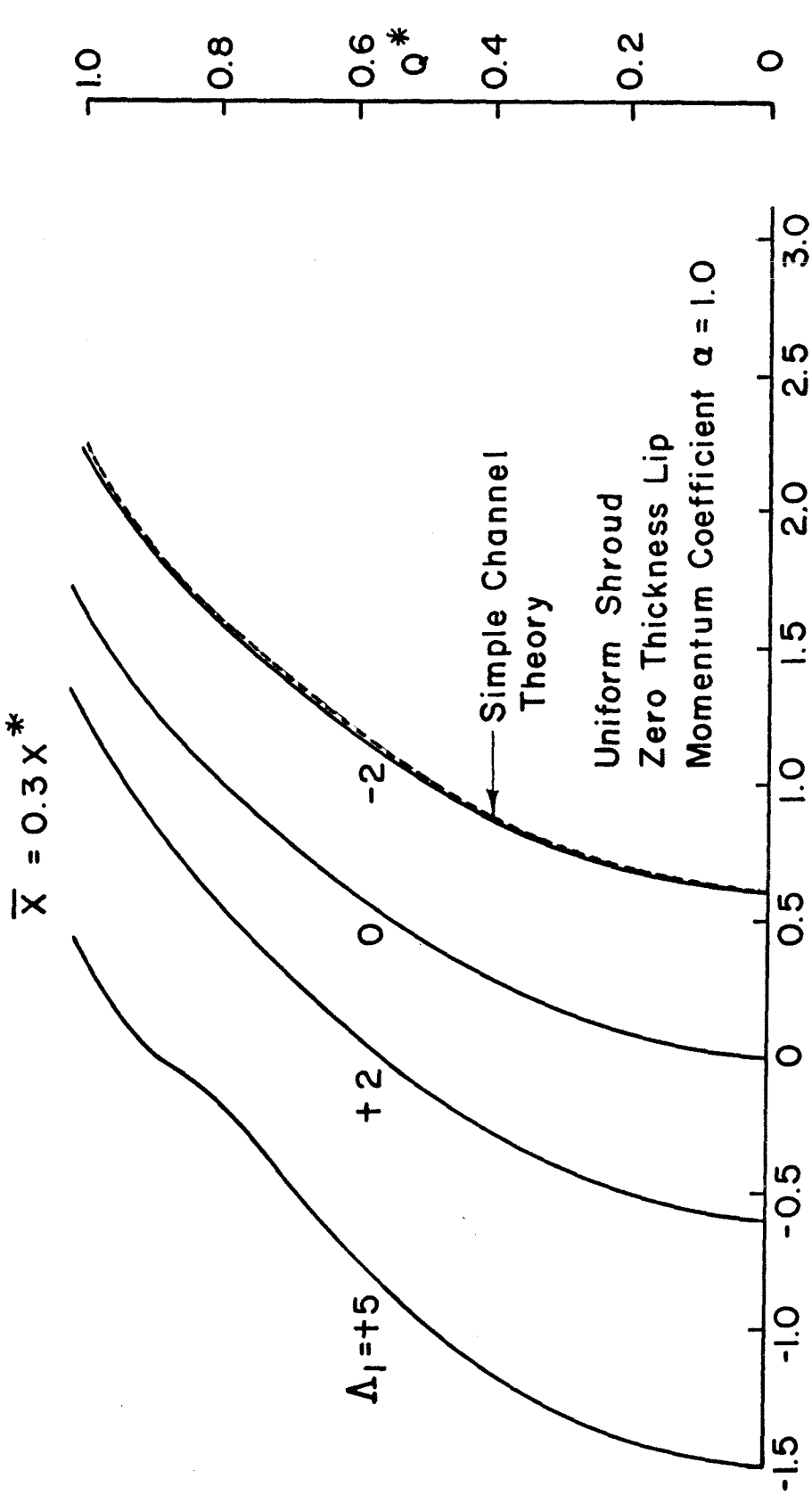

FIG. 16 EFFECT OF Λ_1 ON JET ENTRAINMENT Q^*

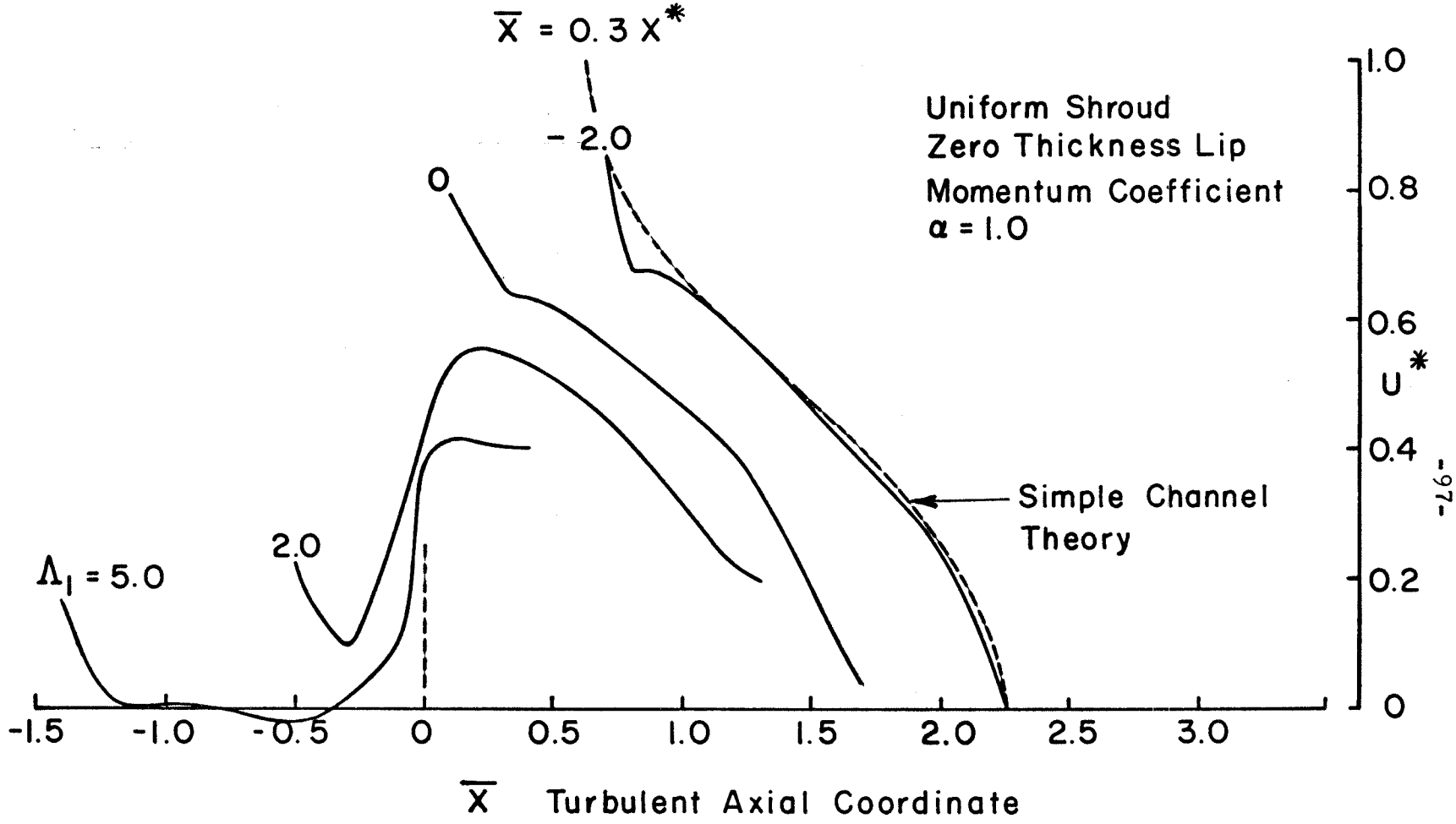

FIG. 17 EFFECT OF Λ_1 ON EDGE VELOCITY U^*

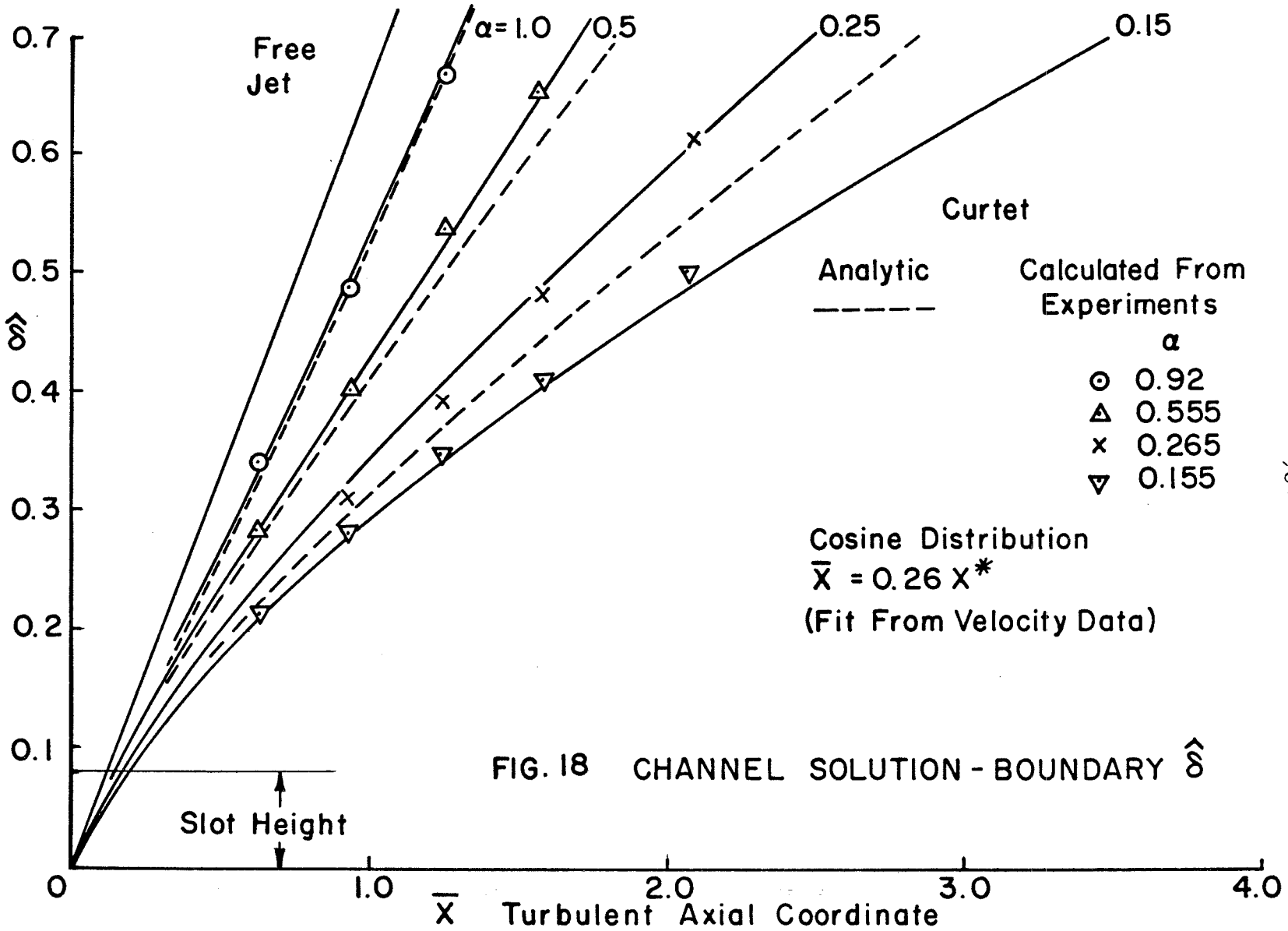

FIG. 18 CHANNEL SOLUTION - BOUNDARY $\hat{\delta}$

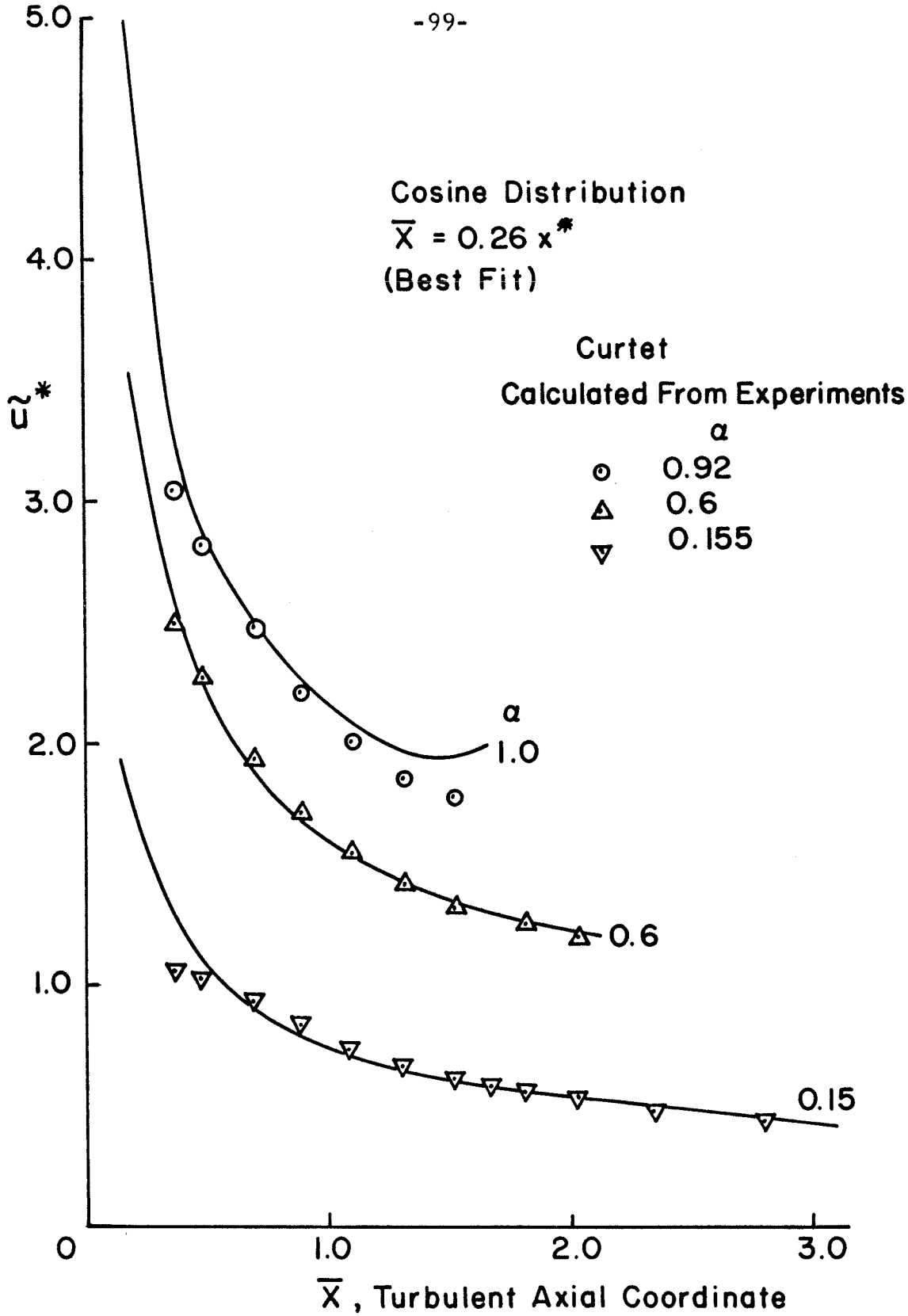

FIG. 19 CHANNEL SOLUTION–SUPERVELOCITY $\tilde{u}^*$

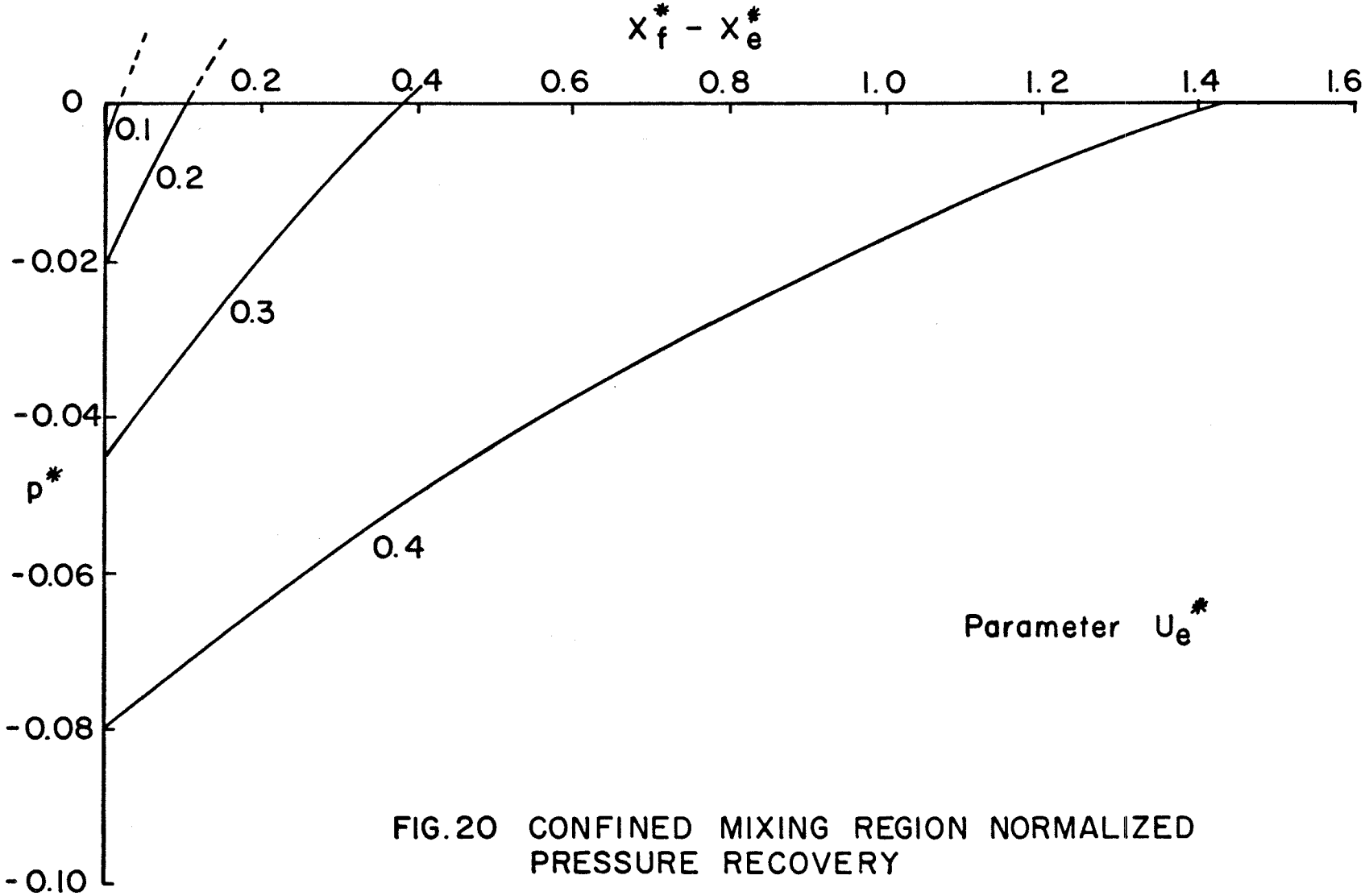

FIG. 20 CONFINED MIXING REGION NORMALIZED PRESSURE RECOVERY

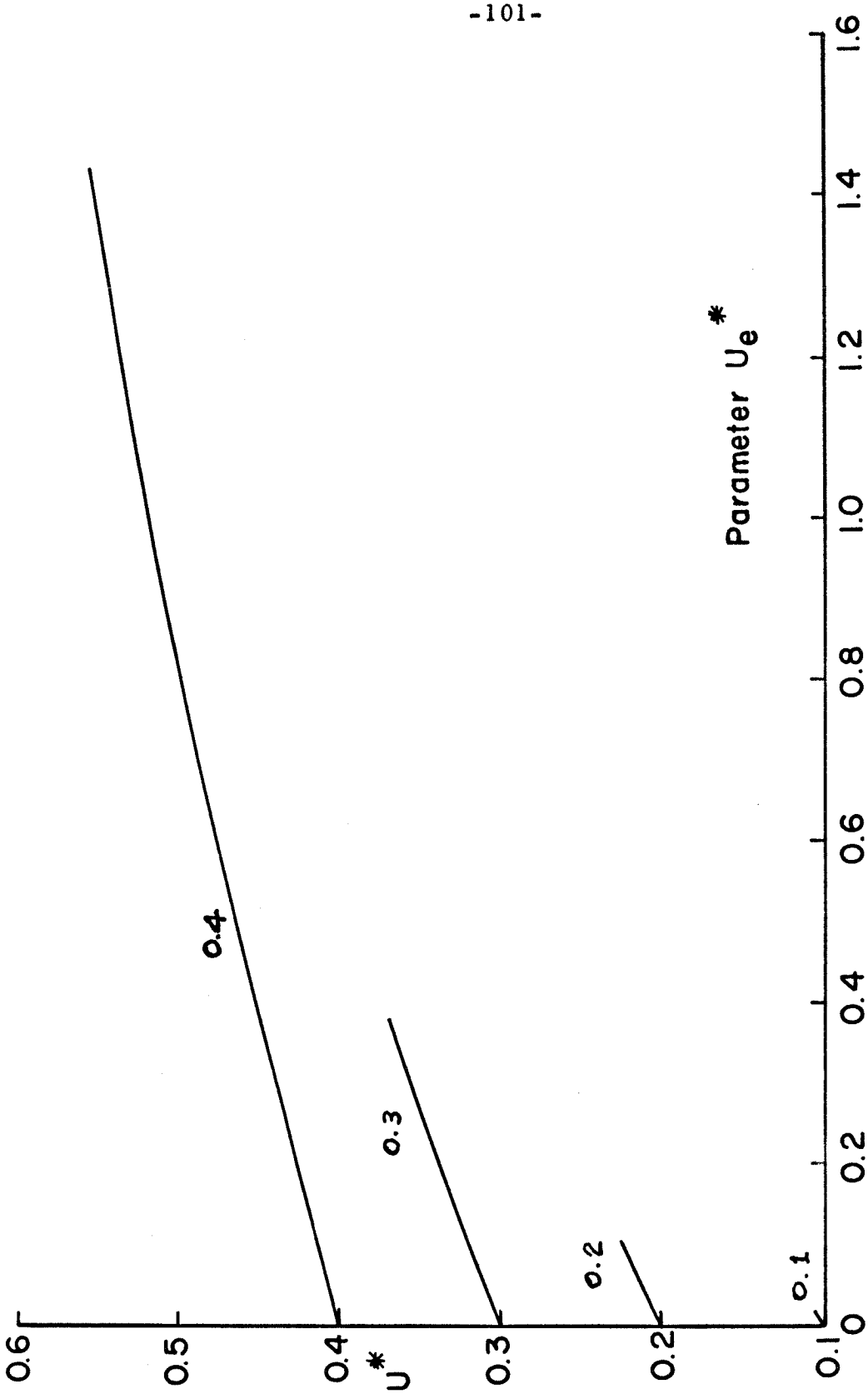

FIG. 21 CONFINED-MIXING REGION, VELOCITY AT THE SHROUD U^*

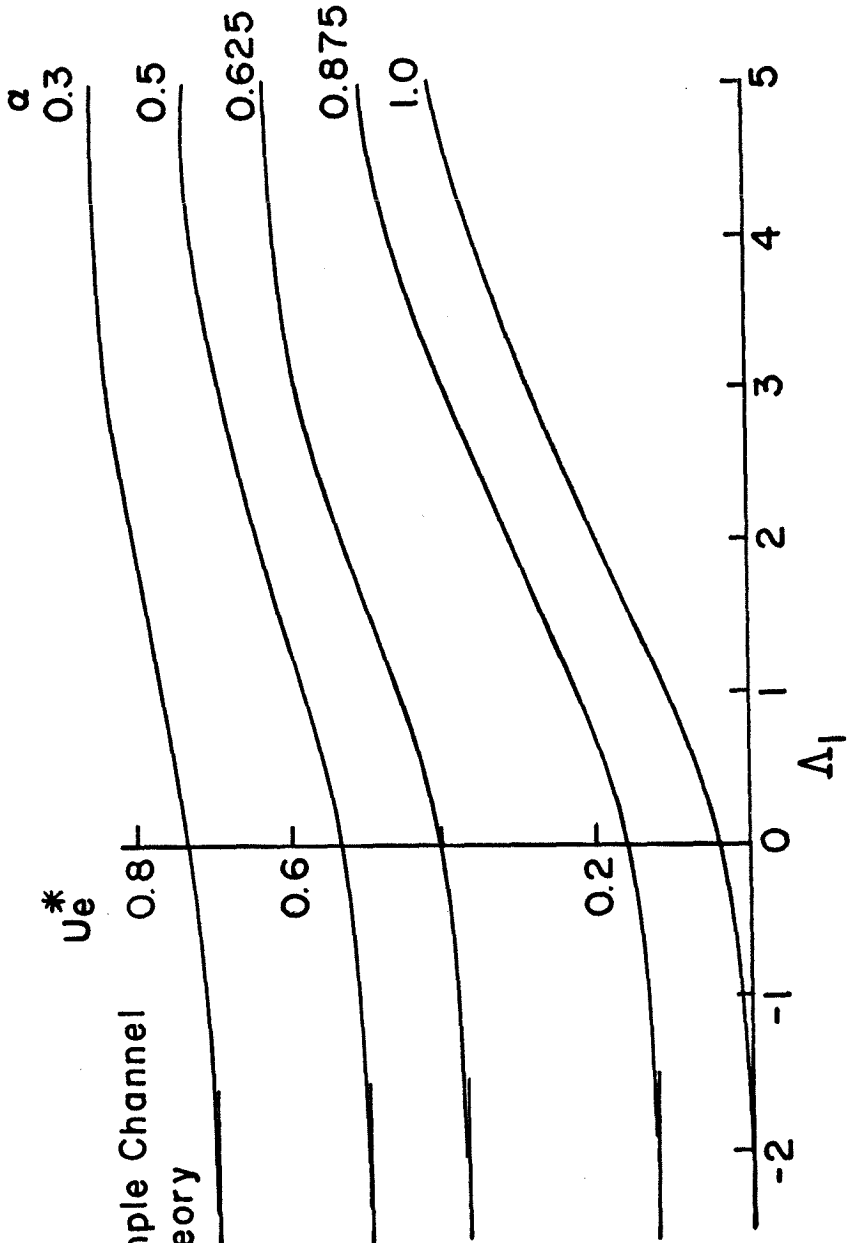

FIG.22 EDGE VELOCITY U_e^* — CORRELATION OF FREE-MIXING PARAMETERS

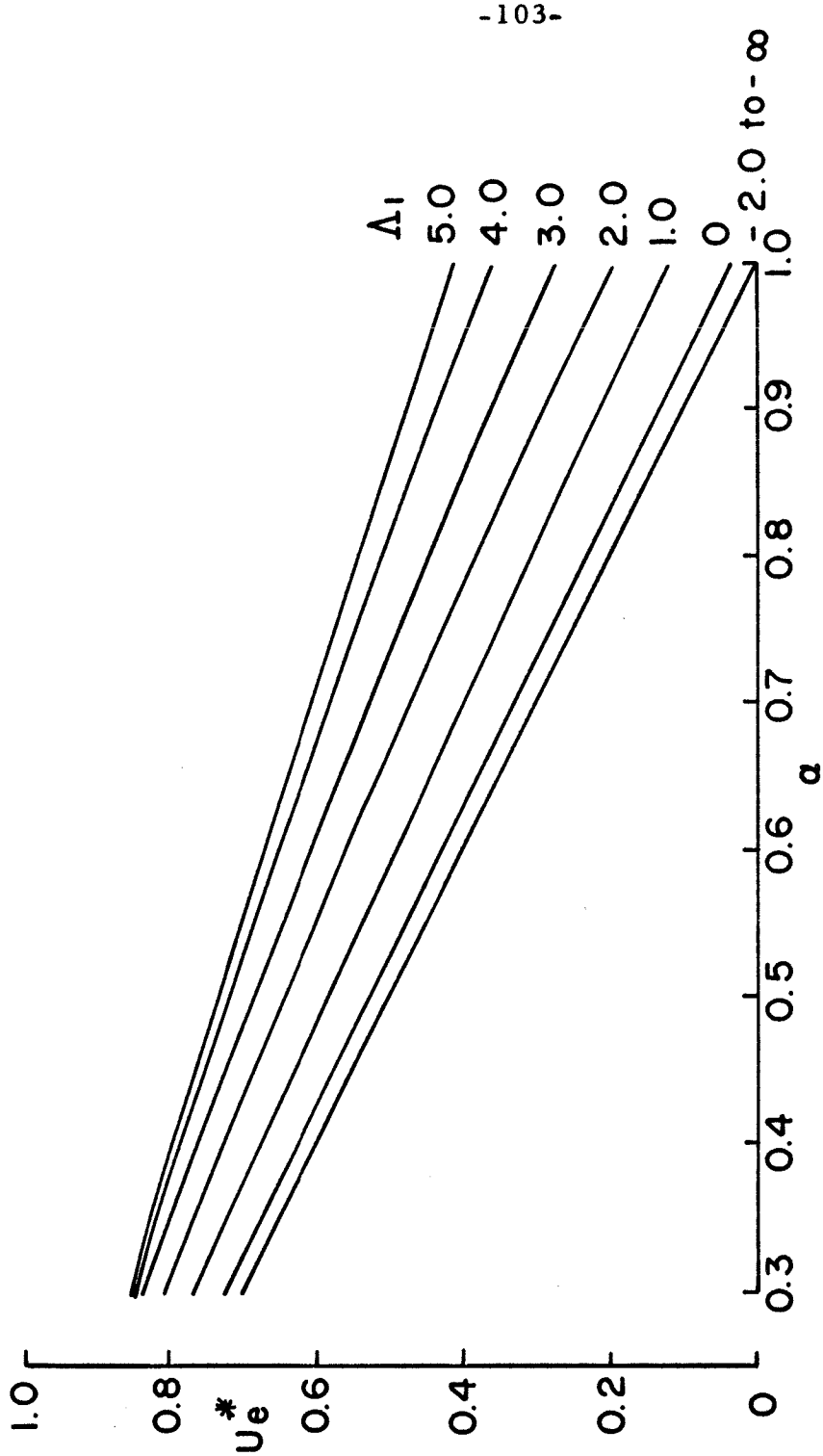

FIG. 23 EDGE VELOCITY U_e^* - CORRELATION OF FREE-MIXING PARAMETERS

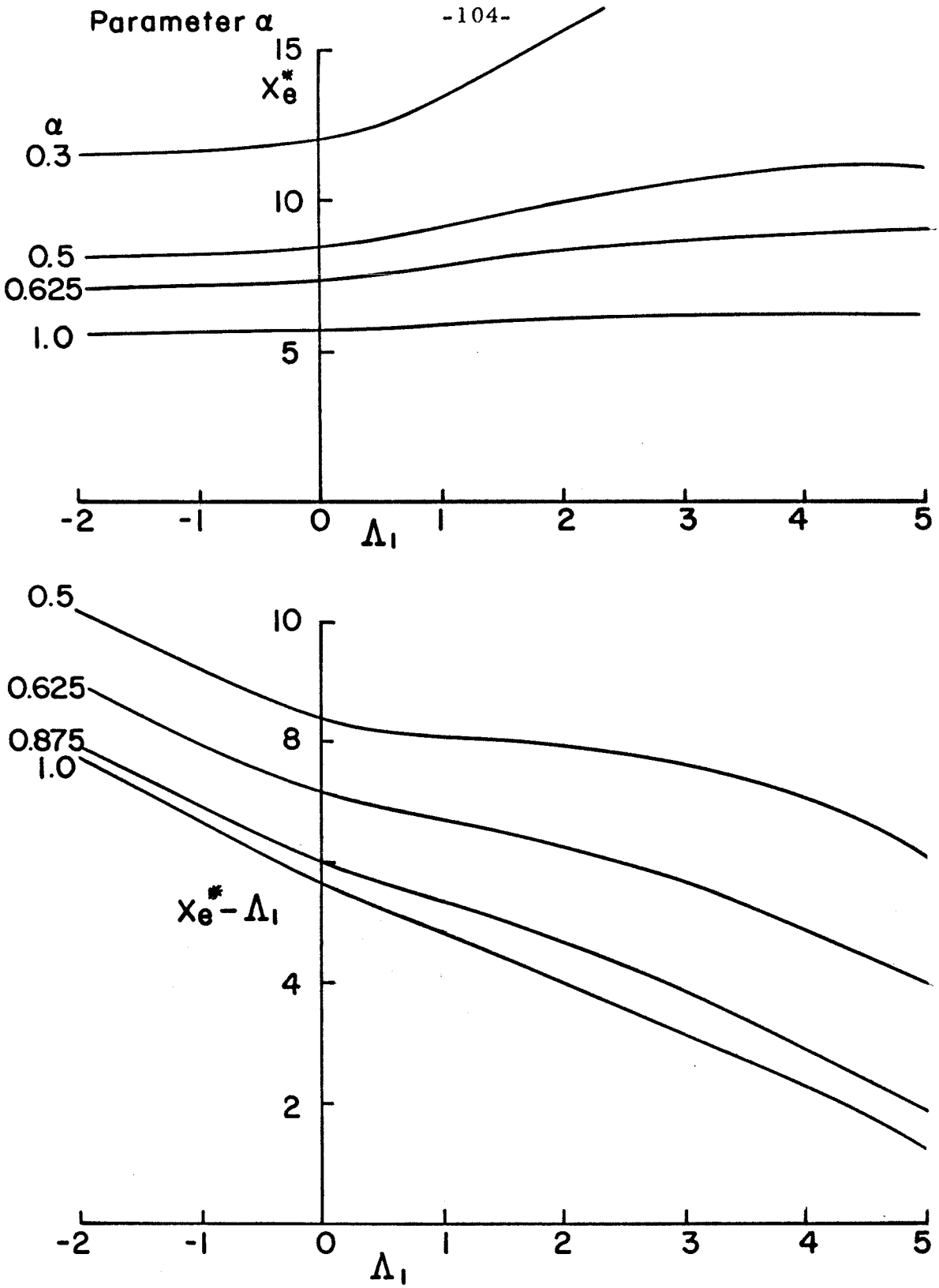

FIG. 24 FREE-MIXING REGION LENGTH X_e^* CORRELATION OF PARAMETERS

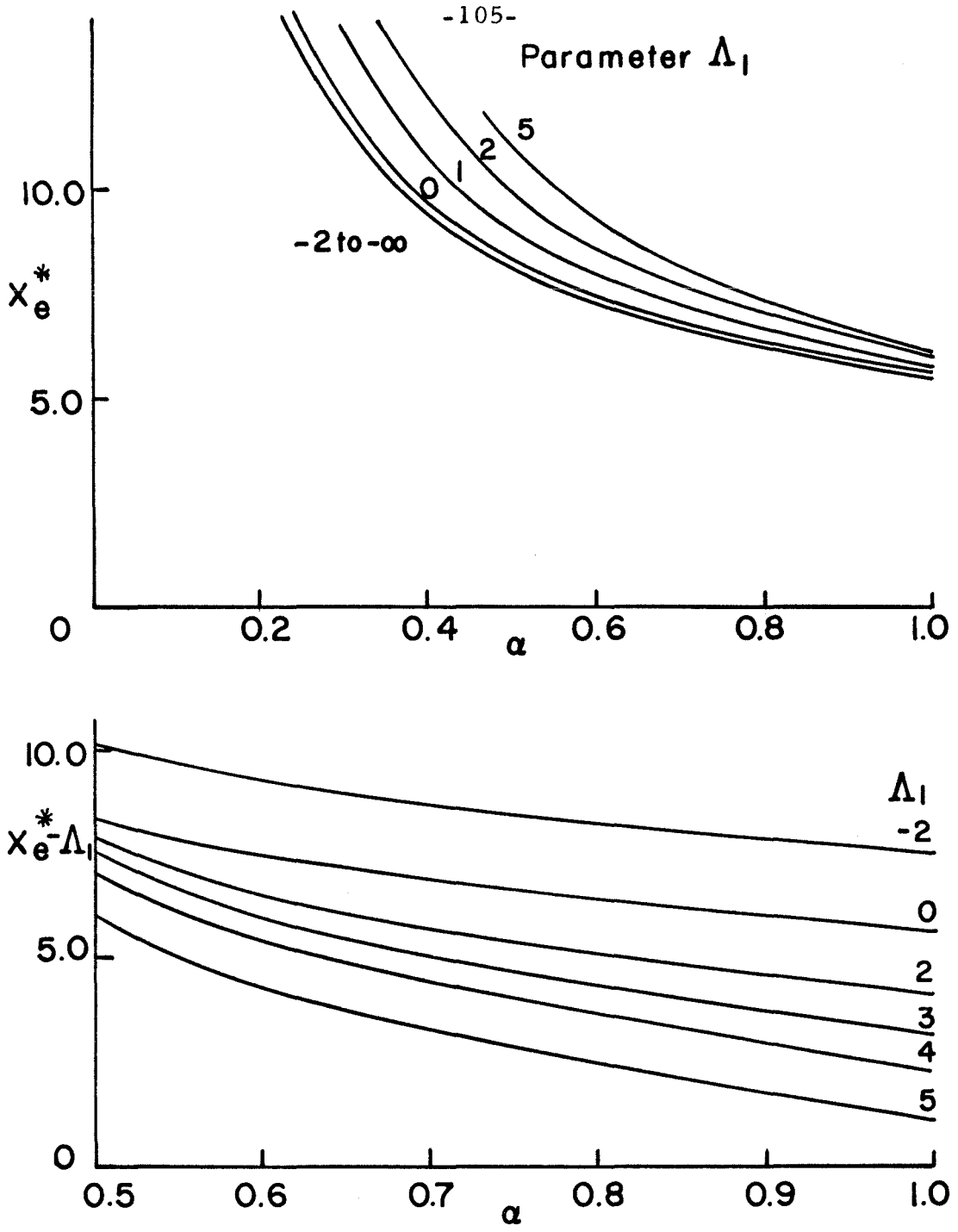

FIG. 25 FREE MIXING REGION LENGTH X_e^* CORRELATION OF PARAMETERS

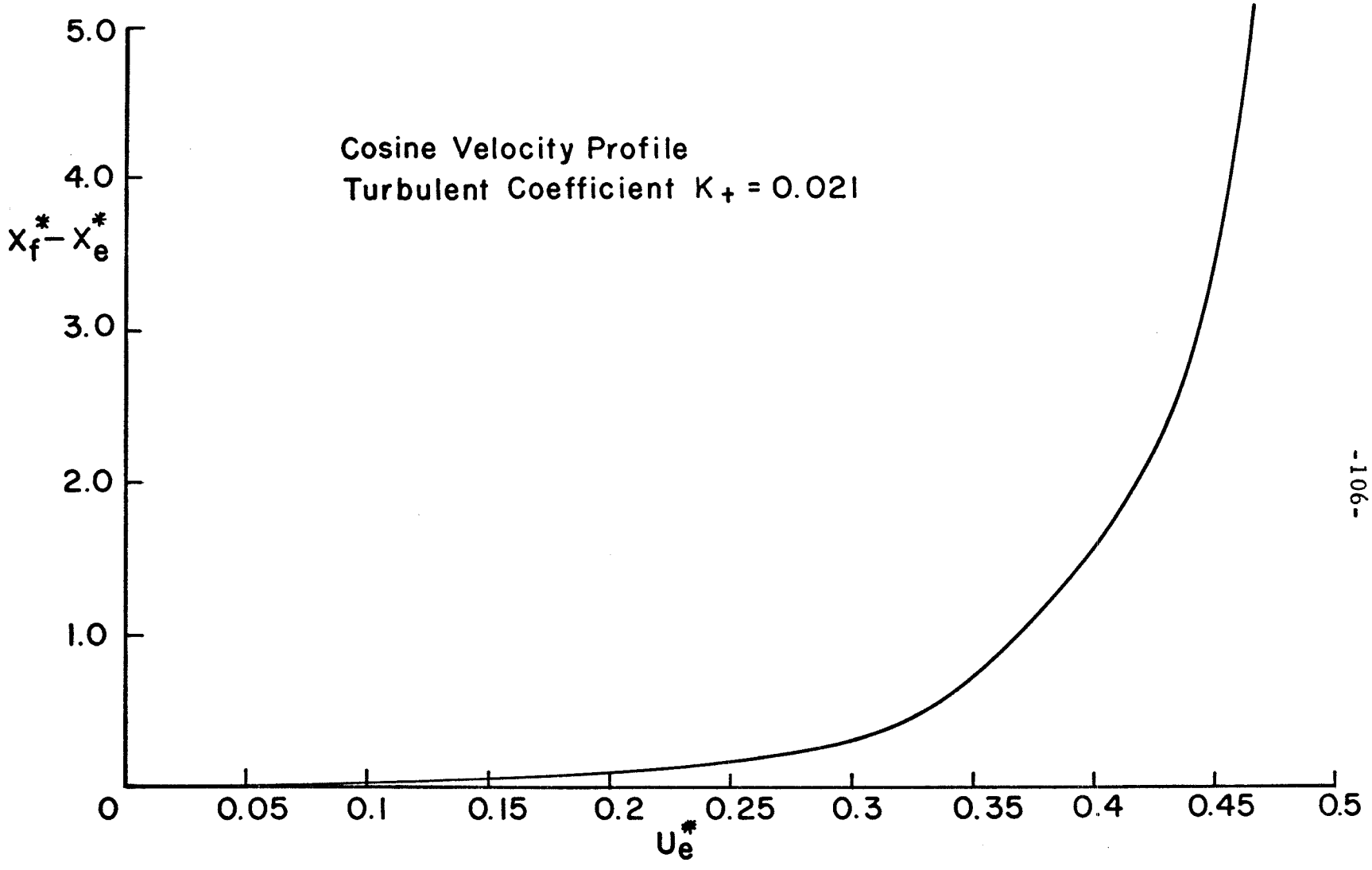

FIG. 26 CONFINED-MIXING REGION LENGTH $X_f^* - X_e^*$

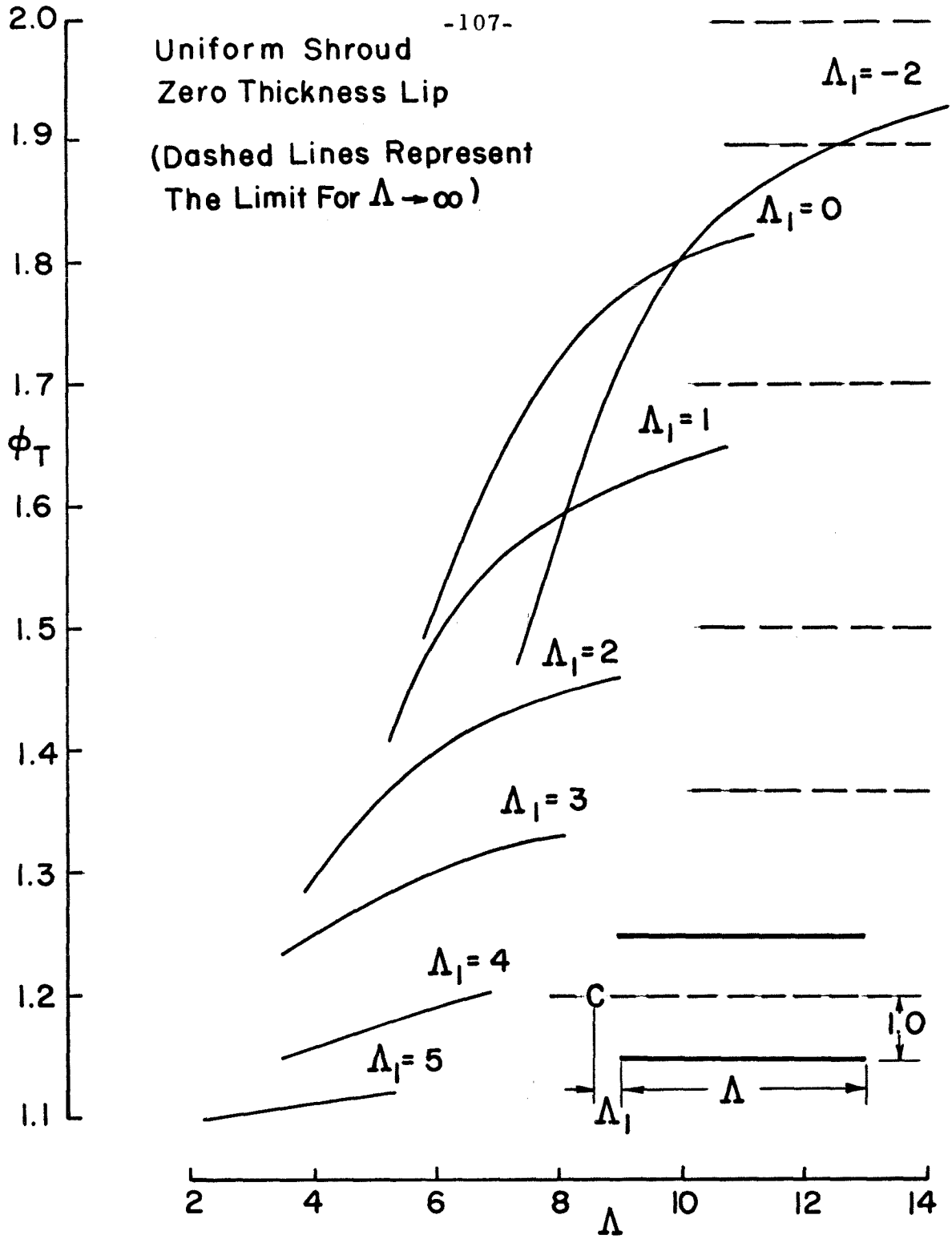

FIG. 27 EFFECT OF SHROUD LENGTH ON THRUST AUGMENTATION

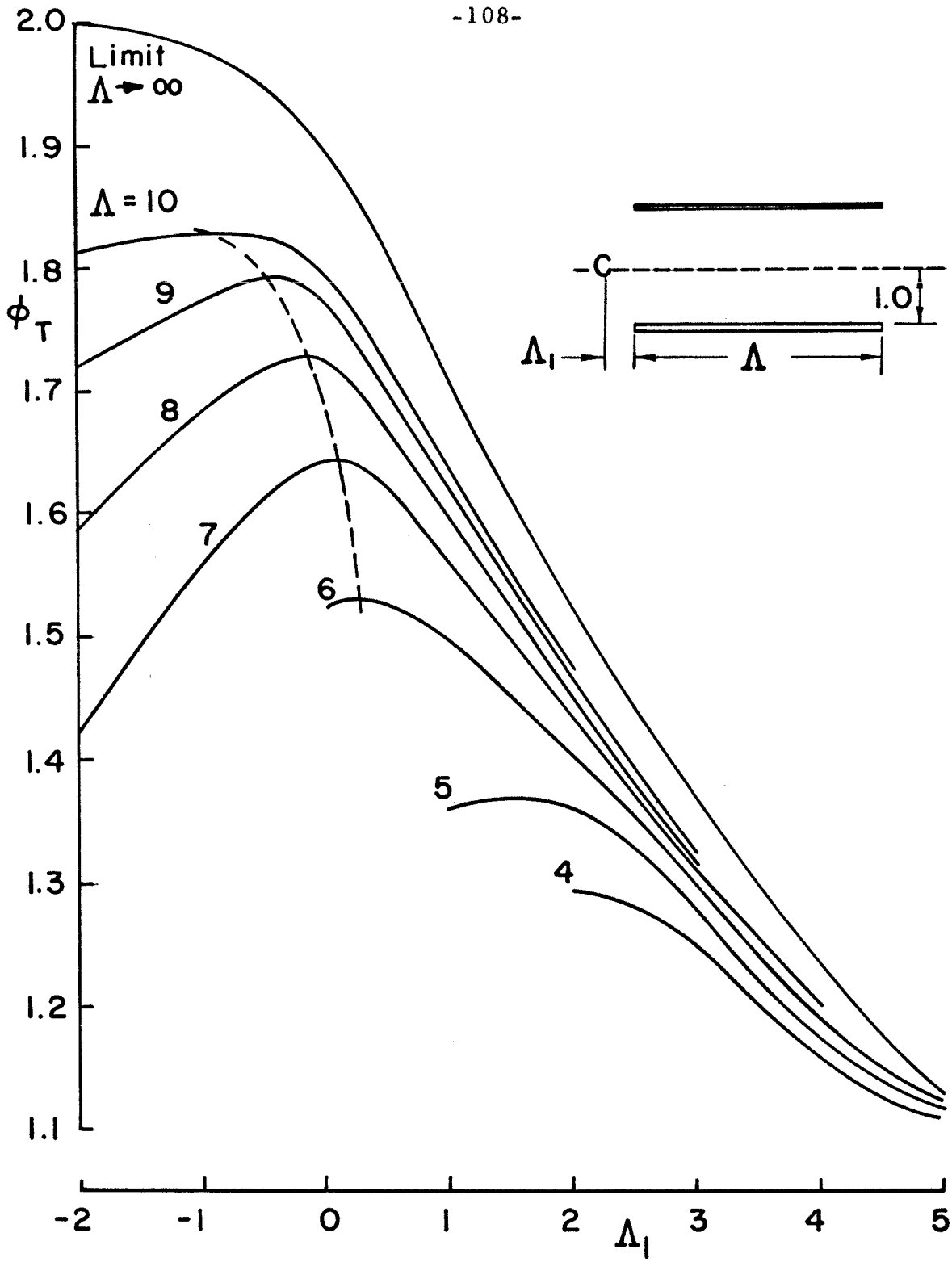

FIG. 28 EFFECT OF LIP-NOZZLE SEPARATION ON THRUST AUGMENTATION

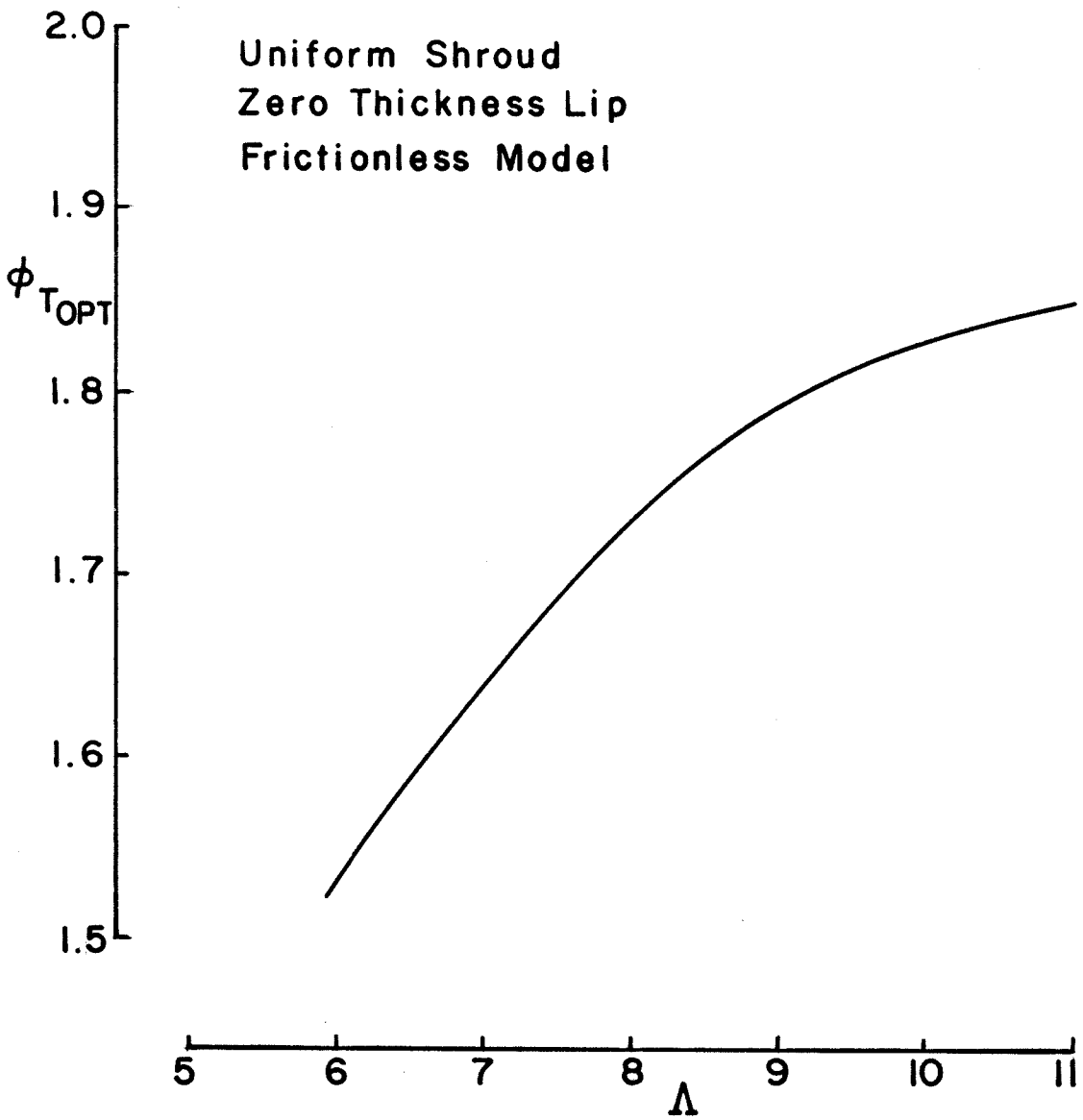

FIG. 29 OPTIMUM THRUST AUGMENTATION

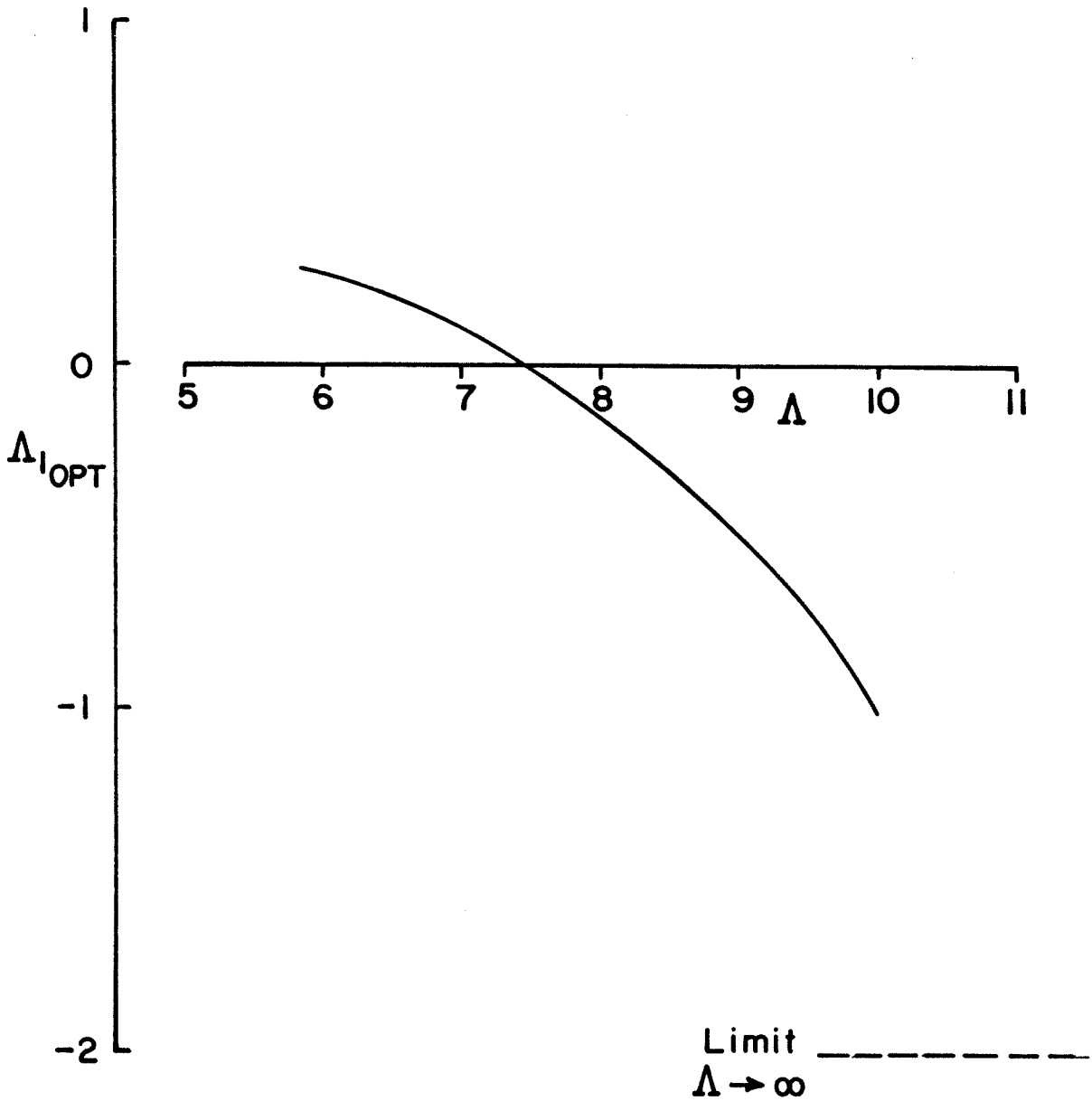

FIG. 30 LIP POSITION FOR OPTIMUM THRUST AUGMENTATION

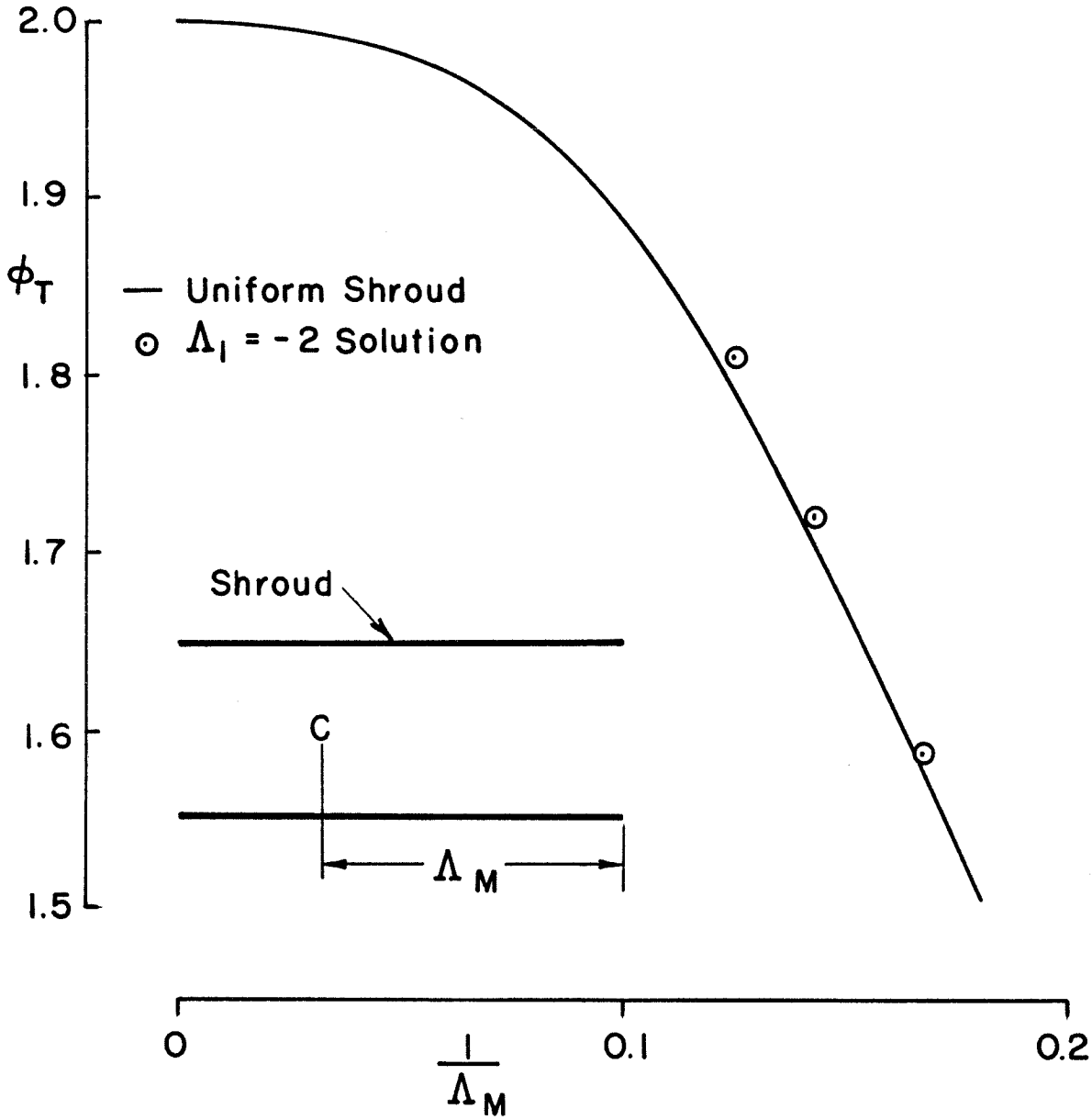

FIG. 31 THRUST AUGMENTATION SIMPLE CHANNEL THEORY

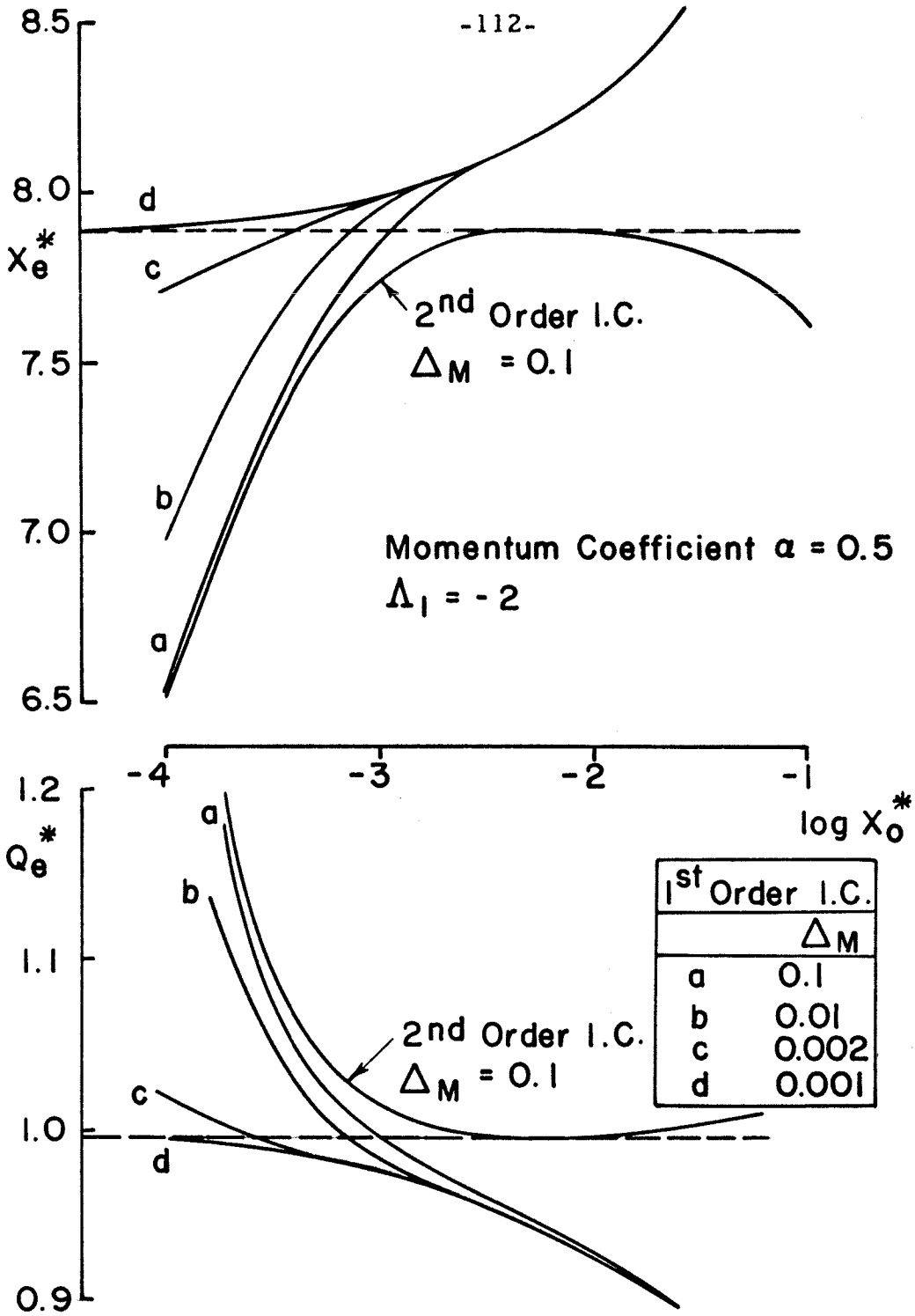

FIG. 32 FREE-MIXING SOLUTION NUMERICAL DETERMINATION OF INITIAL X_o^* AND STEP SIZE Δ_M

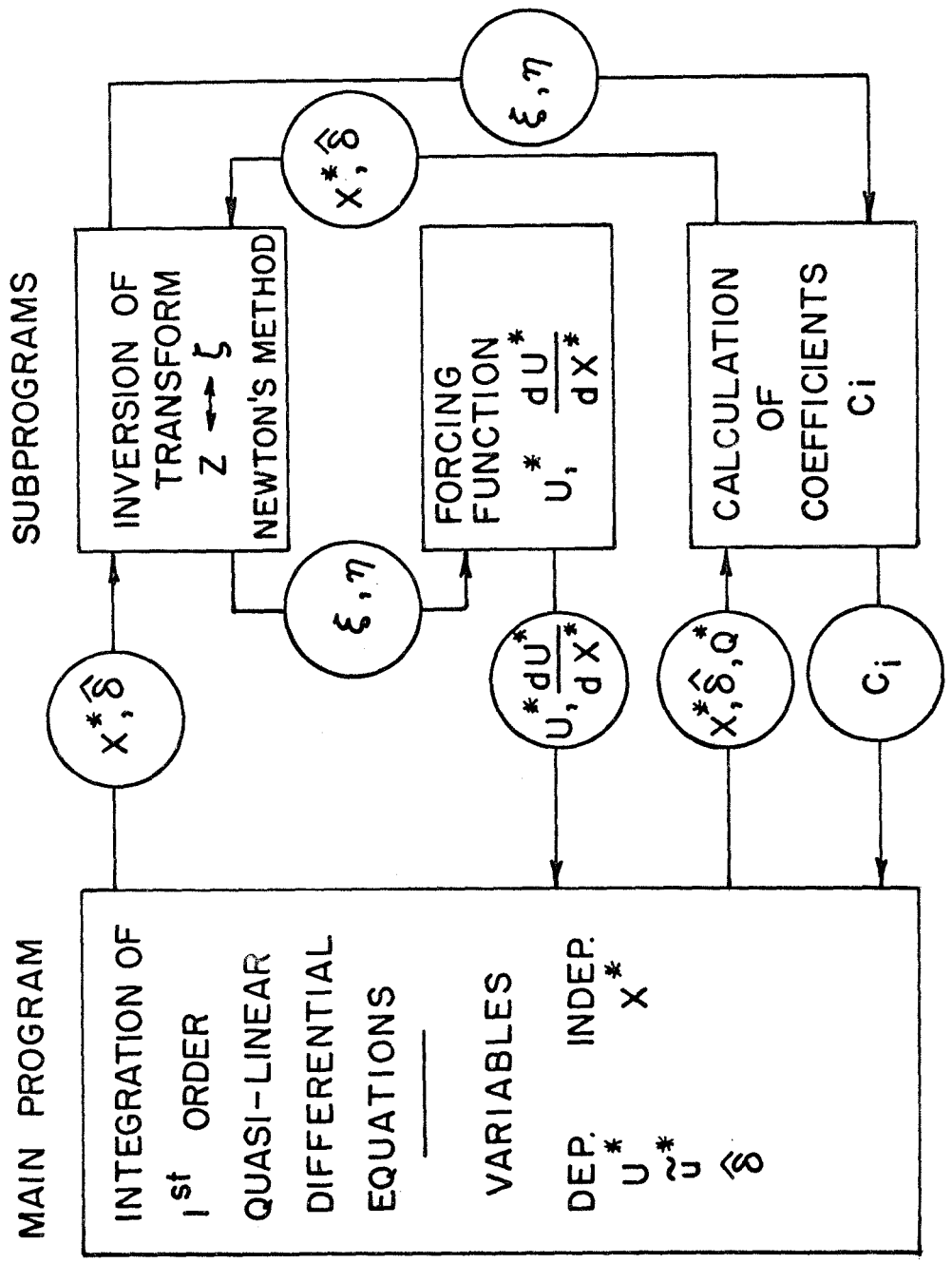

FIG. 33 NUMERICAL ITERATION SCHEME